LARGE EDDY SIMULATION OF FUEL INJECTION AND SPRAY COMBUSTION IN AN ENGINE ENVIRONMENT

by
Krzysztof Jaguś

A Thesis Submitted for the Degree of Doctor of Philosophy

School of Engineering and Design
Brunel University
July 2009

In loving memory of my Dear Uncle,

Stanisław Jaguś

Acknowledgements

First of all I would like to sincerely thank my Supervisor Dr. Xi Jiang for his constant support, knowledge he has provided me with and all the discussions we had during the past three years. This Thesis could not have been accomplished without his guidance, supervision and help he provided me with amply.

I would also like to extend my thanks to Supervisor Prof. Hua Zhao and my industrial Supervisors, Godfrey Greeves, Gavin Dober and Nebojsa Milovanovic. Their assistance throughout duration of my project and extensive knowledge they shared with me contributed greatly to the completion of this Work.

The project would not have been possible without the sponsorship of Delphi Diesel Systems for which I am extremely grateful.

Contents

List of Tables

List of Figures

Nomenclature

Roman Symbols

A	Model constant for the laminar timescale in the combustion model
A_R	Constant in the Arrhenius reaction equation
a_b	Parent blob diameter in the K-H breakup model
C_d	Droplet drag
C_k	Constant in the k-model
C_{MIX}	mixing constant in the expression for mixing timescale
C_p	Specific heat at constant pressure
C_S	Constant in the Smagorinsky model
b_R	Constant in the Arrhenius reaction equation
D_m	Species m diffusion coefficient
D_{SGS}	Subgrid energy dissipation term
E	Specific total energy
E_a	Activation energy
e	Internal energy
e_D	Total energy of droplet
F_i^S	Spray drag
f	Coefficient of the degree of turbulent combustion
G	Filter function
h_m	Sensible enthalpy

h_j^{SGS}	Subgrid scale heat flux
h_d	Seat transfer coefficient for the liquid phase
K	Thermal conductivity
k	Turbulence kinetic energy (RANS)
k_r	Reaction rate
k^{SGS}	Subgrid scale kinetic energy
L_V	Latent heat of evaporation
Q^S	Heat release due to spray
Q^C	Heat release due to chemistry
q_j	Heat flux vector
p	Pressure
Pr_t	Turbulent Prandtl number
R	Universal gas constant
r	Droplet radius
S_{ij}	rate of strain tensor
Sc_t	Turbulent Schmidt number
Ta	Taylor parameter used in the K-H breakup model
T	Temperature
T_A	Activation temperature of a given reaction
u	Velocity
u_r	Relative velocity between gas and liquid phase
V	Volume
V_d	Volume of the droplet

$V_{j,m}$	Diffusion velocity of species m in j direction
We_g	Weber number for the gas phase
We_l	Weber number for the liquid phase
W_F	Molecular weight of the fuel
W_P	Molecular weight of the product
W_O	Molecular weight of the oxidizer
W^S	Subgrid turbulence effect due to spray
Y_m	Mass fraction of species m
Y_F	Concentration of fuel
Y_O	Concentration of oxidizer
Z	Ohnesorge number

Greek symbols

Δ	Filter width
δ_{ij}	Kronecker Delta
ε	Dissipation of the turbulence kinetic energy (RANS)
η_g	Gas viscosity
Θ^{SGS}	Subgrid viscous work
$\theta_{j,m}^{SGS}$	Subgrid species diffusion mass flux
Λ	Wavelength used in a spray model
ν	Viscosity
ν_t	Eddy viscosity

Π^{SGS}	Velocity – pressure gradient correlation
ρ	Density
ρ^{CHEM}	Density change due to spray
ρ_l	Liquid density
ρ_g	Gas density used in the breakup models
ρ_m	Thermodynamic equilibrium value of partial density
ρ_m^C	Contribution to species concentration from chemistry
ρ_m^S	Contribution to species concentration from spray
ρ^S	Density change due to spray
σ	Surface tension
$\tau_{c,m}$	Characteristic timescale in the combustion model
τ_{ij}	Stress tensor
τ_{ij}^{SGS}	Subgrid stress tensor
τ_l	Laminar timescale
τ_{MIX}	Mixing timescale
τ_t	Turbulent timescale
Φ^{SGS}	Subgrid species mass flux
Ω	Growth rate used in a spray model
ω	Frequency
ω_P	Chemical production rate
ω_{KIN}	Kinetically controlled reaction rate
ω_{MIX}	Mixing controlled reaction rate

Abbreviations and miscellaneous:

ATDC	After top dead centre
CA	Crank angle
DNS	Direct numerical simulation
HSDI	High speed direct injection
LES	Large eddy simulation
RANS	Reynolds averaged Navier Stokes
SGS	Subgrid scale
TDC	Top dead centre
$\bar{}$	Filtered Quantity
$\tilde{}$	Density weighted filter

Abstract

Large eddy simulation of spray combustion in an HSDI engine is carried out in this thesis. The implementation of the code was performed in logical steps that allowed both assessment of the performance of the existing KIVA-LES and later development. The analysis of the liquid annular jet confirmed existence of typical, annular jet exclusive structures like head vortices, stagnation point and recirculation in the inner zone. The influence of the swirl in the ambient domain was found to have profound impact on the development, penetration and radial spreading of the jet. Detailed results were reported in Jagus et al. (2008).

The code was further validated by performing an extensive study of large eddy simulation of diesel fuel mixing in an engine environment. The reaction models were switched off in order to isolate the effects of both swirl and the different numerical treatment of LES. Reference RANS simulation was performed and significant differences were found. LES was found to capture much better the influence of the swirl on the liquid and vapour jets, a feature essentially absent in RANS results. Moreover, the predicted penetration of the liquid was much higher for the LES case and more in accordance with experimental measurements. Liquid penetration and subsequent evaporation are very important for prediction of heat release rates and encouraging results formed a good basis to performing a full simulation with models for ignition and combustion employed. The findings were analyzed in the paper by Jagus et al. (2009).

Further modifications were introduced into the LES code, among them changes to the combustion model that was originally developed for RANS and calculation of the filter width. A new way of estimating the turbulent timescale (eddy turnover time) assured that the incompatibilities in the numerical treatment were eliminated and benefits of LES maximized. The new combustion model proved to give a very good agreement with experimental data, especially with regard to pressure and accumulated heat release rates. Both qualitative and

quantitative results presented a significant improvement with respect to RANS results and old LES formulation. The new LES model was proved to give a very good performance on a spectrum of mesh resolutions. Encouraging results were obtained on a coarse mesh sets therefore proving that the new LES code is able to give good prediction even on mesh sizes more suitable for RANS.

Overall, LES was found to be a worthy alternative to the well established RANS methods, surpassing it in many areas, such as liquid penetration prediction, temperature-turbulence coupling and prediction of volume-averaged data. It was also discovered that the improved LES code is capable of producing very good results on under-resolved mesh resolutions, a feature that is especially important in industrial applications and on serial code structure.

1 Background

1.1 Motivation

The last decade saw a huge development in the area of High Speed Direct Injection (HSDI) diesel engines. Diesel technology is now at the forefront of Internal Combustion (IC) engines research due to their wide applications in automotive industry, as well as in many other applications such as ship engines. Ever greater concerns about environment protection and concerns regarding long term availability of fossil fuels have resulted in a very intense research devoted to understanding of combustion processes inside a diesel engine combustion chamber. Fuel efficiency, reduction in soot and NOx emissions are now of paramount importance. Thousands of test rigs gather relevant data from engines to gain a better understanding of the mixing and combustion phenomena.

Along with experimental research, Computational Fluid Dynamics (CFD) is becoming increasingly popular as one of the development tools, or even as a main one used in a design process. Massive increase in available computing power each year means that, what was considered an impossible task a few years ago can now be accomplished on a portable computer. The ability to model complex geometries by means of CFD opened the door to engineering and industrial applications. This was closely followed by development of numerical models and treatments of the flow problems. The well established Reynolds-Averaged Navier-Stokes (RANS) modelling approach although very robust and in certain applications sufficiently accurate, have started to show limitations. Phenomena involving high unsteadiness, including high vorticity flows and transient flows such as fuel injection encountered in liquid atomization and sprays, are typical areas where RANS methods are

severely limited. Fundamental assumption of Reynolds-averaging (time- or ensemble-averaging), and the imperfections of the models themselves ($k - \varepsilon$ and problems with highly swirling flows for instance) are mostly to blame. This turned attention of many researchers and scientists towards more sophisticated procedures of simulating the flow field. The Direct Numerical Simulation (DNS) approach is the most accurate methodology used for flow field prediction. As its name suggests, the governing equations are solved directly on a very fine grid and no modelling is introduced. Errors in the solution arise only due to the numerical algorithm and mathematical procedures of solving the differential equations. That is why the numerical schemes used in DNS are of very high order (typically 4th to 10th-order) to limit the artificial dissipation. This combined with the need for ultra dense meshing and small time-steps renders the DNS infeasible for any real world flow configurations. The second reason why DNS may not be the best solution for engineering flows is that the results contain a lot of information on small, chaotic scales which are of no direct relevance to the results or problems an engineer seeks in simulations. Filtering would probably have to be performed on such results to provide the information about bulk of the flow. The tool is still extremely useful for academic research and validation of models developed for less sophisticated methods like for example the aforementioned RANS formulation.

A method that can be viewed as being a bridge between RANS and DNS is the Large Eddy Simulation (LES) method. LES technique is a relatively novel approach to deal with simulations of turbulent flows. It emerged in the 60's, initially developed with geothermal flows in mind. In the course of time it was deemed promising for engineering flows. Today the power of computers has allowed LES to expand greatly beyond academic applications onto the engineering world. The background of LES can be traced to the Richardson's theory on energy transfer within turbulent flows (Richardson, 1922). To give a brief explanation of

this, Richardson (1922) assumed that the turbulent flow comprises of multiple eddy sizes (akin to turbulent scales) which go smaller in size from the so called integral length scales (known also as the energy containing structures) to the smallest scales. Across this spectra, an energy transfer known as energy cascade is occurring. Large eddies transform energy to the smaller ones. At certain point, viscosity effects begin to have influence and the energy of the smallest eddies is dissipated exclusively by the viscosity forces. LES as its name suggests aims to directly resolve the large, energy containing eddies. The influence of the small turbulent structures (not captured by the simulation) and viscosity is accounted for by modelling, not unlike in RANS approach. This implies that LES principle lies in distinction between resolved and unresolved scales. The spectrum of resolved scales is directly dependent on the grid resolution used. One can only directly resolve eddies larger than the grid size. The subgrid flow (structures smaller in size than the grid) and its effects on the resolved part are then left to modelling. It is beneficial to directly resolve as much structures as possible as this reduces the contribution of the modelling part. The ratio of resolved to modelled energy in a flow is physically determined by the grid size. In mathematical terms it is expressed as a physical filtering operation performed on the flow field. The amount of filtering is controlled by the so called filter width specified by user or calculated during the simulation. Details on the filtering operation and Kolmogorov' assumptions will be presented in Chapter 2. In theory, a very detailed (high mesh resolution) LES can approach a DNS accuracy. In practice however, this is not entirely true, especially with certain turbulence models (Smagorinsky model) that can fail for very small filter widths (Pope, 2008).

1.2   Research objectives

The motivation of this work is to introduce LES to the problems of modelling unsteady, reacting, two-phase flows in HSDI diesel engines. While basic LES in internal combustion engines has been attempted before, this study focuses on the modelling and simulation of complex atomization and spray and the combustion processes with a direct relevance to industrial applications.

While models for combustion and ignition are well established in Reynolds-averaged methods, adaptations or modifications are necessary in order to make them compliant with the LES methodology. It is often the case that the underlying assumptions for a given model are not valid anymore, consequently either a different approach is necessary or the model is simply unsuitable for LES. Looking at it the other way, the time dependent formulation and direct calculation of energy containing eddies may often remove restrictions associated with Reynolds-averaging and open up possibilities to develop new, more accurate modelling assumptions.

To maximize the benefits of time dependent formulation, averaging must be avoided whenever possible. Only then, would it be possible to obtain true instantaneous data. The work presented here aims to develop a robust and reliable LES version of the KIVA-3V code (Amsden, 1993, 1997) that can be successfully used to predict reacting, two-phase flows in a real-world engineering configurations. This means that feasibility, computational performance and applicability of the models used are crucial in achieving this goal. The characteristic time scale combustion model (Abraham et al., 1985) employed in the ERC RANS version (Valentino, 2007) of the KIVA code relies on turbulent timescales to establish the magnitude

of the influence of turbulent flow on the progress of a chemical reaction. This is based on calculation of the averaged turbulent kinetic energy and its dissipation rate by means of the well known $k - \varepsilon$ turbulence model. The main drawback of this approach is that the flow is represented by a single turbulent timescale. Obviously, this is not true for even the simplest configurations and low Reynolds numbers. Therefore there is a need to more accurately estimate the turbulent timescale known also as an eddy turnover time.

One of the objectives of this work is to develop an algorithm for estimation of the turbulent timescales that would be appropriate for LES. This would be achieved by not only dropping the somewhat dubious assumption of a single timescale but also performing estimation based on different quantities other than the large scale turbulent kinetic energy and dissipation from the $k - \varepsilon$ two equation model.

The process of ignition and combustion when considered in terms of numerical descriptions, occurs on the so-called subgrid scales. Subgrid scales are the length scales that are smaller than the grid size. In LES their presence is accounted for by turbulence modelling. Chemical timescales are much smaller than the grid size, hence modelling of turbulence and chemical interactions have to take place or at least take into account the subgrid level. Almost all combustion models to date rely on some sort of averaging or representing subgrid quantities by means of a single variable, for example mixture fraction in the PDF methods (Pope, 1985). The only exception known to the Author's knowledge is the Linear Eddy Model (LEM) formulated by Kerstein (1988, 1992).

In the LEM formulation, all the relevant turbulent time and length scales are accounted for and directly resolved not unlike in DNS (Menon et al., 1993). In order to make them

computationally feasible, scales smaller than the grid size are resolved in a one-dimensional (1D) domain. However the effects of three-dimensional (3D) vortical structures are accounted for by means of a special stochastic process. Extensive research on LEM was conducted by Calhoon (1996) and Sankaran (2003).

The work presented in this thesis was organized in logical steps, outline of which is described as follows. The LES algorithm was assessed in a non-reacting flow for an annular liquid jet configuration, followed by a real HSDI engine configuration for which experimental data exists and E16 engine purpose-built for spray investigations. The results were compared with both the experimental data and RANS simulations conducted using the standard KIVA. The development of combustion model for LES was divided into three main stages. First, the current state was assessed. This was done by employing standard, RANS specific reaction modelling approach in a LES calculated flow field. Identification of LES specific issues was followed by necessary modifications mainly centred on the concept of eddy turnover time and its determination. Implementation of the improved characteristic timescale combustion model is then verified with the experimental data. Based on the results, further refinement is done to the LES model in order to limit the amount of averaging introduced and better reproduce the influence of the smallest scales on the reaction rates in the system. The modified code is validated against experimental, industry supplied data of a real engine configuration. RANS simulations are performed where possible to further highlight the differences and advantages of LES.

2   Review of the Methodology and the Modelling Approach

2.1   Scale range separation, space filtering and mathematical formulation

Turbulent spray combustion, which is of main interest here is an extremely complex phenomenon, involving multiple time and length scales. The largest ones are of the order of the size of the system (for instance dimensions of the gas turbine combustion chamber), while smallest, dissipative Kolmogorov scales are much smaller and dependent on Reynolds number (Kolmogorov, 1991). Combustion and multiphase phenomena add to the diversity and complexity of the system. While reaction always occurs at the molecular level and at the smallest time scales, there are many situations where large scale flow influences the structure of the flame. Each of the species involved has its own reaction characteristic chemical timescale, diffusivity etc. Moreover, combustion in the system can be mixing or reaction rate controlled, depending on many factors such as turbulence levels, chemical species involved, pressure and temperature. This diversity of turbulent reacting flows makes them a very complex modelling task. If this type of physical problem is attempted to be solved by numerical methods, limitations in both mathematical description and the available computer resources immediately arise. Therefore necessity exists to introduce assumptions and simplifications to describe the system in an abridged, reliable way, making the problem feasible for numerical treatment.

Scale range separation is the basis of LES. Figure 2-1 depicts the basics of Kolmogorov theory (Kolmogorov, 1991) and associated turbulent flow scales. Those can be divided into two main ranges: energy containing range and universal equilibrium range. The energy containing range contains the largest eddies which LES should be able to directly capture.

Universal equilibrium range is split into two sub ranges: inertial range and dissipation range. The dissipation range contains the smallest scales of turbulence (associated with Kolmogorov length scale). Viscosity effects play a key role in dissipation of the flow energy in that region. The inertial sub-range sits between dissipation and energy containing ranges and this is where the transfer of energy to successively smaller scales is taking place (Leonard, 1974). An operation of filtering can be applied to the governing equations for fluid flows, which subsequently leads to a set of filtered governing equations, forming the basis of the numerical solution in LES. It needs noting that filtering can in theory be applied at any scales and does not need to follow the distinction between energy containing range and universal equilibrium range. It is however most beneficial in terms of computational costs to adjust the filtering in such a manner that the majority of the energy containing range is directly resolved.
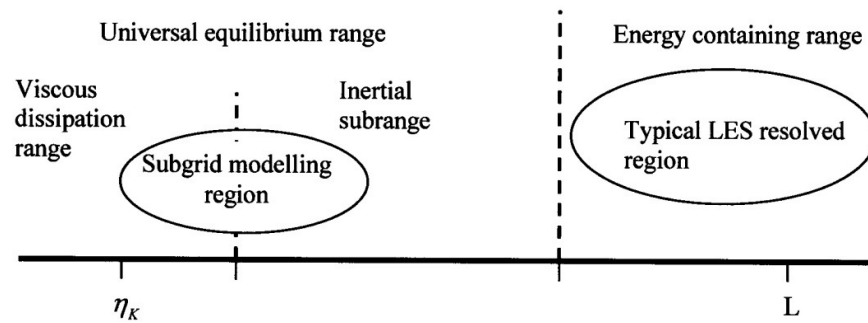
Figure 2-1. Kolmogorov energy spectrum.

Equations describing reacting flows in combustion engines and gas turbine combustors must account for changes in density to be able to predict phenomena like pressure fluctuations, dilatation, and thermal expansion. This is a more complicated approach than that in strictly incompressible flows, although treatment of engine flows can be accomplished by using the low Mach number approximation while still accounting for density changes. Simplification of the filtered, compressible equation set can be accomplished by introducing the density

weighted filtering, known commonly as Favre filtering (also known as mass-weighted filtering), so as to avoid appearance of additional SGS terms when the compressible flow governing equations are filtered. Mass-weighted filtering is used for all parameters of the fluid flow besides the pressure (and body forces in gravitational, electrical and magnetic fields when relevant). The filtering is designated by two symbols, namely, the overbar designates ordinary filtering, while the tilde specifies mass-weighted filtering (Erlebacher & Hussaini, 1992).

$$\tilde{f} = \frac{\overline{\rho f'}}{\overline{\rho}} \tag{2.1}$$

Flow field is then decomposed into the resolved and unresolved parts:

$$f = \tilde{f} + f' \tag{2.2}$$

Here, $\tilde{f}$ represents the resolved scale, while f' is a subgrid scale component. While at first glance this is similar to the way variables are decomposed in RANS, it is important to note that this is not decomposition into mean and fluctuating parts but distinction between resolved and unresolved scales in LES.

The filtered quantity is obtained by applying a filtering function given by

$$\tilde{f}(x,t) = \int_V G(x - x_i')f(x_i',t)dx_i' \tag{2.3}$$

where V represents the domain and G is a filter function which must satisfy:

$$\int_V G(x_i - z_i)dz_i = 1 \tag{2.4}$$

While in theory any filtering function satisfying the above equation can be used, three types of filters have been commonly used in LES, including Fourier space filter, Gaussian filter and box filter. The Fourier space filter requires transformation of Equation (2.3) into the Fourier space using the Fourier transformation:

$$\tilde{f}(\omega) = \int f(x_i) e^{-i\omega x} dx \qquad\qquad (2.5)$$

The filter definition in Equation (2.3) will then read (Froehlich & Rodi, 2002):

$$\hat{\tilde{u}}(\omega) = \hat{G}(\omega)\hat{u}(\omega) \qquad\qquad (2.6)$$

Fourier space filter is of limited feasibility in engineering LES (Froehlich & Rodi, 2002; Lesieur et al., 2005). Therefore the Gaussian and box filters are often used. The Gaussian filter is commonly specified as:

$$G(x, y) = \left(\frac{A}{\pi}\right)^{1/2} \left[-A(y-x)^2\right] \qquad\qquad (2.7)$$

where A is equal to $A = 6/\Delta^2$ according to Speziale (1985) and Δ is a characteristic filter width. For LES calculations it is best to correlate the filter width directly with the grid size. Hence it is convenient to specify it as:

$$\Delta = \sqrt[3]{\Delta x \cdot \Delta y \cdot \Delta z} \qquad\qquad (2.8)$$

where Δx, Δy and Δz are the sizes of a typical grid cell in x, y and z directions respectively. The most common filter used is the box filter. It has a unique feature in that the filtered quantity at the filter centre represents the spatial average of the filtered function within the filter domain. This makes it attractive for application in finite volume method based codes.

Applying the filtering to the fundamental governing equations of fluid flows leads to a set of filtered equations to be solved in LES, consisting of the mass conservation equation, Navier-Stokes momentum equations for the three velocity components, and the energy equation and species conservation equations for each of the species present in the system for reacting flows. Before LES specific equations will be presented, the generic equation set is listed below, so that the differences are more easily outlined.

$$\frac{\partial \rho}{\partial t} + \frac{\partial \rho u_j}{\partial x_j} = \rho^S \qquad (2.9)$$

$$\frac{\partial \rho u_i}{\partial t} + \frac{\partial}{\partial x_j}\left(\rho u_i u_j - \tau_{ij}\right) = F_i^S \qquad (2.10)$$

$$\frac{\partial \rho E}{\partial t} + \frac{\partial y}{\partial x_j}\left(\rho E u_j + q_j + u_i \tau_{ij}\right) = \dot{Q}^C \qquad (2.11)$$

$$\frac{\partial \rho Y_m}{\partial t} + \frac{\partial}{\partial x_j}\left(\rho Y_m \left(u_j + V_{j,m}\right)\right) = \dot{\rho}_m^c + \dot{\rho}_m^S \qquad (2.12)$$

The relevant terms are given as follows:

q_j is a heat flux vector

$$q_j = -K\frac{\partial T}{\partial x_j} + \rho \sum_{m=1}^{N} h_m Y_m V_{j,m} \qquad (2.13)$$

τ_{ij} is the stress tensor, commonly specified as

$$\tau_{ij} = -p\delta_{ij} + 2\mu_g S_{ij} - \frac{2}{3}\mu_g S_{kk} S_{ij} \qquad (2.14)$$

S_{ij} is the rate of strain tensor defined as

$$S_{ij} = \frac{1}{2}\left(\frac{\partial u_i}{\partial x_j} + \frac{\partial u_j}{\partial x_i}\right) \qquad (2.15)$$

The source terms on the right hand sides of Equations (2.9) - (2.12) are due to the spray and chemistry effects, namely ρ^S is the density change due to the liquid phase, $\dot{Q}^C$ is the heat release from the chemical reactions, $\dot{\rho}_m^C$ and $\dot{\rho}_m^S$ are contributions to species concentrations from chemistry and spray. Finally, in the momentum conservation equation, the term F_i^S accounts for drag forces due to the liquid spray present in the system. For the same type of

flow (gas containing liquid phase described in Lagrangian reference frame) LES equation set looks as follows (Sone and Menon, 2003; Sone et al., 2001):

$$\frac{\partial \overline{\rho}}{\partial t} + \frac{\partial \overline{\rho}\widetilde{u}_j}{\partial x_j} = \overline{\rho}^{\,S} \tag{2.16}$$

$$\frac{\partial \overline{\rho}\widetilde{u}_i}{\partial t} + \frac{\partial}{\partial x_j}\left(\overline{\rho}\widetilde{u}_i\widetilde{u}_j - \widetilde{\tau}_{ij} + \tau_{ij}^{SGS}\right) + \frac{\partial \overline{p}}{\partial x_i} = \overline{F}_i^{\,S} \tag{2.17}$$

$$\frac{\partial \overline{\rho}\widetilde{e}}{\partial t} + \frac{\partial}{\partial x_j}\left(\overline{\rho}\widetilde{u}_j\widetilde{e} + \overline{q}_j + h_j^{SGS}\right) + \overline{p}\frac{\partial \widetilde{u}_j}{\partial x_j} - \widetilde{\tau}_{ij}\frac{\partial \widetilde{u}_i}{\partial x_j} + \Pi^{SGS} + \Theta^{SGS} = \overline{\dot{Q}}^{\,C} + \overline{\dot{Q}}^{\,S} \tag{2.18}$$

$$\frac{\partial \overline{\rho}\widetilde{Y}_m}{\partial t} + \frac{\partial}{\partial x_j}\left(\overline{\rho}\widetilde{u}_j\widetilde{Y}_m - \overline{\rho}\overline{D}_m\frac{\partial \widetilde{Y}_m}{\partial x_j} + \Phi_{j,m}^{SGS} + \theta_{j,m}^{SGS}\right) = \overline{\dot{\rho}}_m^{\,C} + \overline{\dot{\rho}}_m^{\,S} \tag{2.19}$$

In the above equations, the subgrid related terms are unclosed and have to be modelled. This includes the subgrid-scale stress tensor τ_{ij}^{SGS}, subgrid heat flux h_j^{SGS}, velocity-pressure gradient correlation Π^{SGS}, viscous work Θ^{SGS}, species mass flux $\Phi_{j,m}^{SGS}$, and species diffusive mass flux $\theta_{j,m}^{SGS}$. Additionally, all the terms on the right-hand-sides of Equations (2.16) – (2.19) which are due to liquid spray and combustion need to be modelled. They may include contributions from both the resolved and sub-grid scales.

The modelling of the unclosed terms in the filtered equations and appropriate treatment of the chemical (combustion) and spray source terms in the governing equations represent the most challenging and important task for LES of reacting spray flows. There have been considerable efforts in modelling all these terms.

The closure of the residual stress tensor is often performed using the $k-$equation model (Menon & Calhoon, 1996), the subgrid stress tensor is given as

$$\tau_{ij}^{SGS} = -2\bar{\rho}\nu_t\left(\tilde{S}_{ij} - \frac{1}{3}\tilde{S}_{kk}\delta_{ij}\right) + \frac{2}{3}\bar{\rho}k^{SGS}\delta_{ij} \tag{2.20}$$

In Equation (2.20), $\tilde{S}_{ij}$ is the resolved strain rate tensor, defined as

$$\tilde{S}_{ij} = \frac{1}{2}\left(\frac{\partial \tilde{u}_i}{\partial x_j} + \frac{\partial \tilde{u}_j}{\partial x_i}\right) \tag{2.21}$$

The eddy viscosity is given by $\nu_t = C_\nu\bar{\rho}\sqrt{k^{SGS}}$ using the subgrid turbulent kinetic

energy k^{SGS}, which is provided by solving the following equation

$$\frac{\partial \bar{\rho}k^{SGS}}{\partial t} + \frac{\partial \bar{\rho}\tilde{u}_j k^{SGS}}{\partial x_j} = -\tau_{ij}^{SGS}\frac{\partial \tilde{u}_i}{\partial x_j} - D^{SGS} + \frac{\partial}{\partial x_j}\left(\frac{\bar{\rho}\nu_t}{\mathrm{Pr}_t}\frac{\partial k^{SGS}}{\partial x_j}\right) + \dot{W}^S \tag{2.22}$$

In the above equation, the subgrid energy dissipation rate term D^{SGS} is closed by

$C_\varepsilon\bar{\rho}^{3/2}\sqrt[3]{k^{SGS}}/\bar{\Delta}$. The values of C_ν and C_ε are chosen to be 0.067 and 0.916 (Sone &

Menon, 2003; Sone et al., 2001). The last term $\dot{W}^s$ is the subgrid turbulence effects due to

spray, which follows the original modelling approach used in RANS version of the KIVA.

The subgrid heat flux, viscous work, and species mass flux may be modelled as (Sone and

Menon 2003; Sone et al., 2001):

$$h_j^{SGS} = -\frac{\bar{\rho}\nu_t C_p}{\mathrm{Pr}_t}\frac{\partial \tilde{T}}{\partial x_j}; \quad \Theta^{SGS} = D^{SGS}; \quad \Phi_{i,m}^{SGS} = -\bar{\rho}\frac{\nu_t}{Sc_t}\frac{\partial \tilde{Y}_m}{\partial x_i} \tag{2.23}$$

In LES of reacting flows, an assumption is often made that in a turbulent reacting flow the

scales of the chemical processes are separated from those of turbulence, based on the

observation that chemical reactions occur at much smaller time scales than those of turbulence

itself. A separate, uncoupled treatment of both turbulent and chemical processes is then

possible. This is a scale separation, which forms the basis of many physical models for

turbulent combustion. There are however situations, where this scale separation fails

completely. For example, it has been shown by Dinkelacker et al. (1998) and Menon and Patel (2006) that lean premixed flames are highly unstable and can be quenched locally or extinguished by turbulent effects. This phenomenon is especially important in the context of gas turbine combustors. Since the design of a modern gas turbine combustor focuses on lean combustion for lower emission and increased fuel efficiency, the risk of flame quenching and local extinction is increased. The so-called lean blow out (LBO) can occur in both premixed and non-premixed flames and substantial amount of research is devoted to this problem (Candel, 2002; Menon and Patel, 2006). The coupling between turbulence and combustion chemistry calls for very sophisticated combustion models effective at all flow scales and this is where the scale separation theory has serious limitations. In addition, heat release due to the reaction causes density and velocity fluctuations which couple the behaviour of small scales back to the large, energy containing eddies. A short review of current state of combustion modelling will be given in 2.3.

In the LES procedure, after operation of filtering, the numerical scheme is then responsible for solution of the filtered equations, with the unknown terms either closed by subgrid modelling or in some instances discarded due to the lack of robust models. In general, more accurate numerical schemes than for RANS are desirable (Hori et al., 2008). One of the most appealing traits of LES is the limited dissipation and the ability to capture instantaneous data. To keep it attractive, use of non-dissipative numerical algorithms is highly desirable (Camarri et al., 2004), although relatively crude schemes like second order upwind which is dissipative by nature can give good results, far superior to those of time averaged methods. Haworth (1999) compared various SGS models to RANS techniques. Even though coarse meshes were used, encouraging results were obtained. Especially variations between cycles were captured, something that is not possible using traditional time-averaged techniques. The aforementioned

diffusion issue is most important in simulations of sprays, where jet penetration prediction is very important. Indeed, one of the aims of this thesis is to take advantage of reduced dissipation in predicting penetration of diesel sprays into the combustion chamber.

Correct estimation of spray travel is very important both in terms of quality of the mixing and emission prediction. Small differences can lead to huge changes in the production of pollutants over an engine cycle. Accurate and reliable predictions of the penetration are therefore highly desirable. It was shown among others by Apte et al. (2003) that LES can be very promising in that area. Very good agreement with experimental data regarding spray tip penetration was achieved. Study regarding turbulent mixing in diesel spray using LES by Kimura et al. (2004) also showed good agreement with experiment. One of the most useful publications concerning abilities of the LES model is by Sone and Menon (2003). In their work LES scheme was implemented into the KIVA code along with sophisticated linear eddy model to account for subgrid mixing. Again, encouraging results were obtained. The field of the evaporated fuel was significantly less diffused than the one predicted by the reference RANS simulation. Although the work concentrated on spark ignition engines and the formulation was non-reacting, it nevertheless showed LES as a promising method for simulation of complex flows, no doubt aided by the Linear Eddy Model formulation as a subgrid scalar transport mechanism. Among LES of internal combustion engines, work of Yavuz et al. (1998) is recognised as pioneering one. Again, KIVA code was used because of its expandability and arbitrary Lagrangian Eulerian scheme that is suitable for moving meshes and convective transport with varying levels of implicitness.

Study was also conducted to estimate the turbulence levels and compare them with experimental data (Auriemma et al., 1998). Interesting remarks were drawn, most important

of which seems to be the existence of cycle to cycle variations. It was also showed that turbulence intensity scales scale linearly with engine operational speed for an engine configuration they used. This remark has to be treated with caution, as the geometry was relatively simple and engine speeds used were low. There was also no swirl imposed in the chamber which is not realistic since all modern direct injection engines rely on strong flow perturbations in the combustion chamber in order to enhance mixing. Finally, no subgrid scale model for turbulence was used.

Some scientists claim that a non-SGS LES can still be a reliable tool (Boris et al., 1992), but this should go in pair with finer resolution of the grid to solve more energy containing eddies and limit the lack of contribution of the subgrid scales. It is often argued that the numerical dissipation can account for the inertial range but the control over this process is very limited at best. Also, the backscatter phenomenon is not accounted for in such cases. Backscatter is a process of reverse energy cascade (from the subgrid scales, back to the resolved ones). It has been confirmed that backscatter can in certain cases account for a significant portion of a modelled energy budget within the flow. It was noted by Schumann (1995) that backscatter is higher in a coarse mesh application, which is where the subgrid energy represents a significant portion of the total kinetic energy. Detailed research on backscatter, the physical phenomena behind it and current ways of numerical representation was conducted by Domaradzki and Saiki (1997).

Most of the LES work performed so far has been conducted using structured grids. In this context the work of Haworth and Jansen (2000) needs to be noted, in which an algorithm for unstructured finite volume elements was used. This of course gives more freedom when simulating complex geometries, at the expense of more complicated coding. Haworth

compared his LES results with experimental, DNS and rapid-distortion theory data. Again, improvement over Reynolds averaged turbulence models was clearly visible. Three subgrid scale models were used. The simplest Smagorinsky formulation, Smagorinsky with dynamic coefficient determination and finally a Lagrangian dynamic subgrid scale model by Meneveau et al. (1996). Trustworthy results for an IC engine configuration have been obtained, and some LES-specific issues have been raised like law of the wall treatment or inflow and outflow boundary treatment.

2.2   Numerical simulations of non-reacting sprays

Modelling of a two-phase flow is an extremely challenging task both in terms of mathematical description and substantial computational requirements. Yet this area of Computational Fluid Dynamics is very significant from the engineering and industrial point of view. Internal Combustion engines, turbo aerospace units and aviation engines all use liquid fuel that is being injected into the combustion chamber. Before the fuel is vaporized, a lot of complex interactions take place between the droplets of fuel that influence the rate of evaporation and subsequently quality of the combustion process. While the mechanisms that govern the disintegration of low speed liquid sprays are reasonably understood in these days (Haenlien, 1932; Reitz, 1987), their relevance to Diesel Engine applications is limited. These days, there is a strong tendency to increase injection pressure while minimizing the amount of fuel injected in a single injection. This combined with the switch to direct injecting and shorter fuel release times has created the need of a better understanding of a behaviour of a high pressure, high speed liquid jet issuing into a high pressure environment.

The work of Patterson and Reitz (1998) within the framework of diesel engines gives a useful feedback on the dependency of the results on the break up model constants chosen and shows that the level of empiricism in the modelling must be reduced. Apte et al. (2009) performed a state-of-the-art LES of a liquid spray in a Pratt and Whitney combustion chamber on an unstructured grid. The liquid phase was modelled using Lagrangian point-particle formulation with stochastic models for breakup. The input constants for the models were determined dynamically during the simulation, overcoming the lack of ad-hoc knowledge of the flow problem. While the dispersion of the droplets was found to be accurate, the number of small diameter droplets was over predicted. Also, the primary breakup region near the nozzle tip was not accounted for. This region while probably not crucial for gas turbines is very important in Diesel engine applications where the confinement of the spray is small. The similar stochastic Lagrangian model used by Vinkovic et al. (2006) does account for droplet coalescence and inter droplet collisions. This makes prediction of secondary breakup possible. The formulation also accounts for subgrid droplet behaviour, a trait that is scarce in LES to date. A dedicated study towards understanding of turbulent mixing in a diesel spray using LES was conducted by Kimura et al. (2004). They tried to address the problem of instabilities near the circular jet axis by modifying the filter size. Both gas jets and particle laden jets were investigated, liquid phase being tracked once again in a Lagrangian framework. The outcome confirmed the issue of modelling of liquid behaviour in the near nozzle region, as the diffusion of particles was underestimated comparing to the experimental data. This was more severe as the mass load increased.

More work has recently been devoted to atomization and sprays in diesel engines. Lee et al. (2002) implemented LES into the KIVA code which is also used in this study. A full two-phase flow simulation has been conducted with combustion. Itoh et al. (2003) concentrated

again on a vaporizing spray in conjunction with a swirling ambient flow. Similar research, albeit concerning gas turbine application was attempted by Caraeni et al. (2002). The outcome of those investigations while undoubtedly useful was questioned by some researchers with regard to validation of numerical procedure.

When high pressure liquid sprays are concerned, experimental and numerical work has been performed by Su et al. (1996). The main goal was the determination of the spray penetration of a multi-hole injector. The models for droplet drag and deformation were included. Tennison and Reitz (2001) compared experimental and computational data of a HSDI engine equipped with a common rail fuel injection and delivery system. Penetration, mean droplet radius and the angle of sprays were his main concerns. Most of the above mentioned literature deals with simulations in the RANS context. Within the LES formulation, work concerning two-phase flows has only recently gained greater interest and the amount of information available is much less extensive.

In a LES as well as in a RANS approach, the common way to describe a two-phase flow is by using Lagrangian frame of reference for droplet tracking. This approach, described in detail by Faeth (1987) has many advantages and some limitations. The advantages are: the ability to provide detailed information of fluid-gas interaction, relatively small diffusion error, ability to account for various droplet sizes. The latter is very important as droplet sizes influence the vapour rate, effectiveness of atomization and break up rate. All of those have an either direct or indirect effect on heat release and reaction rates, especially in lean combustion applications which are increasingly popular. That is why it is crucial to be able to model and account for droplet atomization and breakup in the simulations. The drawback of the Lagrangian approach is the computational efficiency when tracking a large number of droplets. For each droplet, a

set of conservation equations must be solved. This becomes computationally infeasible for very dense sprays with large amount of droplets. While not an issue with very dilute sprays (Faeth, 1987), in applications where spray is dense and effects of near nozzle droplet interactions important this poses a serious problem. In order to at least partially overcome this, a concept of computational parcel has been introduced. This is basically a sampling technique where instead of tracking an individual droplet, a large number of droplets form a parcel, which is then tracked by the code. All droplets within a single computational parcel have identical parameters (temperature, size, velocity etc.) This approach has been broadly used in spray simulations (Menon & Patel, 2006).

Although the "parcel" concept is not ideally suited for LES due to the averaging introduced into the liquid phase, it has nevertheless been used by researchers. The LES version of a well established KIVA3V code (Amsden, 1993) uses computational parcels to simulate dense sprays. A recent work by Salewski and Fuchs (2007) well highlights the issues associated with droplet modelling. Small distances between droplets, large values of Stokes number and higher then expected Weber numbers were observed even in the far field, where models should be able to predict accurately droplet behaviour. This essentially violates the model assumptions. Authors propose some remedies, but the work does highlight the complexity of two-phase modelling of not only dense sprays.

Computational efficiency aside, another drawback of using Lagrangian method for droplet tracking is the time step limitation for the liquid phase and its governing equation integration. In the end though, Lagrangian method now seems to be an industry-standard approach for two phase flow simulations and remainder of this brief review will be devoted to this method. It is however necessary to point out that Eulerian treatment of liquid phase is also possible. De

Villiers et al. (2004) presented an Eulerian liquid phase treatment by means of utilizing the volume of fluid modelling procedure. The Volume of Fluid approach was also utilized by the recent work of Befrui et al. (2008) who investigated a near field spray structure which as mentioned before is very important in Internal Combustion Engine applications. The spray was issued from an Outward Opening GDI Injector and the results were compared with experimental data. Detailed analysis of influence of coupling between liquid and gas phases in LES is described by Pannala (1999). The method used was the LEM method. Interesting comparison of Eulerian/Eulerian and Eulerian/Lagrangian approach for dealing with multiphase flows in LES is assessed by Riber et al. (2009).They used two versions of a numerical code: implicit incompressible and a more sophisticated explicit and compressible. The dispersion of the liquid phase was well predicted in both cases. The root-mean-square values however were in better agreement with experimental configuration in the Eulerian/Lagrangian formulation. Almeida and Jaberi (2008) also performed an LES of a dispersed particle-laden turbulent round jet using a new stochastic subgrid scale closure. The coupling between the particles and ambient medium was predicted correctly. In addition investigations concerning effects of particle size and mass were conducted.

In the Lagrangian formulation, the mathematical relations that govern droplet dynamics and coupling with the gas phase need to be given. The governing equations for droplet motion in LES are given below. The formulation follows that of Menon and Patel (2006), under the assumption that the Kolmogorov scale is of the same order or larger than the largest droplet in the spray field. For such a situation, the interaction between gas and liquid phases is dominated by laminar fluid dynamics. The equations then read

$$\frac{dx_{i,d}}{dt} = u_{i,d} \tag{2.24}$$

$$\frac{dm_d}{dt} = -\dot{m}_d \tag{2.25}$$

$$\frac{du_{i,d}}{dt} = \frac{3}{16} \frac{C_D \mu \operatorname{Re}_d}{\rho_d r_d^{\,2}} \left(u_i - u_{i,d} \right) \tag{2.26}$$

$$m_d C_L \frac{dT_d}{dt} = h_d \pi d_d^{\,2} \left(\tilde{T} - T_d \right) - \dot{m}_d L_v \tag{2.27}$$

In these equations, subscript d denotes a droplet related quantity, while d_d is the droplet diameter, h_d is the heat transfer coefficient calculated by the formula proposed by Faeth and Lazar (1971), L_v is the latent heat of vaporization usually given by the correlation of Miller and Bellan (1999), and m_d is a mass of particle given by $m_d = (4/3)\pi r_d^3 \rho_d$.

The influence of the particles on the gas phase flow is reflected in the spray source terms, such as the F_i^s and ρ_m^s appearing in the momentum equation (2.17) and species conservation equation (2.19) for the gas phase respectively. It can be clearly seen that the coupling between phases is of two way nature. The droplets are influenced by the resolved scale velocity and temperature. The resolved flow in turn receives contributions from evaporated liquid as well as drag of the droplets (momentum change). The procedure for the computation of the liquid-gas phase exchange terms in equations is described in detail in (Menon & Patel, 2006). Here only brief outline is presented. The four coupling terms are calculated as follows

$$
\begin{pmatrix} \dot{\rho}_s \\ \dot{F}_i^{\,s} \\ \dot{Q}^s \\ \dot{\rho}_m^s \end{pmatrix} = - \begin{pmatrix} \dfrac{dm_d}{dt} \\[2mm] \dfrac{dm_d u_i}{dt} \\[2mm] \dfrac{dm_d e_d}{dt} \\[2mm] \dfrac{dm_d Y_m}{dt} \end{pmatrix} = - \begin{pmatrix} \rho_d \dfrac{dV_d}{dt} + V_d \dfrac{d\rho_d}{dt} \\[2mm] m_d \dfrac{du_{i,d}}{dt} + u_{i,d} \dfrac{dm_d}{dt} \\[2mm] m_d \dfrac{de_d}{dt} + e_d \dfrac{dm_d}{dt} \\[2mm] m_d \dfrac{dY_{n,d}}{dt} + Y_{m,d} \dfrac{dm_d}{dt} \end{pmatrix} \tag{2.28}
$$

In Equation (2.28), e_d is the total energy of fuel droplet and V_d is the volume of the droplet. The volume-averaged source terms for all of the droplet group trajectories that cross a computational cell are computed by summing the contribution from every droplet group for n number of droplets as follows

$$
\begin{pmatrix} \tilde{\rho}_S \\ \tilde{F}_S^i \\ \tilde{Q}^S \\ \tilde{S}_{s,k} \end{pmatrix} = - \begin{pmatrix} \sum_n \dfrac{dm_d}{dt} \\ \sum_n \dfrac{dm_d u_i}{dt} \\ \sum_n \dfrac{dm_d e_d}{dt} \\ \sum \dfrac{dm_d Y_m}{dt} \end{pmatrix}
\tag{2.29}
$$

The state-of-the-art droplet modelling in LES should account for subgrid turbulent motion and its effect on turbulence. In Menon and Patel (2006), the stochastic dispersion of droplets caused by turbulent motion is incorporated by representing the gas-phase velocity at particle location as

$$
u_i = \tilde{u}_i + X \sqrt{2k^{SGS}/3}
\tag{2.30}
$$

In Equation (2.30), X is a randomly generated number sampled from a uniform distribution with zero mean. The fluctuating subgrid part of the velocity can be also modelled using different expressions and stochastic methods (Vinkovic et al., 2006).

In both LES and RANS of spray flows, droplet breakup modelling has to be introduced. Although many models have been used in the past like the TAB model (O'Rourke & Amsden, 1987) or the "wave" model (Reitz, 1987) with success in RANS simulations, LES has introduced more challenges into the droplet breakup modelling with which existing models are not always able to cope. There is still a lack of well-established liquid breakup models that

are highly suitable for LES. There have been some recent attempts in the field, for instance, the model of Gorokhovski (2001) that is able to account for highly varying droplet breakup sizes. This model was coupled with LES of an atomizing spray flow (Apte, 2003), where the results included a broad spectrum of droplet diameters. They also developed an algorithm for simultaneous treatment of computational parcels and individual droplets in the flow which is very beneficial for unsteady, highly turbulent LES. A complex review of multiphase modelling was performed by van Wachem and Almstedt (2003), which can give further insight into this complex problem.

2.3   Numerical simulations of spray combustion

An extension of LES to reacting flows has gained much interest in the last decade. The modelling of the additional terms arising from the production and destruction of chemical species are challenging even for a traditional RANS approach. LES adds to the complexity because of the presence of subgrid quantities and unsteadiness. Since combustion occurs at the molecular scales, only the finest scales of turbulence have direct influence on the reaction rate. This implies that the interaction of molecular diffusion, reaction rate and turbulent stirring occurs somewhere in the inertial range of turbulent flow and even in the viscosity influenced dissipative range. For automotive engines, those scales can be as small as 10^{-3} mm (Lumley, 1999). Those interactions are highly non-linear and development of reliable models is a difficult task.

Phenomena like flame-generated turbulence, flame instability and counter-gradient diffusion should all be taken into consideration. As noted by Pope (2008), molecular and viscous dissipation ranges are not resolved by traditional LES, hence information about interaction of

turbulence and chemical rates is contained within the subgrid scales. Naturally, the energy containing eddies also influence the flame, especially in the premixed cases where quenching due to the excessive turbulence is possible. Turbulent structures are also often used to stabilize and anchor the flame in the burner. As a result, chemical and turbulent interactions are present throughout the turbulent spectrum (Bray, 1996). Many subgrid models for reacting LES have been developed over time with varying degree of success. In the following, a short summary of the approaches most commonly used in engineering applications is presented.

The main difficulties in modelling the reaction rate term is the highly non-linear character of the expression used to describe it. This is clear when we look at a simplest reaction where fuel and oxidizer create a product: $F + O \rightarrow P$. The production rate is specified by the following equation

$$\overline{\overline{\dot{\omega}}}_P = W_P k_R \rho^2 Y_F Y_O \tag{2.31}$$

where W_P is the molecular weight of the product and the reaction rate is given as

$$k_r = A_R T^{b_R} \exp\left(\frac{-T_A}{T}\right) \tag{2.32}$$

This is an Arrhenius type dependence which is a simple description of the finite-rate chemical kinetics, where A_R and b_R are constants and T_A is the activation temperature of the specific reaction. The $\overline{\overline{\dot{\omega}}}_P$ term in Equation (2.31) is closely related to heat release source term $\overline{\dot{Q}^c}$ in Equation (2.18).

Expanding this expression into a Taylor power series shows that the reaction rate $\overline{\overline{\dot{\omega}}}_P$ is dependent not only on resolved variables like density, concentration of fuel and oxidizer but also on higher order fluctuations. It has been proved that those higher order correlations cannot be neglected. On the other hand, direct modelling would be extremely complex and

41

computationally not feasible. Therefore the most accurate approximation of this term is a fundamental trait of a quality model. The basic approach for dealing with the filtered reaction term is its estimation on the basis of the resolved quantities only. Subgrid contribution is neglected and the higher order correlation terms are not accounted for. In this assumption, lack of information from the subgrid scales leads to an assumption of perfect subgrid mixing. When a mesh is sufficiently fine this is to some extent justifiable. Unfortunately a sufficiently fine mesh is rarely possible in flows of engineering interest. Overall, while the model can serve to provide mean statistics under the above assumptions, most of them can often fail in most engineering applications. One point that has to be noted is that some researchers argue that neglecting subgrid contributions can be compensated by the dissipative nature of numerical procedure. This may be reasonable for low order numerical schemes, but for the state-of-the-art high order schemes the justification does not seem to hold well.

Further up the hierarchy of LES combustion models is an eddy-dissipation based approach. A fundament condition that needs to be fulfilled is that the combustion process is either kinetic controlled or turbulent mixing controlled. The basis of this model was presented by Magnussen and Hjertager (1976). The feasibility of the approach is justified by the fact that the fluctuations of the reactants are related to the mean values and therefore the mixing controlled rate can be expressed by the mean reactant species. Fureby (1996) then extended their model for LES framework by modifying the expression for reaction rate. This was expressed as

$$\bar{\dot{\omega}}_P = W_P \min\left(\bar{\dot{\omega}}_{KIN}, \bar{\dot{\omega}}_{MIX}\right) \tag{2.33}$$

The reaction rate depends on kinetically controlled and mixing controlled parts which are specified as follows

$$\bar{\dot{\omega}}_{KIN} = k_R \bar{p}^2 \bar{Y}_F \bar{Y}_O \tag{2.34}$$

$$\overline{\dot{\omega}}_{MIX} = \frac{\overline{\rho}}{\tau_{MIX}} \min\left(\frac{\overline{Y}_F}{W_F}, \frac{\overline{Y}_O}{W_O}\right) \qquad (2.35)$$

The mixing timescale τ_{mix} is equal to

$$\tau_{MIX} = \frac{C_{MIX}\Delta}{\sqrt{k_{SGS}}} \qquad (2.36)$$

where C_{mix} is a constant.

The presence of subgrid kinetic energy in the formula makes the model particularly suitable in simulations where the k-equation model (Menon et al., 1996) is used for subgrid stress tensor closure. Inability to predict slow chemistry effects aside, the biggest drawback of eddy-dissipation based models is the presence of constants which in theory require fine tuning for specific cases. In practice experimental data is usually unavailable and therefore *a priori* analysis is impossible. There are other modelling approaches, like the well established PDF methods or Conditional Moment Closure (CMC) formulations, but it is beyond the scope of this Thesis to present a complex review. Detailed coverage of the topic can be found in work of Pitsch (2006) and Bray (1996).

3   LES of an Annular Jet in a Diesel Engine Environment

3.1   Introduction

Jets in a swirling environment are important subjects encountered in many engineering and industrial applications including gas turbine combustors and combustion engines. Swirling flows are often used in gas turbine burners to stabilize the flame. In combustion engines, swirling can enhance the air-fuel mixing. Most HSDI engines these days rely on swirl to augment the droplet breakup and dispersion that aids mixing and improves quality of the subsequent combustion process.

In addition to swirling, nozzle configuration can also directly influence the mixing process. Round nozzles are commonly used and significant amount of work has been devoted to the simulations of round jets. However, work concerning the behaviour of an annular jet is very limited.   Annular jets have unique fluid dynamic characteristics which could influence significantly the mixing of the fuel. The main feature is the existence of both the inner and outer shear layers which interact differently with the ambient medium compared to a round jet. The existence of two adjacent shear layers leads to the formation of the recirculation zone and stagnation point inside the jet (Chan & Ko, 1979). This causes the flow in the inner region to travel upstream, causing additional disturbances to the inner shear layer. On the outer side of the jet vortex roll up and breakdown take place. Those effects when combined with a swirling ambient medium create a very complex two-phase flow which is highly unsteady and difficult to investigate using traditional CFD.

Predictions of an annular-jet induced flow field carried out numerically using traditional time averaged techniques inherently cause serious problems. As just mentioned, the unique features are all highly unsteady and applying time averaging leads to the disappearance of those structures. Because of this, a RANS simulation of an annular liquid jet is expected to give poor results, similar to those of a classic round jet, with the unique flow features missing from the representation. Even when investigating the time averaged flow, there are still limitations when using RANS. The industry standard $k - \varepsilon$ model has difficulties when predicting flows with high levels of vorticity. Since in this study the influence of the swirl is investigated, the unsuitability of $k - \varepsilon$ mode in that regard effectively rules out RANS based tools. While DNS simulations of an annular liquid jet have been performed recently and the results obtained were encouraging (Siamas et al., 2009), the cost of running a simulation on 512 node cluster is usually very limiting due to the excessive cost. LES is a viable alternative for capturing instantaneous flow physics and computational cost is substantially smaller, making it viable both in research and industrial applications. LES is adopted in this study, which aims at providing an insight into the fluid dynamic behaviour of an annular fuel jet and especially the effects of the initial ambient swirl on the flow field.

There is only a limited amount of research carried out on annular jets. Patte-Rouland et al. (2001) performed particle image velocimetry measurements of the velocity field which had been analyzed using proper orthogonal decomposition. They identified the presence of a recirculation zone in the flow field. The presence of the vortical structures localized on the external mixing layer was also identified. Garcia-Villalba et al. (2006) presented comprehensive results of LES of turbulent unconfined annular swirling jet. They mentioned the existence of stagnation points due to the two distinct phenomena: presence of the inner and outer shear layers and the instability of the spiralling motion in the swirling flow. Del

Taglia et al. (2004) investigated the behaviour of an annular air jet with a large blockage ratio and found that the flow inside the recirculation zone is asymmetric. This was also observed by Pinho and Whitelaw (1991). Del Taglia (2004), Chen et al. (2003) investigated the instabilities in the developing annular jet. Del Taglia observed interesting regions of asymmetry within the recirculation zone in the inner region of the jet. The agreement with experimental data was quite poor. According to Authors, this was due to the asymmetries in the experimental jet exit velocities. However, these existing studies mainly concentrated on single-phase non-reacting annular jets. Two-phase flow is much more difficult to study, both in terms of methodology and resources (computational cost).

The main reason behind this work is to confirm the existence of typical, annular jet specific turbulent structures using a LES version of the KIVA code. This would serve as a validation of the LES scheme employed, as well as provide additional insight into the complex physics of liquid annular jets in a high pressure swirling environment that would resemble HSDI engine conditions.

3.2   Flow configuration and initial conditions

3.2.1   Mesh resolution for LES

Computations on different grid resolutions were performed to establish a stage where a balance was reached between direct resolution of the energy containing eddies and computational time. It must be noted, that unlike RANS, Large eddy simulation does not reach a stage where the results become mesh independent. The division of the flow into the resolved and unresolved parts leads to a situation where theoretically a very dense LES would

resolve all the flow structures and the contribution of subgrid energy would vanish at which point we would approach DNS accuracy. In practice, such a situation is not desirable as subgrid models are usually designed for operation in a certain regime and their behaviour in the region where $\Delta \cong 0$ can be either unpredictable or not optimal, to say the least. Interesting analysis of this issue with the popular Smagorinsky model was conducted by Pope (2008). His findings show that in the extreme departures from the optimal range, the constant in the model does need adjustment in order to compensate for the different turbulent regime. The Smagorinsky model was designed to work most effectively and reliably within the inertial range of the turbulent spectrum.

Pope (2008) showed that for a very small filter width:

$$\frac{\Delta}{\eta} << 1 \tag{3.1}$$

The C_s constant needs to be lowered to about 0.13 in order to correctly estimate the mean rate of energy transfer to the residual scales. C_s is a constant in the Smagorinsky formula for the eddy viscosity, $\nu_t = (C_S \Delta)^2 \overline{S}_{ij}$ and in general should be proportional to the filter width.

On the other end of the spectrum, we may deal with situation where the filter width is comparable in size to the integral scale of the turbulence. When the ratio:

$$\frac{\Delta}{L} \cong \infty \tag{3.2}$$

The filtered velocity $\overline{U(x,t)}$ tends to the mean velocity $\langle U(x,t) \rangle$ and consequently the residual stress from the model approaches the Reynolds Stress tensor. The eddy viscosity approaches the turbulent viscosity of the fluid. With regard to the C_s, its value tends to zero since:

$$C_s = \frac{l_m}{\Delta}$$

(3.3)

In reality however, we do not used either very coarse or very dense meshing because of the following reasons:

- Coarse mesh is unable to capture important turbulent structures and causes the subgrid model to account for too high a percentage of the turbulent kinetic energy of the flow.

- Very dense mesh is reserved for DNS simulations and in this region benefits of LES clearly vanish.

Ideally, the mesh resolution would allow resolving all eddies from the energy containing range, leaving the rest of the turbulence to be modelled by the subgrid model or numerical dissipation of the algorithm. This state can be reached by careful analysis of the results in terms of the presence of turbulent eddies and foremost by the ratio of resolved to modelled turbulent kinetic energy. As an example, Figure 3.1 shows the amount of modelled kinetic energy present in the flow for two LES using different mesh and a reference RANS simulation, where all of the energy is being modelled. The results are from a simulation from a motored engine going through a full cycle with piston starting near BDC (Bottom Dead Centre). The computational case is outlined in Chapter 4. The LES coarse case stands for coarse mesh and LES fine for the fine one. RANS formulation uses the same grid as the coarse LES. This study shows that performing even the so called coarse LES by using a RANS specific mesh can potentially yield much benefit in terms of the amount of modelled energy in the simulation.
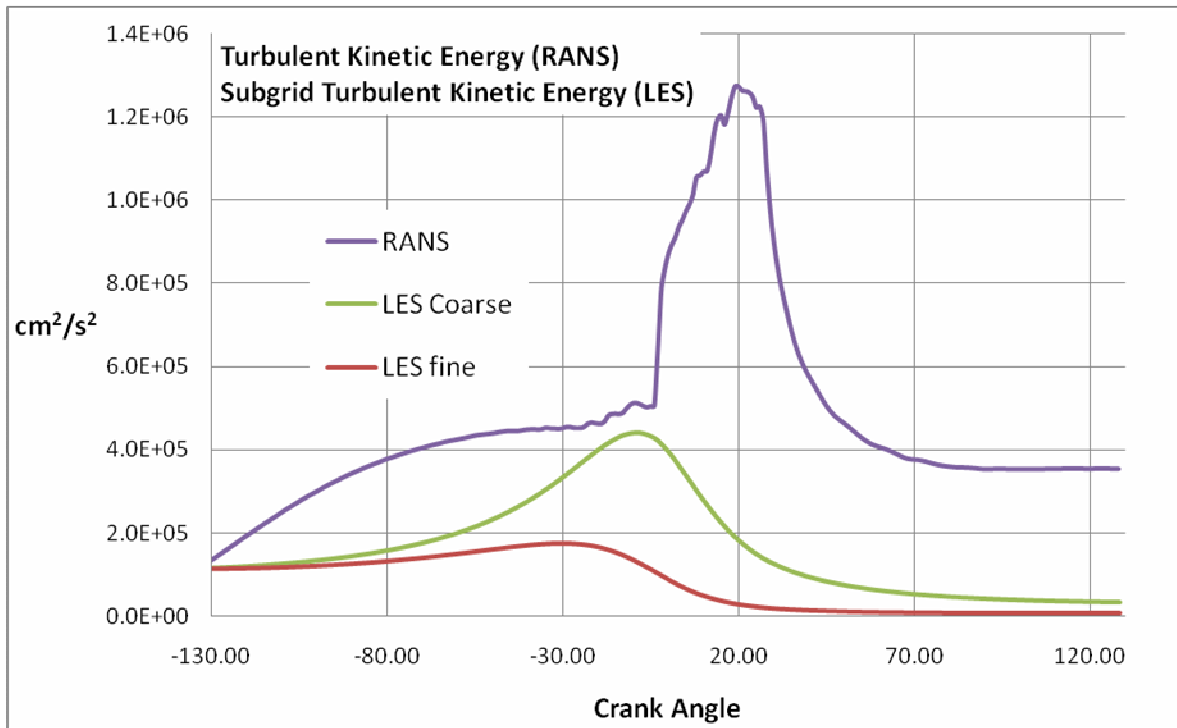
Figure 3-1. Levels of turbulent kinetic energy for LES and RANS.

In this work, the comparative study performed used $k - \varepsilon$ turbulence model in the RANS modelling approach and k –equation model in the SGS turbulence modelling in the LES, which share commonality in the formulation although they are fundamentally different. Both the $k - \varepsilon$ turbulence model and the k –equation SGS turbulence model rely on a kinetic energy term, albeit with the fact that RANS approach models the turbulent kinetic energy for the entire flow field while LES only models the subgrid turbulent energy. In principle, small scales below the grid size of a fine mesh are more uniform than the large ones, therefore modelling is less challenging and should be more accurate. Obviously subgrid turbulent kinetic energy is only a portion of contribution to the overall turbulence level in the simulated flow.

Figure 3.1 shows the differences between modelling of turbulent kinetic energy using RANS and LES formulations. In Figure 3.1, it can be observed that the levels of modelled kinetic energy in LES are not only lower by a few magnitudes but also the progress of the curve is smoother than the RANS. The RANS curve appears jagged and peaks about 20° CA later than LES with a strong jump at the Top Dead Centre (TDC). This can be explained as that the evaluated turbulent kinetic energy in RANS reflects the whole flow field, which changes significantly as the piston nears the TDC and then travels downwards. The flow field predicted in the RANS simulation is especially affected by the change in the tumbling motion in the chamber. The strong jump at 0° CA is probably due to the tumbling motion around the X axis which changes direction at this point. This, however, does not cause a serious problem in the LES where a sudden change is absent from the distribution of the subgrid turbulent kinetic energy because grid-resolved flow can reflect this.

The smooth distribution of subgrid turbulent kinetic energy is a confirmation of earlier statement about uniformity of small scales of the flow. For the LES with coarse mesh (LES_C) case there is only one slight jump present in the vicinity of the squish region, where the pressure is the highest, tumbling flow changes direction and the turbulence is generally intense. This increase may signify a need for a slightly better mesh resolution to resolve more of the large scale flow structures and further reduce the contribution of modelled energy. Indeed, the LES_F (LES with fine mesh) case curve fully supports this explanation. The subgrid turbulent kinetic energy in LES_F simulation yields different values than LES_C. The levels are much lower, there is no peak and the magnitude decays after the TDC, reaching very low levels of subgrid turbulent kinetic energy. The comparison clearly indicates the modelling efficacy of LES. LES can significantly reduce the modelled or approximated amount of turbulence in the flow, thereby leading to much better numerical predictions.

Comparing the both LES cases, the benefits of using fine mesh in LES are highlighted, which is a natural consequence of the principles of SGS turbulence modelling. The finer the resolution, the more structures and flow characteristics can be captured by the grid and reproduced without modelling errors, while the contribution of modelled part is reduced and the accuracy of the numerical prediction of the flow fields is increased. Low levels of the subgrid energy in the case of the fine mesh also prove that there is no further need to refine the resolution, most, if not all of the large, energy containing eddies are being resolved.

The issues of mesh resolution are also quite apparent when simulating dense sprays. The Lagrangian particle tracking and the behaviour of the droplet is directly dependent on the nearest grid node. Increasing the distance between nodes can cause "jumps" and discontinuities in the particle motion. The evaporation rate might also be affected as the temperature gradients between neighbouring nodes will obviously be larger on a coarse mesh. On the other hand, most of the two-phase models have limitations imposed on the amount of liquid phase present within a given volume of the ambient medium. As we decrease the cell size, the volume becomes smaller, but the presence of the amount of liquid is not affected. What follows is the increased liquid mass fraction rate within a cell. This may lead to inaccurate predictions of the two-phase flows as the liquid load will be too much for the code to handle. The average distance between droplets will also be reduced when extremely fine mesh is used which causes strong interactions between droplets, like secondary breakup, coalescence and deferring from the round shape. Al those areas are where the modelling procedures are not sufficiently developed and the phenomena either very simplified or not accounted for at all. This problem does not appear very often, contrary to the issues associated with under-resolved mesh, it is however worth remembering that limitations exist on both ends of the mesh resolution spectrum.

3.2.2   Numerical method

In accordance with KIVA scheme, a structured type of grid is used. The physical domain has a diameter of 80 [mm] and height of 100 [mm]. Full 360 degree section is simulated in order to capture any possible influence of the coexisting vortical structures as well as investigate asymmetry of the developing jet. The mesh used in the computations of an annular jet consists of 760000 structured elements. This gives a typical cell size in the Z direction of around 0.5 mm which is enough to capture the bulk of the energy containing eddies. The Z direction is considered crucial in computations because it is the downstream direction of the issuing jet. The overview of the mesh is presented in Figure 3.2. It was found that this mesh size was the best compromise between calculation time and accuracy. Further refinement lead to increased computational times with negligible benefit regarding the ability to capture additional turbulent structures.

The methodology of simulating the liquid annular jet is not straightforward. In order to capture the interactions of two shear layers (inner and outer region) the liquid film must have a certain thickness. Otherwise we would deal with a round jet with a negligible thickness. This is accomplished by specifying 18 single nozzles placed circumferentially in the middle of the domain with the radius of 5 [mm]. Each single nozzle then has an initial spread of the issuing liquid equal to the angle of 15 degrees. The spray cone of each of the nozzles is not hollow to better reproduce the effect of the liquid film. This procedure allows for successful simulations of the liquid jet influenced flow field in the ambient domain that is fundamentally different from a gas jet.

The summary of conditions used for the simulations are presented in the Table 3.1, along with positioning of the injection points. Figure 3.2 also shows the location of the circle on which 18 nozzles are placed.
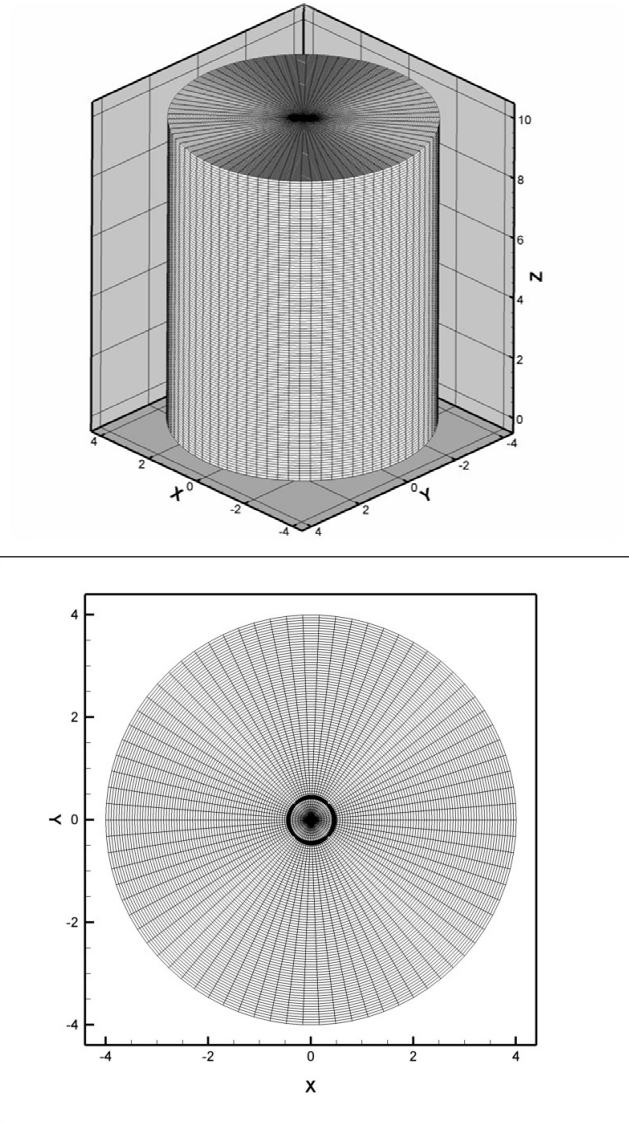
Figure 3-2. Overview of the annular jet mesh and the location of injectors.

The composition of the gas phase is that of a standard air with 73% of N_2 and 27% of O_2. The liquid injected is a diesel fuel Cummins model. The boundary conditions that are of a serious concern in LES are dealt here with by using a closed domain. Initially the gas phase is stationary with a low, residual level of turbulence. The turbulence generation throughout the simulation can then be attributed exclusively to the injection of the liquid and subsequent two-phase interactions.

The boundary condition at the solid walls is currently set to the no-slip condition which is believed to be a most appropriate one given the questionable usability of RANS-specific law of the wall functions present in the original version of the KIVA. There is also a free-slip condition available but in the light of internal combustion engine application with a swirl this was deemed unrealistic because no decay of turbulence at the walls would be observed. Although the pressure in the domain is very high to reflect the conditions encountered in the diesel engine, the combustion has been suppressed in all three cases. Non-reacting case allows a better understanding of elementary jet behaviour. Combustion with its heat release rates, rapid density gradients and fluctuating pressure would be likely to significantly influence the results.

Table 3.1. Annular jet computational cases

|	Case A_1	Case A_2	Case A_3
Mesh resolution	760000	76000	760000
Ambient pressure	8 MPa	8 MPa	8 MPa
Swirl Number	0.0	0.5	1.2
Initial Temperature [K]	298.0	298.0	298.0
LES filter width [mm]	0.60	0.60	0.60
Injection Velocity [m/s]	300	300	300
Number of injected particles	4.0e+04	4.0e+04	4.0e+04
Total mass of the injected liquid [g]	20	20	20
Initial radius of the droplet [mm]	0.107	0.107	0.107
Z location of the nozzles [cm]	10.0	10.0	10.0
Radius of the circumferential nozzle placement [cm]	0.5	0.5	0.5

3.3   LES results and discussions

Significant amount of instantaneous flow data have been obtained. The initial stage of the injection will be firstly examined, where unsteady turbulent structures are already visible and influence of the swirling ambient medium is present. Figure 3.3 shows the developing annular jet for three cases, at the time instance of 2.5e-03[s] after the start of injection. The cross-section is created on the middle YZ plane and only upper part of the domain is shown because jet at the initial stage does not penetrate far. The annular jet is characterized among many features by the so-called vortex roll-up at the tip. Time averaged methods have difficulty in capturing this, since the vortex is highly unsteady. Once a structure is generated at the face of the issuing jet, a roll-up then occurs along the outer boundary of the jet and to some extent in the inner region. Existence of inner and outer shear layers is a reason for different behaviour in those regions. The head vortex can be seen clearly in the Figures 3.3a and 3.3b. As the vortex rolls up along the shear layers, a new one is created at the head and the process is repeated. Generation of those structures is triggered by the large difference of velocity between the liquid phase and ambient medium which is stationary or has some initial level of swirl. Looking at the Figure 3.3, roll-up structures are captured in all three cases, although the high-swirling case (Figure 3.3c) tends to dissipate them very quickly. The vortices travelling upstream in the vicinity of the outer shear layer are captured by the code especially well in the non and medium swirl cases. Case A3 does not appear to contain the roll-up vortex in the inner region. The outer vortex is positioned more sideways at about Y = 1.7[cm], where A1 and A2 detect its presence at approximately 1.5[cm]. This situation is most likely caused by the high deformation of the liquid film in the lower portions of the jet.
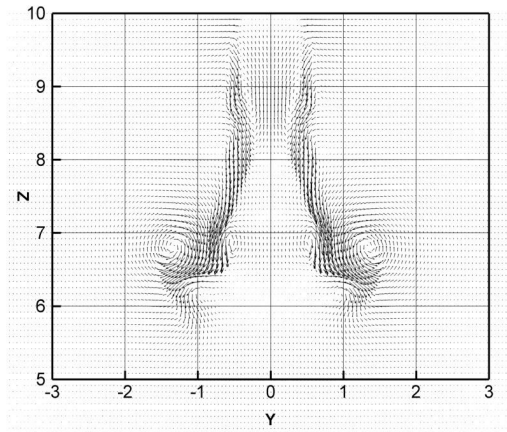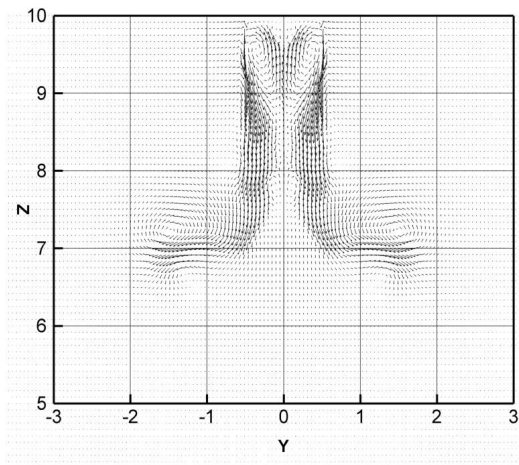
a)
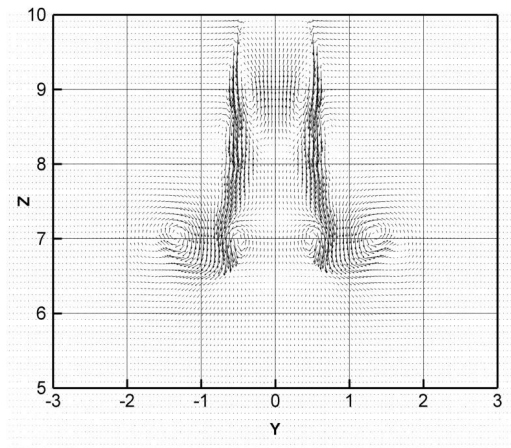
b)

c)

Figure 3-3. Velocity vectors at the initial injection stage (2.5e-03[s]): a) swirl number 0.0;

b) swirl number 0.5; c) swirl number 1.2.

Close-ups of the structures shown in Figure 3.3 are shown in Figure 3.4. The rotating ambient medium appears to increase the sideways diffusivity of the jet. Indeed, the spreading in the case A3 is more pronounced. This is followed by the subsequent reduced penetration, especially in comparison with the case A1. Very distinctive is the "flattening" of the A3 jet at its caused most likely by the high momentum exchange with the swirling gas phase. As a result the jet penetrates less, up to about Z=7. The A1 case has the jet penetrated up to Z=6 and the A2 case up to Z=7.5. In a domain that is 10[cm] high this is a very indicative difference.

With regard to the head vortices, it was previously noted that they are formed at the tip and then travel a certain distance upstream along inner and outer layers. This has been confirmed in all three instances. The distance they move upstream before being dissipated is governed a number of parameters. The value of swirl number seems to be playing the key role, as angular momentum can be dominant and dissipate the structures. The inner region of an annular jet contains specific turbulent structures of an elongated form that circulate in the upstream region. They coexist with the phenomena of a reversed, upstream flow. Although these vortices are most likely to exist near the nozzle, it has been observed that for longer injection times and consequently increased jet penetration, two sets of vortices can be present in between the inner shear layers in the upper and lower region. They cause the reversed flow, which in turn has influence on the travel of rotating vortex just described. Worth noting is the fact that roll-up vortices in case A1 and A2 are smaller than in A3 but have higher intensity, as confirmed by the investigation of vorticity levels.

Close-up of the structure in the inner region of the jet at the initial injection stage is presented in Figure 3.4, for the left-hand side. Arguably, this is where most differences can be observed.

The baseline case is the A1 case, where all the typical flow features should be observed. Cases with initial swirl will then showcase the influence of the swirl on those typical, annular jet specific features. The reversed flow is captured and visible on the close-up in Figure 3.4. It is formed near the nozzle due to the interactions between stationary gas and inner shear layer of the liquid film travelling at the high speed downstream. The flow is perfectly symmetrical at this stage and elongated vortices are visible. They are responsible for the upwash. Existence of those has also been confirmed by Garcia-Villalba et al. (2006). Their form, which is significantly different from that of a typical round vortex emerges from gradual and relatively undisturbed shearing process at the outer edge. The perturbations of the liquid film in the non-swirling environment are relatively small at the early injection stage which also influences the downstream penetration, highest in the A1 case.

Another flow feature, exclusive to the structure of an annular jet is the presence of the stagnation point. This is the point when the flow is being reversed and in the A1 it is located at approximately Z=8. Downstream of that location the flow activity is limited, the velocity gradients are much lower. That may be a consequence of the jet spreading and gradual air entrainment as well as gradually decreasing liquid phase momentum. Overall, the flow in the core is very symmetrical (please note, that this is an early injection stage) with two elongated vortices dominating the turbulent behaviour in the upstream region.

Introduction of the ambient swirl has a pronounced effect on the field. First of all, the elongated vortices have a different length to width ratio which is lower. They penetrate further into the core, at the expense of absolute length. For the A2 case, the vortex is about 10 mm long, comparing to 13mm for A1. The difference is even more pronounced when referring to the high case swirl. Over there, the vortices are shifted upwards and are created almost at the

tip of the injection nozzle. They are wider and interact with each other at the axis forming a very strong flow moving upwards. Their length is about 5 mm, so roughly half the size of previous cases. The stagnation point is less pronounced and shifted upstream as well. The broad, low velocity region downstream of the stagnation point in the A1 is gone and the inner region is much narrower, reduced by two high velocity streams parallel to the inner shear layer. In fact, A3 appears to have two stagnation points at Z=8.7 and Z=8 cm, although they are much more abrupt and the velocity changes are not as gradual as it is both in the case of A1 and A2. Looking again at the Figure 3.3, what is apparent is the absence of large liquid perturbation for the swirling cases. In the A1, at the location of Z=8.2 there is a large instability in the film that is reduced in the A2 and not present in A3. An obvious conclusion would be that the swirl does increase the stability of the liquid film, most likely due to the angular motion of the gas acting in a protective way and preventing the jet from earlier disintegration. This is in contrast to the swirl induced increased sideways penetration at more downstream locations. Possible explanation is the momentum of the liquid phase, high injection velocity. Strong flow downstream at the initial stage is shrouded by the swirling gas, and only after the initial entrainment does the swirl augment the penetration/breakup of the jet.

To sum up, the first stage of the injection already contains some typical flow features that had been confirmed to exist in experimental data (Patte-Rouland et al., 2001). Swirling flows had been shown to differ meaningfully with strong differences especially in the inner region and the values of jet penetration. In order to further assess the characteristics, data set from the later time after injection needs to be analyzed. A time of 4.5e-03 [s] was chosen as an intermediate step between the initial and final stages.
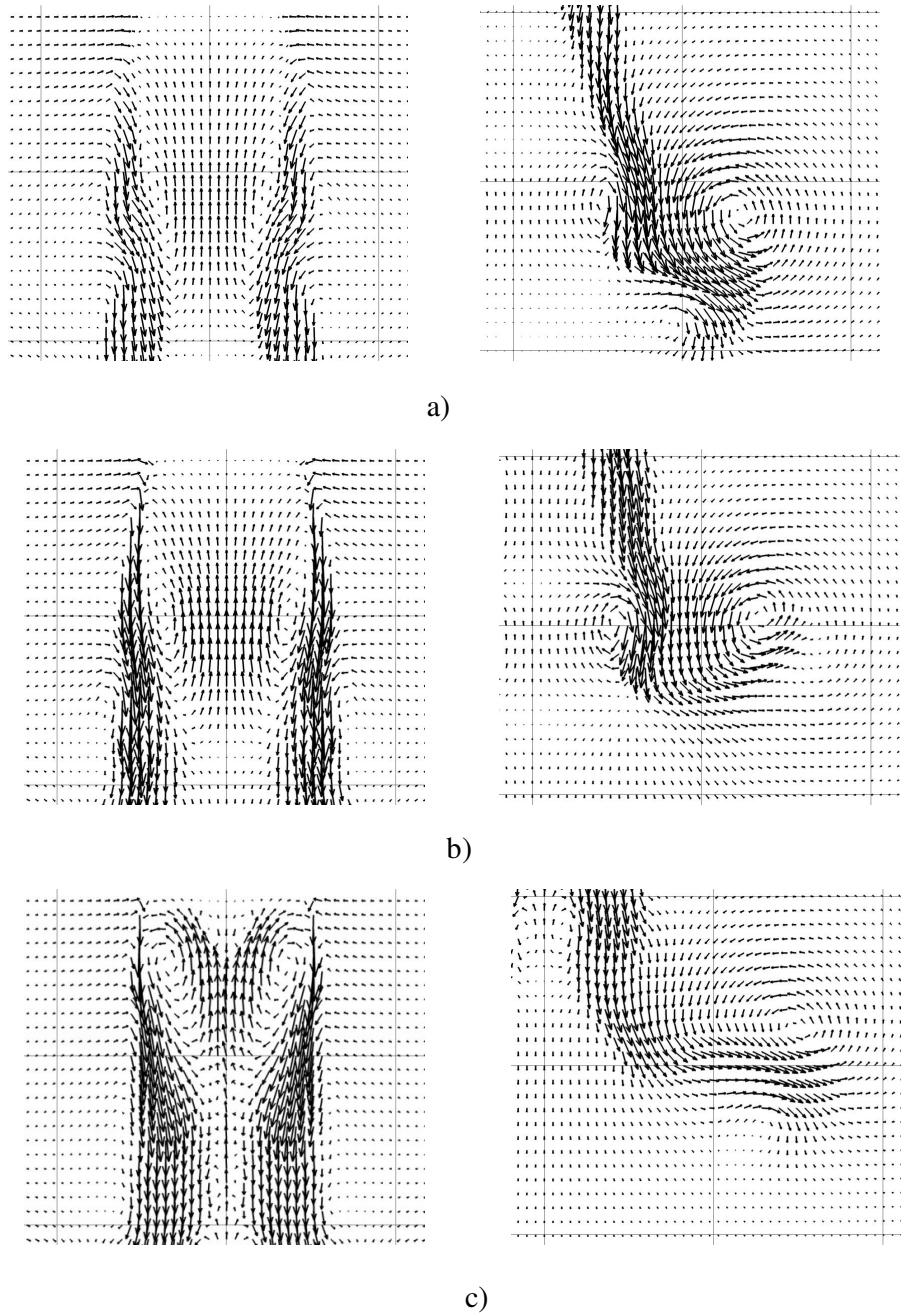
Figure 3-4. Close-up of the jet at 2.5e-03 [s], inner region (left) and vortex rollup (right): a) swirl number 0.0; b) swirl number 0.5; c) swirl number 1.2.

Figure 3.5 shows the cross section of the developed jet for three cases. This time, whole domain boundaries are visible. The most important difference is of course farther penetration

of the jet which is increased by approximately 20 mm. This is equal for A1 and A2 with slightly reduced value for A3. The sideways spreading of the jet has similar discrepancies. In the cases A1 and A2 the radial increase of the penetration is marginal, both at the tip and upstream. In the case of high-swirling flow, the radial penetration had not only failed to increase, it has been reduced at the tip. The wide "collar" visible in Figure 3.3 for the A3 case at Z=7 does not exist anymore and the jet is much more confined. It is likely that this "collar" structure was broken into smaller vortices that can be seen in Figure 3.5 both along the outer shear layer in the upstream locations at Z=7.9, 8.9, 6.5. Those vortices are also present further upstream in the jet core. This is the most striking difference when viewed alongside cases A1 and A2. Presence of small, rotating vortical structures within the jet is exclusive to the high swirling case. The possible reason for their existence is the complex interactions between the gas phase with a very high angular momentum and liquid carrying a high momentum downstream.

Three dimensional effects may be responsible for early breakup of the jet symmetry and disintegration of the liquid film. Regarding the penetration, it is clear, that in the A3 case it is severely limited. Again, highest penetrating case is the one with non-swirling ambient medium. With regard to the symmetry, cases A1 and A2 are much better then the high swirl number calculation. This can be seen in the Figure 3.5. The only deviation seems to be at the tip in the A1 case, but this can be attributed to the nature of viewing instantaneous results and symmetry can therefore be assumed to exist in the jets. There is also strong entrainment near the tip and that can cause additional instabilities and generation of random turbulence. Features like stagnation point and counter rotating vortices are well preserved.

One more interesting feature that is exclusive to the calculation with the medium swirl number is the presence of small vortices right near the injection points (Figure 3.5). They seem to break up the liquid layer that is uninterrupted in the remaining simulations. The vortices are symmetrical and increase the entrainment of the ambient air right at the nozzle. In other cases we are not likely to observe any entrainment at such a vicinity of the nozzle. There is also another area of increased ambient air transport to the inner region and that is located at Z=6.7 and visible in Figure 3.5.

The liquid layer is likely broken up in that region and an area of low flow velocity is created. It re-emerges at about Z=6 to again create a strong flow downstream. This longitudinal breakup of the jet is highest for the A2 case but similar, although much smaller area can be distinguished for the A1 case at about Z=8 where roll-up vortices exist at the area's external boundaries. Coexistence of those vortices in the stagnation region may affect the flow structure. The vortices can weaken the jet development in the streamwise direction as they roll up, which along with perturbations of the liquid may lead to early breakup of the jet column. The swirling effect seems to work in favour of the process, as can be seen in the cases A2 and A3 where the breakup region is significantly bigger.

Finally, analysis of the fully developed annular jet is provided. This corresponds to the time of 10.5e-03 [s] after the start of injection. Figure 3.6 presents the necessary details. Analyzing the penetration first, the highest one is for the A1 case, followed closely by the A2. High swirl number limits the penetration severely for the developed jet structure. In fact the baseline structure is not conserved as the violent breakup occurs as high downstream as Z = 7 cm, followed by creation of turbulent structures of varying size, some of them approaching the characteristic length which is taken to be diameter of the nozzle.
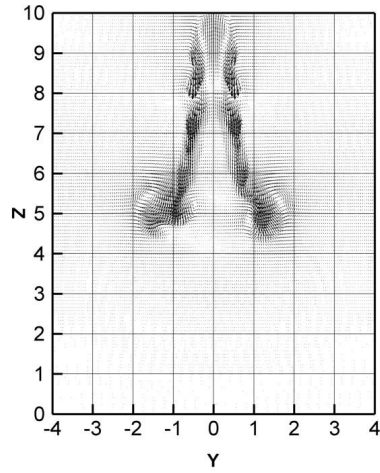
a)
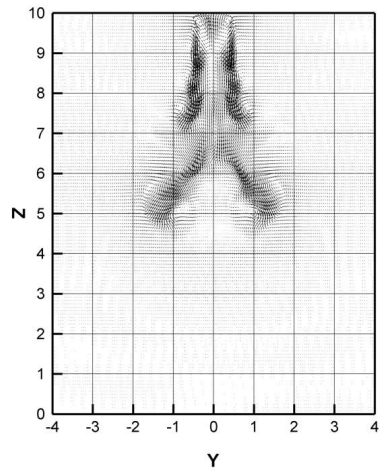
b)
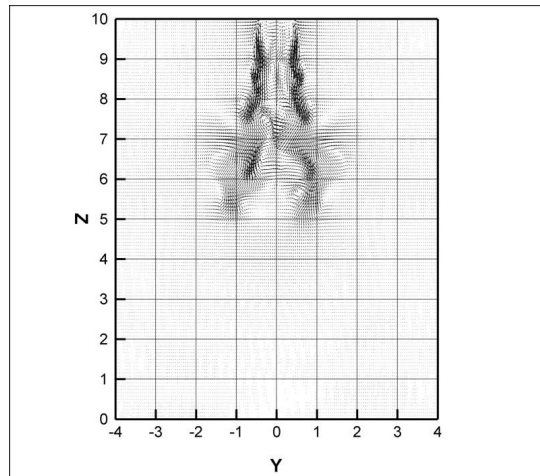
c)

Figure 3-5. Jet velocity fields at 4.5e-03 [s]: a) swirl number 0.0, b) swirl number 0.5, c)

swirl number 1.2.

Those structures spread sideways very quickly enhancing the mixing with ambient medium at the cost of longitudinal penetration of the jet. The lack of a typical jet structure below Z=6 is an indication that the swirl number equal to 1.2 is too high for this particular Reynolds number to aid the mixing process as far as whole domain is concerned (radial mixing in the upper parts is however improved). The best mixing is achieved using the moderate swirl number where compromise between radial and downstream penetration strikes the best balance. With regard to the structure of the jet, earlier statement concerning swirl affecting the inner region of the jet still stands. Comparison of snapshots of A1 and A2 in Figure 3.6 confirms that the flow field is less turbulent in that area than in the high swirl case. There are no random structures, the stagnation point is easy to locate and the flow is very symmetrical. Although up to about Z=7 the A2 case also displays symmetry, further downstream it is broken up and random fluctuations take over. Very interesting is the presence of large, elongated vortical structures that are separated from the main jet body visible in Figure 3.6b. They are about 10 mm in length and present at Z=4.5. They act as an important mixing aid and their existence is therefore beneficial. To certain extent, such structures can also be observed in the Figure 3.6a, although their location is further down the domain at about Z=2.5. The shape is different and they are not as well separated from the jet.

Figure 3.6 highlights important differences in the section between Z=8 and Z=9 which is basically at the top of the domain, near injection nozzles. All three cases present substantial differences. The lack of swirl in Figure 3.6a causes the flow field to be less turbulent, with small velocity gradients and characteristic flow upstream. The stagnation point is pronounced and velocity values in its vicinity are very low. The inner elongated vortices, visible at the Figure 3.3 are barely visible and most likely almost completely dissipated.
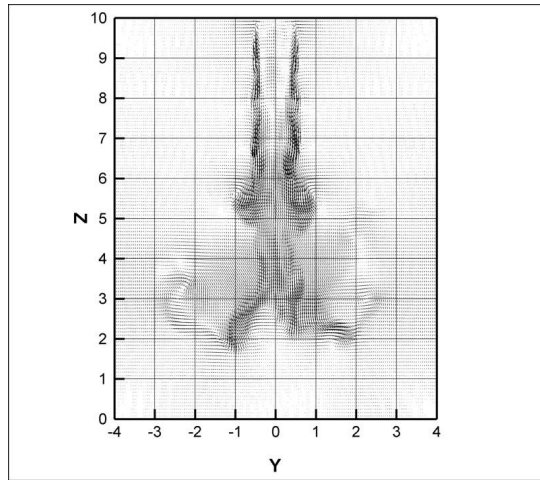
a)
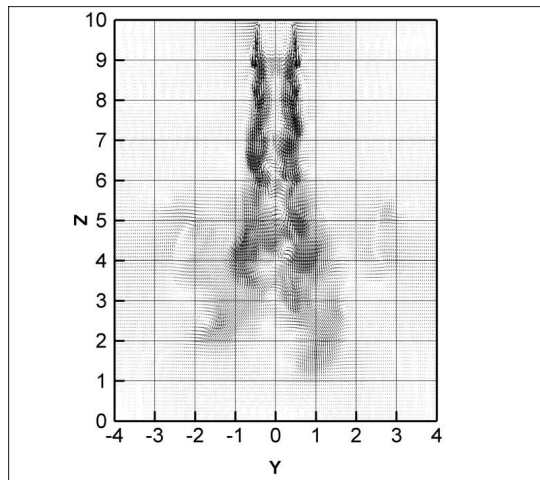
b)
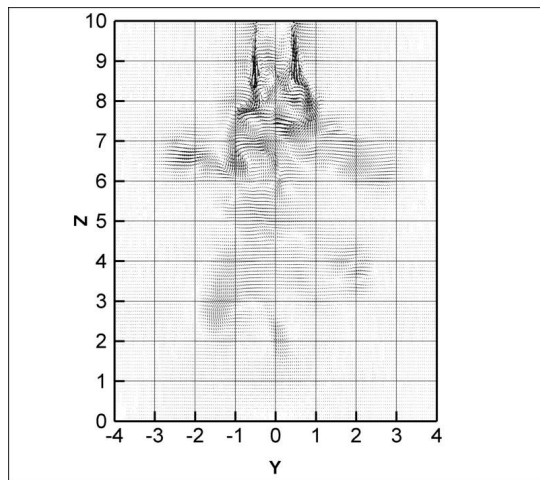
c)

Figure 3-6. Velocity fields of the developed annular jet (10.5e-03 [s]): a) swirl=0.0, b)

swirl=0.5, c) swirl=1.2.

Case A2 in Figure 3.6b displays much more turbulent state with higher velocity gradients. The stagnation point is shifted slightly downstream and the area where velocity gradients are small (case A1) has vanished. The body of the jet seems to be much thicker and more perturbed leading to more pronounced vortex generation at the outer shear layer. In the inside area below Z=7 some small, random vortices can be observed. Case A3 in Figure 3.6c structure is the one least resembling the typical annular jet. Swirl number of 1.2 is high enough to be able to break the structure completely. Some form of liquid sheet is only present up to Z=8.5, after which the pattern disappears and large vortices coexist along with smaller ones to create high amount of mixing but no jet structure. That is why at the high downstream locations the mixing actually suffers, even though the swirl is high. The inner region of A3 is very turbulent, again with large number of small scale vortices coexisting with each other. The elongated structures however and stagnation point cannot be distinguished anymore. Lower swirl is much more effective combining the features of an annular jet with enhanced vorticity levels comparing to the baseline A1 case.

Finally, some three-dimensional iso-surfaces of vorticity are presented in Figure 3.7. Vorticity gives a very good indication of turbulence levels. It is related to the amount of circulation within the flow. In physical terms it is defined as a local angular rate of rotation of a fluid. The other popular definition is that the vorticity is the curl of velocity

$$\vec{\zeta} = \vec{\nabla} \times \vec{u}$$
(3.4)

The three-dimensional snapshots shown in Figure 3.7 confirm the earlier discussion with regard to the penetration in the radial and vertical direction. The jet in the A3 case has more spreading and significantly limited downstream penetration. This is in contrast to the A1 case,

where the situation is reversed. In between sits the A2 case with slightly smaller length of the jet then in the A1 case but with more swirling effect in the upper regions.
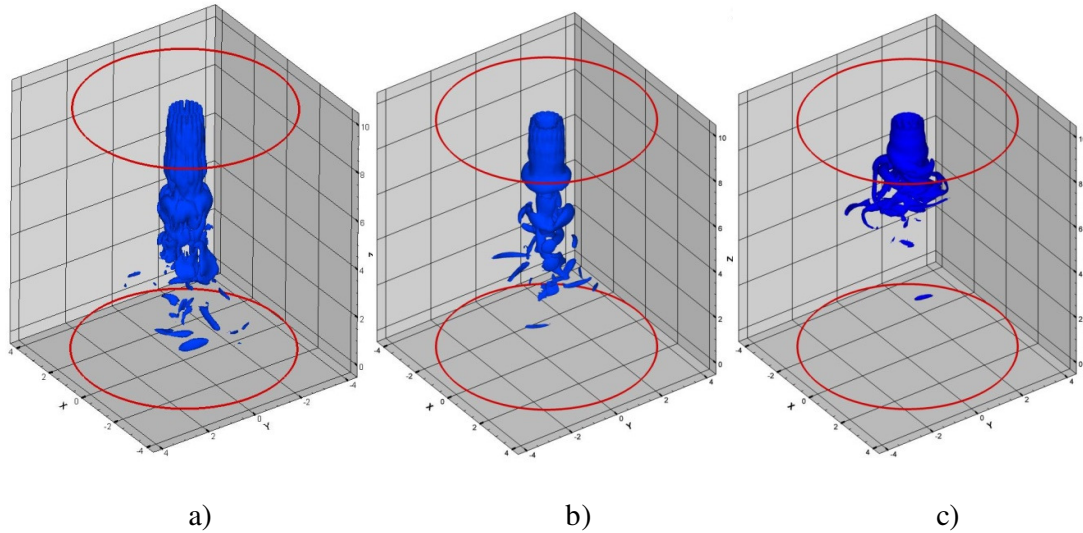
Figure 3-7. Instantaneous vorticity at 10.5e-3s after injection for different swirl numbers: a) swirl number 0.0, b) swirl number 0.5, c) swirl number 1.2.

3.4   Concluding remarks

Careful analysis of the structure of a liquid annular jet issuing into the ambient domain with varying degree of initial swirl by means of a LES version of the KIVA code allowed both useful insight into the behaviour of turbulent structures, as well as served as an assessment of the performance of the code. Roll up vortices at the tip of the jet, recirculation zone in the inner region of the jet are some among characteristic fluid phenomena encountered in an annular jet and confirmed both by experimental investigations and DNS simulations. LES version of the KIVA code used was able to capture those highly instantaneous formations

correctly. It was found out that the penetration of the jet varies greatly with changing swirl number of the ambient gas phase. The higher the swirl number, the smaller the downstream penetration of the jet, although radial penetration and mass entrainment are at the same time increased. Highest swirl number of 1.2 was found to break up the jet very early on, up to the point where typical features like symmetrical recirculation zone near the tip and stagnation point were no longer easily distinguished. In all three cases, turbulent structures that disintegrated from the main core and travelled into the domain were observed. The symmetry of the jet body was breaking up at various downstream penetrations, depending again on the swirl number. In general, the higher the swirl, the stronger the perturbations and what follows amplified breakup.

Overall, the LES code was able to reproduce the behaviour of an annular jet with its typical structures due to the coexistence of two shear layers. The sensitivity of the jet behaviour with regard to swirl number was found to be very high.

4 A Comparative LES/RANS Simulations of the Air/Fuel Mixing in an HSDI Diesel Engine

## 4.1 Introduction and liquid phase modelling

Chapter 3 described in detail the behaviour of an annular jet and abilities to capture some typical structures using LES modified version of the KIVA3V code (Valentino, 2006). This chapter will focus on HSDI engine related simulations, specifically assessment of the quality of fuel dispersion and mixing in a swirling environment. Comparison with RANS has been made to outline the differences between formulations and show the advantages of LES and typical drawbacks of Reynolds averaged methods. The lack of combustion does not eliminate the evaporation of liquid particles because the motion of the piston is accounted for and therefore compression stroke increases the temperature, significantly encouraging the evaporation process.

Predictions of dynamic vortical structures is an area where traditional $k-\varepsilon$ model often fails, whereas an advantage of LES is that it captures the unsteady vortical structures by avoiding the time or ensemble averaging. Rotational flow prediction by LES has been a subject of detailed analysis by Devesa et al. (2004) where high unsteadiness and multiple types of vortical structures were proved to exist. Their existence significantly enhances the fluid mixing. On the contrary, RANS does not capture unsteady vortical structures, but only large recirculation structures which are not time-dependent. This was noted by Jhavar & Rutland (2006), where LES of diesel engine fuel injection was investigated. The clear advantage of LES in predicting unsteady mixing was also recognised by Kimura et al. (2004). Their simulations of unsteady particle laden jet provided insight among other into turbulent

intensity dependence on the filter width. Another significant disadvantage of RANS approach using the standard $k-\varepsilon$ model is that the model is over-dissipative, therefore it may significantly under-predict the streamwise penetration of transient gas and spray jets while over-predicting the jet spreading at the same time (Valentino et al., 2007).

In the following, the fuel and particle dispersions obtained from the three simulations are discussed first, followed by the analysis of liquid jet penetration and particle breakup. In addition to the results from the HSDI Hydra engine, Section 4.3.3 describes results from another configuration along with comparison with optical images. The HSDI engine discussions are focused on the differences between the three cases with swirl. The expected outcome of the simulations is the much increased penetration of liquid (and subsequently vaporised fuel) into the domain predicted by the LES cases. What follows, reduced numerical dissipation of the LES formulation should limit the unphysical sideways spreading of the RANS predicted jets. The structure of the jet should also prove to be more influenced by the strong swirl action of the ambient gas. The swirl number of 2.05 is large enough to predominantly control the dispersion of the liquid particles and evaporated fuel. This would be expected to both influence the main core of the liquid jet and encourage droplet break up and dispersion throughout the domain, possibly separating liquid from the main jet and carrying packets of fuel into the combustion chamber. This phenomenon is crucial in terms of quality of combustion as the fuel should possibly be transported into more distant regions of the combustion chamber in order to ensure complete burning and low emissions. The aforementioned penetration of the liquid jet significantly influences the accumulated heat release in the engine, whose prediction was poor in the original version of the KIVA code (modifications that led to improvements in that area are presented in Chapter 5).

If analysis of droplet behaviour is to be carried out, models responsible for breakup used in the code must be presented. ERC version of the KIVA uses two well established models that are designed to cover two main regimes of liquid breakup. They are the Kelvin-Helmholtz (Reitz, 1987; Chigier & Reitz, 1996; Lin & Reitz, 1998) model and Rayleigh-Taylor model (Reitz & Diwakar, 1986; Su et al., 1996). The computational procedure follows the computational parcel concept described in Section 2.2 which has become industry standard for liquid injections from orifices, nozzles etc. The liquid phase is introduced into the chamber as blobs, i.e., big drops with a radius equal to the orifice size. In this way, the problem of the disintegration of the intact liquid core in the nozzle is bypassed.
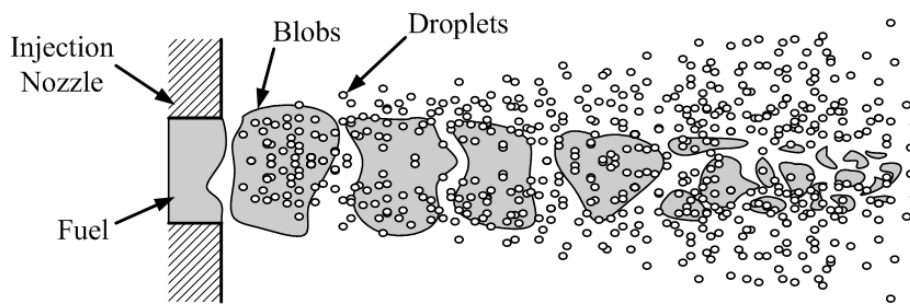
Figure 4-1. Concept of a numerical drop and its breakup.

The breakup of these blobs is thought to be due to the growth of Kelvin–Helmholtz (KH) instabilities, which occur when there is a shear motion of two fluids flowing alongside each other. The "wave" or KH breakup model has been combined with the so-called Rayleigh-Taylor (RT) breakup model based on the recognition of Rayleigh-Taylor instabilities that occur when a low density fluid is supporting a higher density fluid against a force, in order to estimate the disintegration of the blobs into secondary droplets. Close to the injector nozzle where the droplet velocities are high, the KH-breakup is usually the governing mechanism, whereas the RT-breakup becomes more dominant further downstream. The K-H model is based on the linear stability theory which was found to be well descriptive when it comes to

diesel spray atomization. One of the assumptions of the model is that the initial atomization of the injected liquid and subsequent breakup is indistinguishable in a dense spray. The model considers the instabilities which grow at the liquid gas interface. Their origin can be traced to a shear motion of two liquid films next to each other. The instability caused then leads to the dispersion equation that contains two main parameters in addition to liquid and gas phase properties. Those parameters are the growth rate (Ω) and wavelength (Λ):

$$\Omega = \frac{0.34 + 0.385We_g^{1.5}}{(1+Z)(1+1.4T^{0.6})} \left(\frac{\sigma}{\rho_l a_b^{\,3}} \right)^{0.5} \tag{4.1}$$

$$\Lambda = 9.02r \frac{(1+0.45Z^{0.5})(1+0.4T^{0.7})}{(1+0.865We_g^{1.67})^{0.6}} \tag{4.2}$$

Where We_g is the Weber number for the gas phase

$$We_g = \rho_g u^2 \frac{r}{\sigma} \tag{4.3}$$

Where $\square$ is the droplet radius and ρ_g density of gas phase. Z is the Ohnesorge number $Z = We_l^{0.5} / \mathrm{Re}_l$ with Reynolds number for the liquid equal to $\mathrm{Re}_l = \rho_l Ua / \mu_l$, We_l being the Weber number for the liquid phase and $Ta = ZWe_g^{0.5}$ is the Taylor parameter.

Those relations form a model that has been proved to be in good agreement with experimental results. Unfortunately, the wave analogy is best suited for low speed liquid jets. For diesel sprays that are both very dense and of very high velocity, some assumptions and physics may not be sufficient for accurate prediction. This is especially the case in more downstream locations, where we do not deal with large liquid ligaments, but with a large amount of very fine droplets. The presence of the R-T breakup model accounts for the breakup of fine droplets at more downstream locations.

The instabilities that the R-T model accounts for arise from existence of two fluids with different densities. The instabilities generally occur whenever lighter fluid is pushing the heavier fluid (in this case, ambient gas acting on diesel liquid droplets). Those instabilities result in perforation of the liquid film (Gelfand, 1996). In terms of acceleration of phases, the original underlying assumption is that the acceleration normal to the interface between phases may cause instabilities. Going back to diesel liquid and ambient gas, the interface between them would be stable if the acceleration were directed towards the liquid. The acceleration of the droplet can be calculated from the following formula (Patterson & Reitz, 1998)

$$a = \frac{3}{8} C_d \frac{\rho_g u_r^2}{\rho_l a} \tag{4.4}$$

With u_r being the relative velocity between the droplet and gas, C_d being the drag coefficient of the droplet. As in the previous model, wavelength and frequency has to be determined for fastest growing waves (Patterson & Reitz, 1998)

$$\Lambda = 2\pi \sqrt{\frac{3\sigma}{r\rho_l}} \tag{4.5}$$

$$\Omega = \sqrt{\frac{2a}{3} \left(\frac{a\rho_l}{3\sigma} \right)^{1/4}} \tag{4.6}$$

The breakup time is estimated by using dimensionless variable, formula which was given by Patterson and Reitz (1998)

$$T = \sqrt{\frac{4\sqrt{3}}{C_d} \frac{\rho_l}{\rho_g} \sqrt{\frac{8}{3C_d We_g}}} \tag{4.7}$$

The droplet would be then subject to breakup if following was true:

$$r > \Lambda \tag{4.8}$$

Equation (4.7) contains the value of droplet drag. Very often droplets are assumed to be spherical shape and therefore drag is calculated as for a sphere with an appropriate radius. In high velocity diesel sprays however, the deviation from the spherical shape can be significant and droplet can deform to form a disk rather than a sphere. This is accounted for in the code used. The droplet deviation from the spherical shape is calculated that influences the formula for droplet drag calculation (Reitz, 1999)

$$C_d = C_d \left(1.0 + 2.632 y_0\right) \qquad \text{(4.9)}$$

Where y_0 is the unit-less parameter of droplet deviation. Further details of the procedure are described in detail in (Liu et al., 1993). The inclusion of those three models completes the mathematical description of the breakup modelling procedure in the code.

4.2   Engine test conditions and numerical treatment

The engine for which experimental data were available and consequently simulations were performed is a four-valve HSDI diesel engine with common rail fuel delivery system. Important engine parameters are summarized in Table 4.1 with the injection parameters given. The fuel injected was a DF2 diesel fuel (Cummins model), and the injection duration was 30 crank angle degrees. The rail pressure was set to 1550 bars and the total mass of the injected fuel was equal to 0.03875 grams. The data was chosen to be in accordance with previous simulations conducted at Delphi Diesel Systems, with corresponding experimental results available. The exact injection process was governed by a special injection table which contains 120 values of injection velocity changing with respect to ignition stage. This was specified to exactly reproduce the real injection process, where the injected fuel velocity varies inevitably due to the design and operation of the injector and its needle.

In order to take advantage of as fine a mesh resolution as possible, the simulation involved a 60 degree sector representing one-sixth of the full 360 degree cylinder. This involved one nozzle spray hole placed in the middle of the sector. The sectional mesh is indicated in Figure 4.2. It has to be noted, that the code is capable of moving mesh treatment, which was utilized here and therefore actual mesh size changes during the cycle with the piston movement. The angle of the solid cone spray was set to 15 degree angle. This value was dictated by the measurements of the real nozzle. Some explanation is however in order as to the real importance and reasoning behind correct specification of this parameter. Since simulations of complete engine configuration, cylinder, moving piston etc inherently do not deal with in-nozzle turbulent effects; one can argue that the specified angle does not need to follow precisely real life measurements. If so, then the angle of the nozzle could be treated to some extent as a parameter by which penetration of the liquid fuel could be adjusted. To verify this theory, simulation has been performed with 5 degree nozzle angle. As expected, some differences in penetration were observed with smaller angle penetrating further into the domain. For the discussed results however, the original angle of 15° was used.

Three computational cases have been carefully investigated, with one of them being a baseline RANS simulation, in order to highlight the differences between the RANS and LES approaches. The other two cases are LES with significantly different grid resolutions. Changing the grid resolution should be followed by change in filter width and this was also accounted for. Key features of the computational cases are given in Table 4.2. For the case A shown in Table 4.2, the mesh size represents a typical RANS resolution. It was tested that further refining the mesh size did not lead to appreciable changes in the solution.

Table 4.1. Key Hydra engine parameters

Bore diameter	84.46 [mm]
Stroke	88.95 [mm]
Squish	0.8 [mm]
Displacement	500 [cc]
Compression ratio	18.4
Number if injectors	6
Nozzle hole diameter	0.145 [mm]
Spray cone angle	15 [deg]
Injector location in the Z dimension	10.501
Inclination of the injector in the XZ plane	72.5 deg
Distance of the injector from the mesh axis (protrusion)	0.1554 [cm]
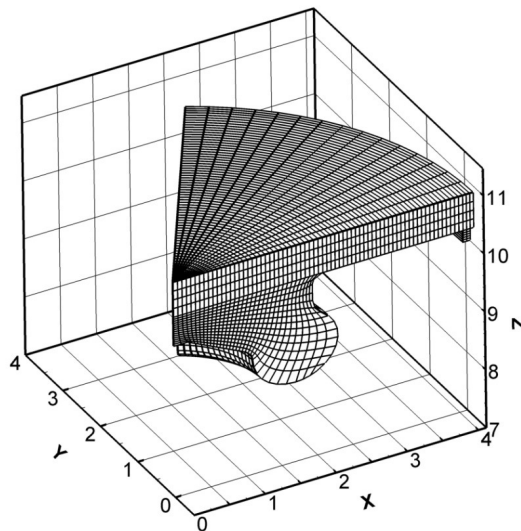
Figure 4-2. Computational mesh of the Hydra engine.

In order to compare the RANS and LES approaches, case B uses identical resolution as case A, representing a coarse mesh which is insufficient for a reliable LES. The aim of this was to establish, whether LES results could be trustworthy or accurate enough when performed on a RANS mesh. In addition, it was expected that major differences in spray penetration would emerge and those would be attributable to different numerical scheme used, taking the mesh sensitivity out of the equation. The constants used for breakup models had not been changed between three cases investigated. The grid resolution in case C, with grid points more than doubled in each direction in comparison to cases A and B, is considered to be fine enough for the LES test, since further refining the mesh size did not lead to significant changes in the solution. It needs to be pointed out that the simulations carried out are non-reacting (both ignition and combustion models are disabled). Reasoning behind this is twofold. First of all, some compatibility issues were present with the combustion model and LES which are addressed in Chapter 5 and second, switching off the reaction gives more detailed insight into the behaviour of both liquid and vaporised fuel jet. Although experimental data available are for combusting cases, liquid penetrations, distribution of the fuel mass fractions and in cylinder-pressures can still be used as a means of validation, provided data after ignition will be discarded and taken out of the equation.

A range of three-dimensional instantaneous flow fields have been obtained. Significant differences between cases A, B and C have emerged, which was expected, given the fundamentally different approaches between the RANS and LES formulations. For the LES, the filter width used in this study was the local grid size.

Table 4.2. Numerical cases for non-reacting spray investigation

	Case A (RANS)	Case B (LES_C)	Case C (LES_F)
Formulation	RANS	LES	LES
Mesh resolution	22000	22000	432300
LES Filter width	N/A	0.6 [mm]	0.1 [mm]
Turbulence model	$k-\varepsilon$	$k-$equation (subgrid)	$k-$equation (subgrid)
SOI	-3.5° CA	-3.5° CA	-3.5° CA
Injection duration	30° CA	30° CA	30° CA
Swirl ratio	2.05	2.05	2.05
Injected mass	0.038725 [g]	0.038725 [g]	0.038725 [g]

4.3   LES/RANS results and discussions

4.3.1   Liquid dispersion and vapour fuel phase distribution

This sub-section presents the distribution of both liquid and vapour phase of the fuel that is being injected into the cylinder. Since the initial conditions in the cylinder were set up to reproduce a significant amount of swirl, it is expected that this will profoundly affect the pattern of injected liquid phase as well as the subsequent vapour phase as the simulation advances in time. This was observed in the experimental tests and a CFD prediction should in theory be able to reproduce this effect. A high swirl number of 2.05 used in the simulation is consistent with the experimental condition, under which the turbulent flow and the dispersion

of the liquid particles and the distribution of the evaporated fuel are predominantly control by the swirl.

The spray motion is coupled with the gas phase velocity, which subsequently affects vapour distribution in the domain. Figure 4.3 presents the fuel distribution and 3D particle position with the piston position at 11° CA which is 14.5° CA after the start of the injection. By that time spray structure is developed already. The particles are coloured by their respective diameter, red end of the spectrum being the largest, blue the smallest. The scale at the bottom of the Figure 4.3 refers to the vapour mass fraction only. The exact distribution and spectrum of particle sizes will be analyzed later. When studying the Figures it is necessary to know that the fuel vapour mass fraction is presented on a two dimensional plane, inclined to follow the jet direction. Figure 4.4 shows the exact location of the post-processing plane used. The particles however, are shown in the entire 3D domain due to their dispersed nature.

All three cases show spray and vapour structure penetrating into the domain. The amount of penetration of liquid parcels is significantly different. LES cases penetrate much further into the domain, up to x=1.8, whereas RANS case reaches the value of x=1.2. In terms of detailed spray characteristics this is a critical difference. In-house experimental observation at Delphi showed a penetration of around x=1.9. In Figure 4.3, it is also evident that the primary liquid jet predicted by the RANS has larger spreading, while the ones predicted by the LES cases have less spreading. It is now established that the insufficient prediction of liquid penetration for the RANS case is a consequence of overly dissipative nature of the $k - \varepsilon$ turbulence model and cannot be avoided. This $k - \varepsilon$ trait is apparent when comparing the radial penetration of the fuel jet. RANS over-predicts the radial spreading of the jet core.
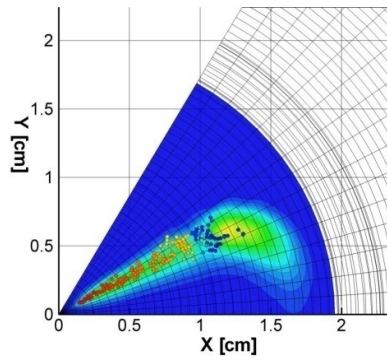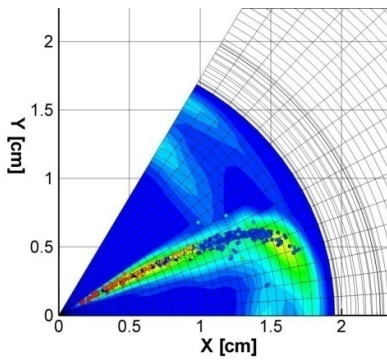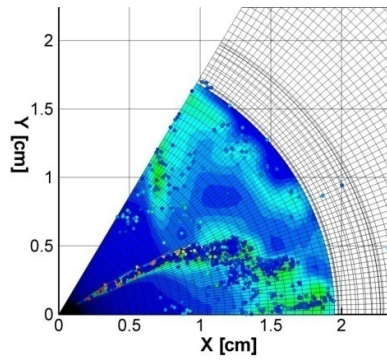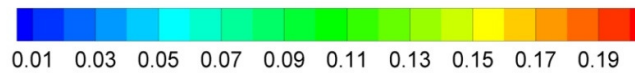
Figure 4-3. Two-dimensional contours of vapour mass fraction and 3D liquid droplet positions at 11°, particles coloured by their sizes, oversized for clarity: a) RANS , b) LES_C, c) LES_F.

Case A does not show any liquid particles outside the main liquid jet. Both LES cases (B and C), however, are able to predict presence of the dispersed fuel that is not part of the primary liquid jet core. For the LES with finer mesh, it is observed that smaller liquid droplets spread out together with more fuel vapour dispersed in the domain, which is believed to be a more realistic prediction considering the high-speed injection and strong swirling conditions in the engine. In terms of differences between the two LES cases, it is apparent that case C predicts fuel in the whole domain. The particles are spread throughout the cylinder, a situation that influences the vapour distribution.
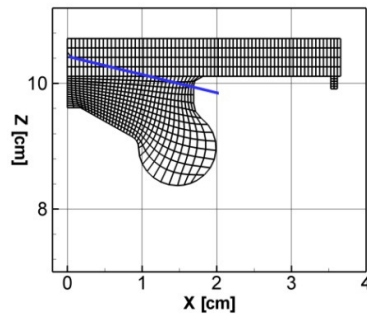
**Figure 4-4. Location of the contour plane for spray analysis, in line with the injector.**

The more uniform presence of the fuel does promote efficient burning which is desirable. In a vortical flow field predicted by LES, the location of particles and vapour is influenced by the vorticity captured by the fine mesh and the more realistic simulation of the swirling effect. Turbulent structures then carry packets of fuel disintegrated from the liquid core. This subsequently causes increased rate of fuel evaporation due to the smaller particle sizes. It is expected that this situation will have a significant impact on the rate of combustion and the amount of pollutants produced over an engine cycle. Especially soot formation could be affected. Fuel rich regions are more pronounced in RANS, where there is less penetration in the domain.

When examining Figure 4.3 one has to bear in mind that the results shown are of periodical nature. This is important especially in LES cases, where the fuel vapour is mostly influenced by the swirl and hence the presence of the fuel on the left side of the domain (this is a spray cloud from the main jet, transferred to the left by the periodic boundary condition). One therefore needs to look at the vapour distribution as a continuous cloud of vapour that is strongly inclined in the clockwise direction, following the direction of the swirl of ambient medium. As in experimental data, all three cases show that the vapour penetrates further into the domain than the liquid jet itself. Case A shows a very clear distinction between liquid and vapour penetration, although quantitatively, the prediction is poor. Significant difference between liquid and vapour penetration in case A is most likely a direct result of excessive dissipation and limited ability of the model to account for strong interaction between ambient swirl and liquid phase movement. LES cases show somewhat different behaviour, with the liquid vapour more closely following the main vapour jet. The clear distinction between regions of liquid and vaporised fuel is less distinct due to the higher influence of turbulence on the jet and the aforementioned increased breakup rates.

To gain more insight on the presence fuel in the cylinder, Figure 4.5 was plotted, which shows the instantaneous contours of vapour mass fraction and 3D liquid droplet positions in a vertical plane cutting through the middle of the 60 degree section grid. The droplet colouring and legend for vapour mass fraction along with three dimensional representation for the droplets follow those in Figure 4.3. The Case C is in stark contrast when it comes to fuel presence in the areas distanced further from the injector. LES_F predicts the presence of fuel vapour up to x=3. RANS under-predicts the penetration in the outward direction by almost a factor of two. There is no presence of liquid of vapour phase in the squish region at all.

While this could be attributed to certain extent to the coarse mesh, LES_C does predict fuel in the squish using the same mesh resolution. The comparison between cases A and B shows case B predicting a much larger fuel vapour penetration although a very coarse mesh (by LES standards) was used in this test. Clearly, the fuel vapour penetrates more and the fuel distribution in the squish region is substantial in case C, which is the LES test case with sufficient resolution. In Figure 4.5, it is also observed that the dispersed small particles in LES computation do travel much further downstream into the squish, where they are subjected to further breakup by the tumble flow.

Another interesting feature captured by the case C simulation is the fuel presence in the lower portions of the cylinder volume, reflecting the objective of the bowl design which is to produce significant flow movements when paired with piston motion to enhance the in-cylinder fuel mixing. This is a common procedure in both diesel and gasoline direct injection engines as there is no swirl created either by the pre-chamber or intake port. The tumble of the intake flow must therefore be generated by another means and special shape of piston top is a common way to do this. Once again, presence of the fuel in the bowl ensures that the mixing is efficient. The dependence of liquid penetration on gas phase modelling is an interesting observation in Figure 4.5. Even though the $k - \varepsilon$ model is for gas phase and is not directly responsible for the motion of particles, the turbulent flow field is a direct consequence of both phases involving strong inter-phase coupling, and the modelling of the gas phase has a pronounced effect on the liquid distribution since liquid particles are being transported by the gas phase flow field. While the liquid distribution is governed largely by the breakup models, the influence of the turbulent flow field on the liquid phase is significant and hence the distribution and evolution of the liquid jet is governed by the predicted turbulent swirling flow field. The behaviour of the curved jets in LES_C and LES_F seems to support this.
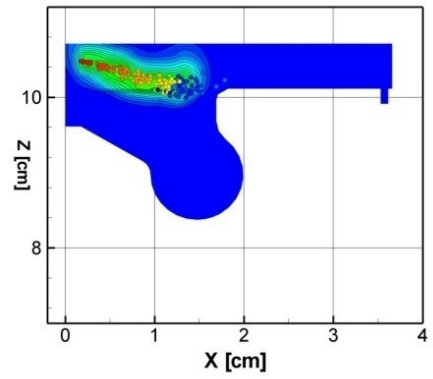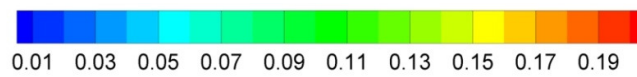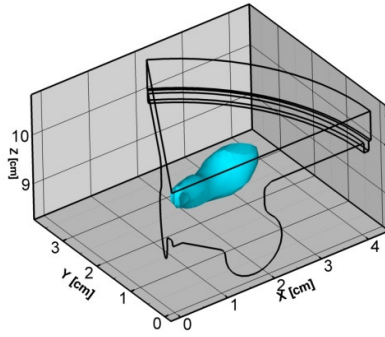
(a)
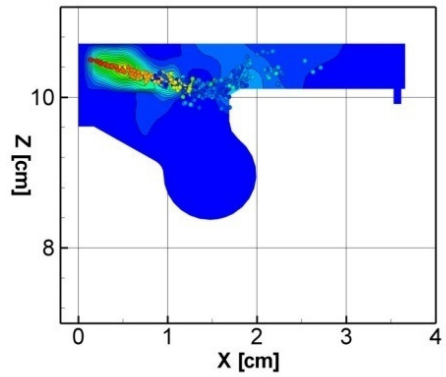
(b)
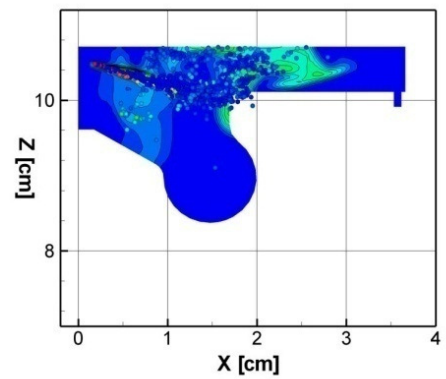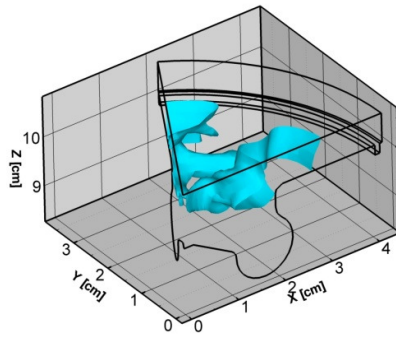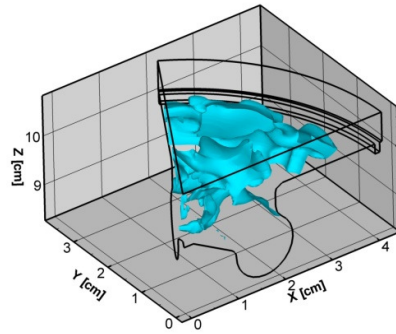
(c)

Figure 4-5. Two-dimensional contours of vapour mass fraction and 3D liquid droplet positions in a vertical cross-section at 11° CA, particles coloured by their sizes: a) RANS, b) LES_C, c) LES_F.

a)

b)

c)

Figure 4-6. Iso-surfaces of fuel vapour for mass fraction (0.035): a) RANS, b) LES_C

(b), c)LES_F

The absolute penetration is limited by the action of the swirl that is evident in LES where spray follows the angular rotation. Such behaviour of the liquid jet is not obvious in the RANS case. This further proves that the high swirl is largely responsible for liquid dispersion and vapour phase distribution as well. Another fact that seems to be supporting the influence of turbulence modelling on fluid phase behaviour is the section of the jet near the nozzle. Large particles are issued into the domain there with a high velocity and initially they follow injection parameters. It is only after approximately 1cm (Figure 4.3) that the droplets are break up, exchange momentum with the gas phase and are from then on much more prone to follow the turbulent flow.

Finally, to get a better insight into the fuel mass fraction distribution differences visible in Figure 4.3 and 4.5 three dimensional plots of fuel vapour mass fraction iso-surfaces are given in Figure 4.6. The differences are even more pronounced than with the contours on the two dimensional plane. LES on both mesh sets is capable of capturing much more wrinkled structure. Influence of the turbulence is directly visible. RANS case shows no such behaviour, in fact, as mentioned before the distribution of the fuel seems to be governed solely by the injection process. LES cases are able to capture instantaneous structures that act on the injected fuel creating a much more complex distribution that is spread throughout much larger portion of the domain. Even the LES_C case which is under resolved in terms of number of grid points does give a good indication of the mixing quality, although it cannot compete with LES_F in terms of number of detail that is captured.

4.3.2   Penetration, particle breakup and evaporation rates

Liquid particle sizes and distributions and fuel evaporation are important characteristics of spray flows. The liquid injection and its dispersion in a gas environment are very complex and

their prediction critical in simulations as it affects the combustion and pollutant formation directly. Figs. 4.3 and 4.5 discussed before both show the liquid particles coloured by their respective diameters. The jet has an initial angle of spreading equal to a nominal input of 15 degrees for a real nozzle (4.1). Vapour contours in Figs. 4.3 and 4.5 show that the droplet breakup in the RANS case is limited and less vapour is present, since larger droplets evaporate slower than larger amount of smaller ones. Case A is not much affected by the surrounding gas phase flow field and the spray development is driven primarily by the initial injection conditions. There is not much fuel present in the spanwise or downstream locations, which does not seem to be realistic under the strong swirling condition. LES cases capture the jet in a meaningfully different manner. The transient vortical structures and gas-phase motion (especially the swirl) have influence on the spray structure including the droplet dispersion and breakup, which were not captured in the RANS case.

The initial swirl in the cylinder (clockwise direction when viewed from the top of the cylinder) does affect the spray pattern in LES, which was also observed in the experimental data. In the LES case with fine grid resolution, the small liquid droplets move away from the main trajectory of the spray at downstream locations due to the swirl and tumble motions, which is a phenomenon observed in the experiments. In the LES, significant droplet breakup occurs which allows for easier liquid transport by the gas flow. Case B shows the influence of the high swirl on the downstream spray structure. The tip of the liquid jet is curved to reflect the action of the swirling angular momentum of the flow (Figure 4.3).

Breakup of the liquid jet in this region is also enhanced. The effect of the swirl on the jet is most evident in case C. There are much more dispersed droplets of smaller diameter present further downstream. Those are carried by the turbulent structures across the cylinder volume.

In case C, the swirl does break the jet earlier and stronger than case B. This is an explanation why at a first glance the structure in case C appears to be less affected by the swirl.

Figure 4.7 shows the injection rate used for the analysis of subsequent paragraphs. Figure 4.7 presents a curve describing the values of injection velocity comprising of 120 velocity values that are used throughout the injection duration (30° CA). This reflects the manner in which fuel particles are injected into the code and together with specification of the total mass injected and area of the nozzle allows the code to estimate the correct mass flow rate. The manner of injection with its high initial velocities was provided by the company and is justified by the nozzle geometry used. In a typical engine, initial injection velocities are likely to be lower due to the injector opening phase.

 Figure 4.8 shows penetration values of the liquid spray in [cm] with respect to ATDC crank angle changes. The criterion for the value of penetration is 95% accumulated mass distance from the injector. A number of conclusions can be drawn from the Figure 4.8. The data before 0° must be viewed with caution because this is the early stage of particle injection and the numerical procedure of issuing parcels into the domain does not guarantee correct spray prediction in the vicinity of the nozzle at the start of injection. In addition, turbulence effects at the very beginning do not influence the spray as the injection velocity is very high. This was discussed before with the respect to case A, but the logic can be applied to the LES cases as well (however only at the very start of the injection process). Bearing this in mind, we can now proceed to the explanation of the Figure 4.8.
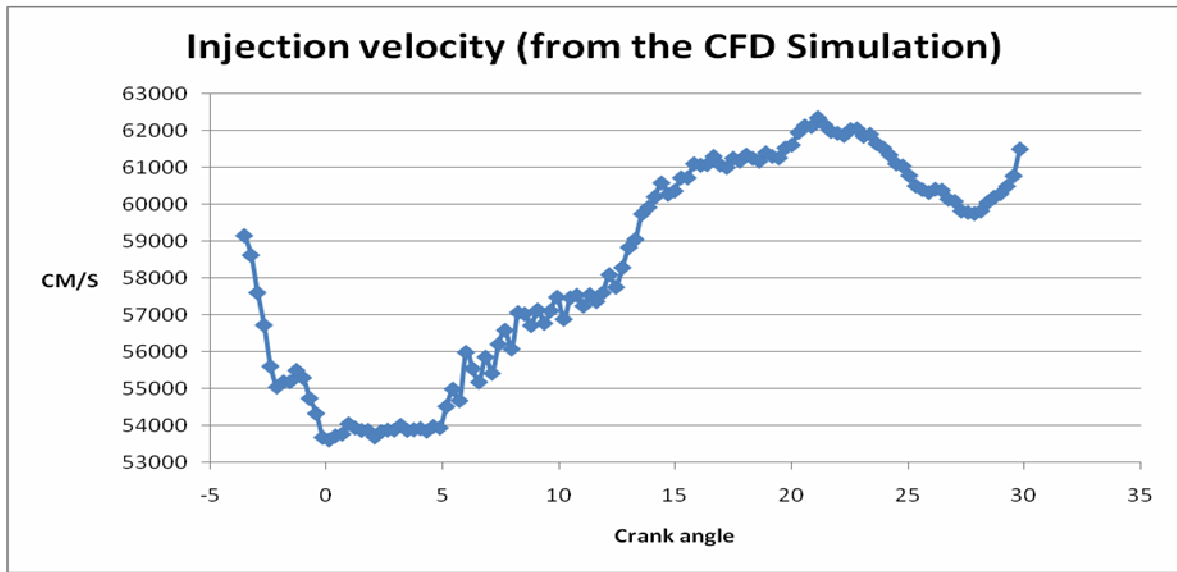
Figure 4-7. Injection velocity with respect to crank angle (duration 30°).
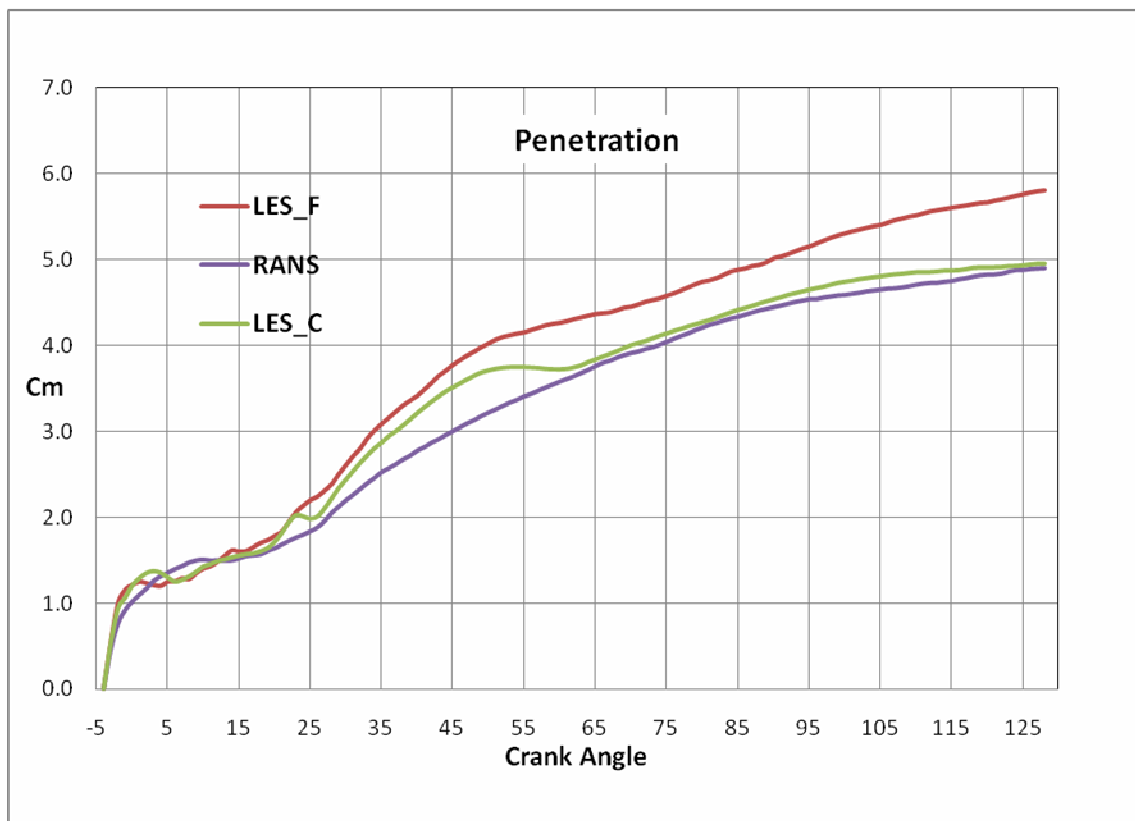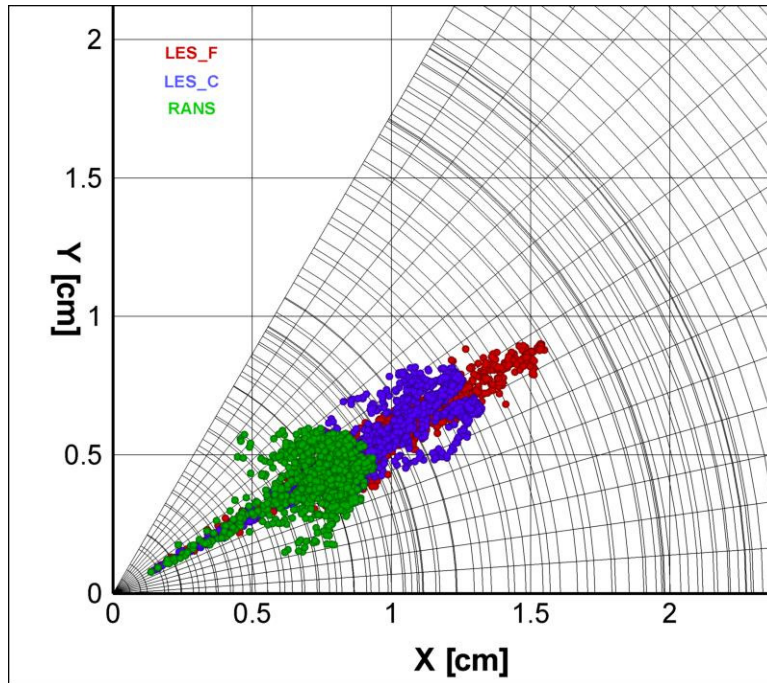

Figure 4-8. Liquid spray penetration for RANS, LES_C and LES_F.

The RANS curve has the most gradual increase without any visible jumps or dips. This would suggest that the injection process and subsequent behaviour of the droplets does not change meaningfully throughout the engine cycle. Indeed, this would also imply that he turbulent flow field does not significantly influence the liquid phase and the injection is driven by the initially specified parameters like the angle and velocity. There is up to 1cm difference in penetration between RANS and LES_F in simulations. In a domain of an 8cm diameter, this difference can be regarded as significant. LES_F is more in line with experimental findings of diesel sprays. The reason why penetration does not reach steady state and is increasing throughout the simulation is twofold. First of all, the lack of combustion means that the evaporation is much less intense and the fuel is not consumed. This means that the liquid jet is penetrating much further into the domain. This is also the reason why the criterion of 95% accumulated mass predicts the presence of the liquid in the domain. The liquid travels further downstream even after the injection process is finished.

In Figure 4.8, interestingly, all three curves behave almost identically up to a crank angle of approximately 26°. The only possible explanation is the gradual momentum exchange with the gas phase and increasing influence of the swirl in cylinder. Penetration of the LES_C resembles that of the time averaged results and it is in this area, where the insufficient resolution for LES method comes into play. Apart from an increase between 26° and 66° the curve does not show improvement with regard to penetration. One must remember however, that those are averaged values and the actual flow field is much different than in RANS as was shown in Figures 4.3 and 4.5. There is no doubt, that the Figure 4.8 would look very different when subtracted from a reacting simulation as the spray would be unlikely to travel that much downstream. To assess the ability of the LES code to correctly predict penetration of the liquid jet (vapour concentration follows) one should possibly isolate all the other

variables that may affect the droplet behaviour and are not directly related to the numerical performance of the code. In this case, it was clearly established before, that the in-cylinder swirl has a profound impact on the pattern of the diesel spray. This situation, while correct and expected for the engine cycle being simulated, is not necessarily ideal for judging the performance of numerical code. Therefore, additional simulation was established without the presence of ambient swirl. This would ensure that the spray results will reflect only the performance of the RANS/LES methodology and not the influence of other physical phenomena such as the swirl as well.

Figure 4.9 therefore shows three spray penetrations for RANS, LES_C and LES_F, respectively. The crank angle is 3.5° ATDC, which is 7 degrees after the start of injection. Comparison at 11°C A was not possible because the spray deposits on the cylinder wall very quickly due to the very high axial momentum of the spray (the injection pressure is as high as 1550 bar) in the absence of the swirl. The input data into the simulation is identical to the previous cases with the same names, bar the swirl which is now absent. All the parameters discussed before like penetration and radial diffusion are augmented by the lack of swirl. It can be seen that the penetration of LES_F is almost twice the value of that of RANS. Using the 95% mass criterion, the penetration data now shows 1.42 [cm] for LES_F and 0.81 [cm] for RANS, while the LES_C case is in between with a value of 1.17 [cm]. Figure 4.9 clearly shows different penetration and radial spreading of the three cases. Superiority of LES calculations is even more evident as the LES_F case has twice the penetration of the RANS case.

Figure 4-9. Liquid spray penetration at 3.5°CA after SOI, non-swirling cases.

For the baseline, swirling cases, the presence of liquid and vapour in the system needs to be examined, as an indication of the effectiveness of evaporation process. The evaporation is only due to the increase in temperature because of the changing cylinder volume during the compression stroke. Figure 4.10 shows accumulated amounts of, liquid and vapour phase in the system, again with respect to crank angle. The evaporation rates can be easily determined by comparing the liquid and vapour contributions. The total amount of fuel was determined by the injection parameters and was identical for all three cases. The LES_F case has by far the most effective evaporation process. As mentioned in the previous section this is because of the increased droplet breakup and particle dispersion. LES_C case again behaves similarly to RANS with less vapour and more liquid. While cases A and B are quite close to each other, the C case does have higher content of vapour present in the system, due to the more efficient evaporation of the fuel in this case. The amount of fuel evaporated depends on the temperature of the ambient gas and the turbulence level as predicted by the evaporation model.

Comprehensive review of fuel evaporation prediction is given by (Birouk & Gokalp, 2006). In Figure 4.10, it is worth noting that the content of liquid does not drop to zero in all cases as it would happen in a real engine combustion situation, which is a result of switching off the combustion modelling in the simulations performed. The results shown in Figure 4.10 were obtained from integration over the cylinder volume. It is noticed that the RANS case and the LES with coarse mesh case LES_C show almost identical results, which is due to the fact that the quantities shown are averaged results across the entire domain. Although the results of these two cases differ from each other significantly in the specific location as shown in instantaneous results, the averaged results are not so different due to the identical mesh used in the simulations. In Figure 4.10, the peak visible at approximately 27° CA signifies the end of injection process. After that the amount of liquid drops and stabilises at about 70° CA.


a)

94
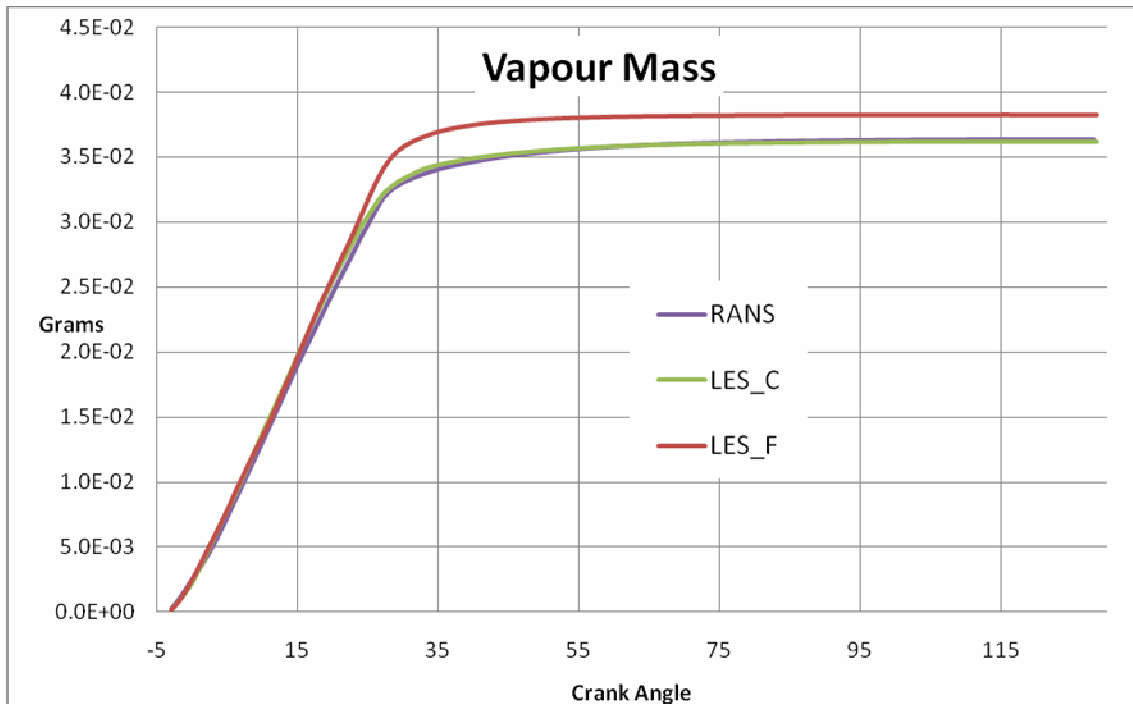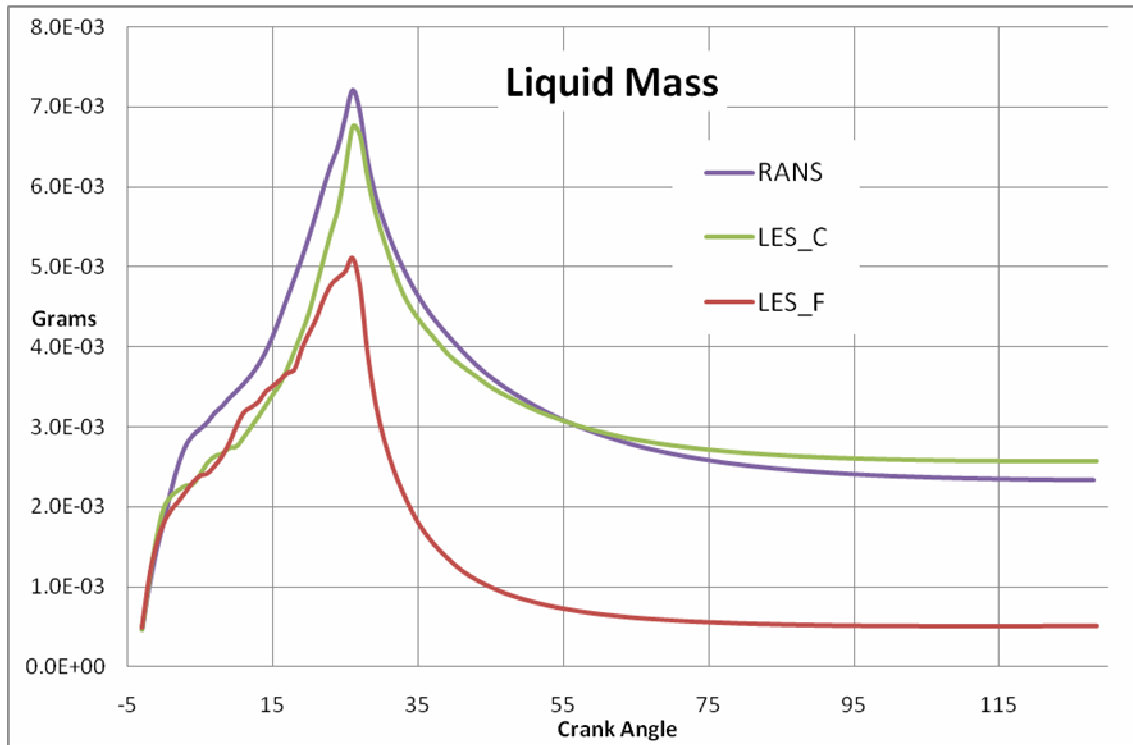
b)

Figure 4-10. Liquid and vapour mass contents for RANS, LES_C and LES_F

Vapour content reaches a constant value at about 52° CA, so does the liquid mass content. One must remember that this is a non-reacting case and the total amount of fuel in the system is constant as no fuel is consumed by the chemical processes.

As noted before, the evaporation is influenced by the liquid breakup. Figure 4.11 shows exactly how different the breakup is in each of the cases. The graph represents SMR (Sauter Mean Radius) values with respect to crank angle. LES_F has the smallest SMR of all with the maximum SMR not exceeding 6 microns. Surprisingly, RANS predicts smaller droplets than the LES_C case. The RANS gives Sauter mean radius smaller than 10 microns, while Case B has the biggest droplets at SMR equal to approximately 13. This poor performance of LES_C may signify the need for calibration of the liquid breakup models when LES is performed on a coarse mesh with insufficient resolution. The initial SMR of injected droplets was set to be

72.5 microns so all three cases are able to predict significant breakup of the droplets. Since the aim of the study was to get the spray penetration predictions as reliably as possible with respect to real engine data (accumulated heat release rates depend strongly on fuel penetration) and the LES_F still under-predicts the penetration slightly, the advantages of performing LES on a sufficiently fine mesh are justifiable in this context. In Figure 4.11, it must be noted that the SMR distributions up to around 30° CA might not be physically meaningful, due to the initial conditions of the injection without much of the influence of the gas phase turbulence modelling. This was also the case in Figure 4.8.

Figure 4.11 shows the superiority of the LES on a dense mesh when it comes to performance of the breakup models, especially the R-T model which is responsible for breakup of the droplets into the smaller ones further downstream. The LES_C case needs some adjustments of breakup constants in order to produce finer droplets. This has to be beard in mind when attempting LES on coarse meshes.
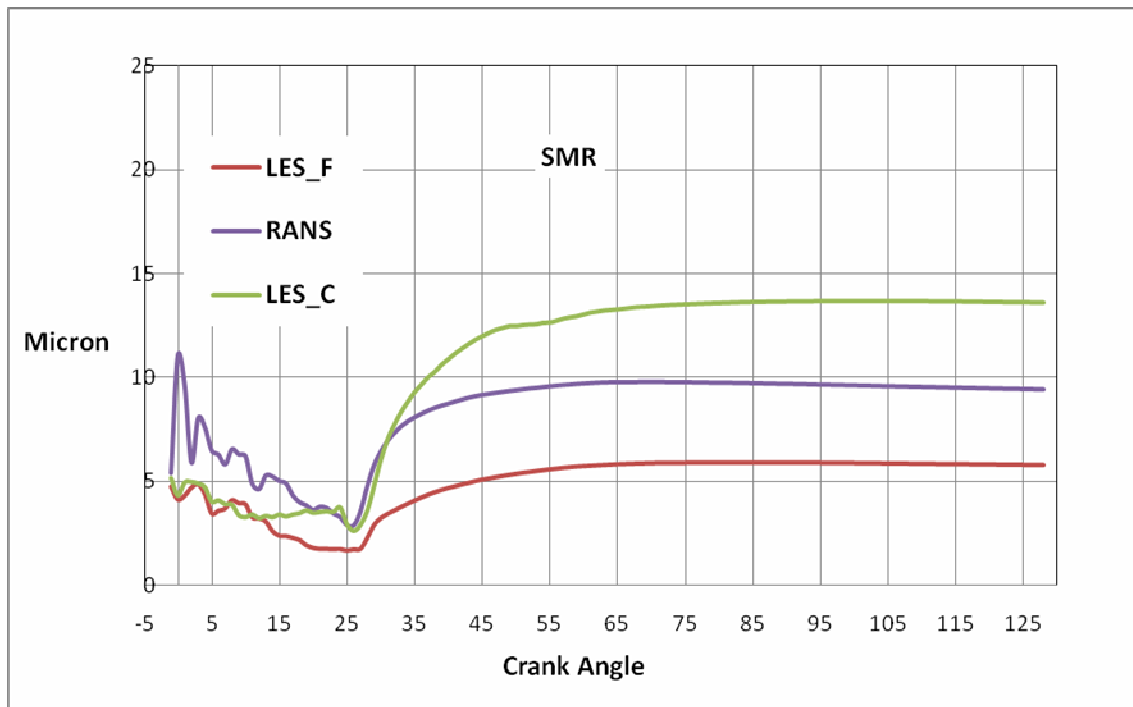
Figure 4-11. Sauter mean radius of fuel droplets for RANS, LES_C and LES_F.

4.3.3 Results from the E16 experimental engine

This subsection deals with the simulation results for the special experimental engine with pre-chamber configuration, built specifically to investigate the behaviour of diesel sprays at the Delphi Diesel Systems. Since the experimental configuration had the reaction suppressed by means of using nitrogen as a gas phase, the same procedure was applied in the simulations. To closely follow the experimental data available from the sponsoring company, initial flow data of the gas phase, along with detailed spray injection pattern were obtained. Those data were then implemented into the code by means of additional subroutines to make sure the initial flow field and injection conditions are in accordance with the measurements obtained from the experimental configuration.

Two numerical cases were investigated by means of LES, varying in mesh resolution. The aim of this task was to try to reproduce the correct spray pattern seen in the optical images, investigate the penetration and again assess the LES sensitivity to mesh resolution. Important parameters of the engine related data are summarized in Table 4.3. The injection rate is given in Figure 4.12. Piston motion was disabled in the simulation to discard any changes in the pressure related to the change in cylinder volume. Two mesh sets were used, a coarse one with 80000 elements (this will now be referred to as the E16_C case) and a fine one with a resolution of 260000 (E16_F). The mesh used was a 60 degree sector of the full cylinder with a single jet issuing from the middle of the domain. The original injector nozzle is a 6 hole unit, however to save computational resources, only one hole was simulated with periodic boundary condition applied at the right and left side. Figure 4.13 shows an overview of the mesh sets used.

Table 4.3. E16 experimental engine simulation parameters

RPM	666
Bore	6.35 [cm]
Stroke	20.9015 [cm]
Squish	2.0985 [cm]
Simulation start	-5.5° ATDC
Simulation end	10.0° ATDC
Start of injection	-1.75° ATDC
Injection duration	7.28°
Spray cone angle	15°
Total mass injected	0.0465 [grams]
Initial chamber pressure	1.5e+06 [dynes/square cm]
Injector location in the Z dimension	22.826 [cm]
Inclination of the injector in the XZ plane	76.5
Protrusion	0.1554 [cm]

Figure 4.14 shows the spray development for different crank angles after the start of injection, along with the optical image from the camera. The images were obtained from the sponsoring company and while they do not correspond exactly to the crank angle presented, comparison of the spray structure can nonetheless be attempted. In Figure 4.14 the results from the simulation are on the left, followed by optical image on the right. We can see that the penetration values predicted by the code are in accordance with the optical images. At 1.6 CA the spray hits the wall and this is correctly predicted by the code. The curvature of the spray caused by the swirl is also in line with the experiment and can be already distinguished at -0.4° CA.
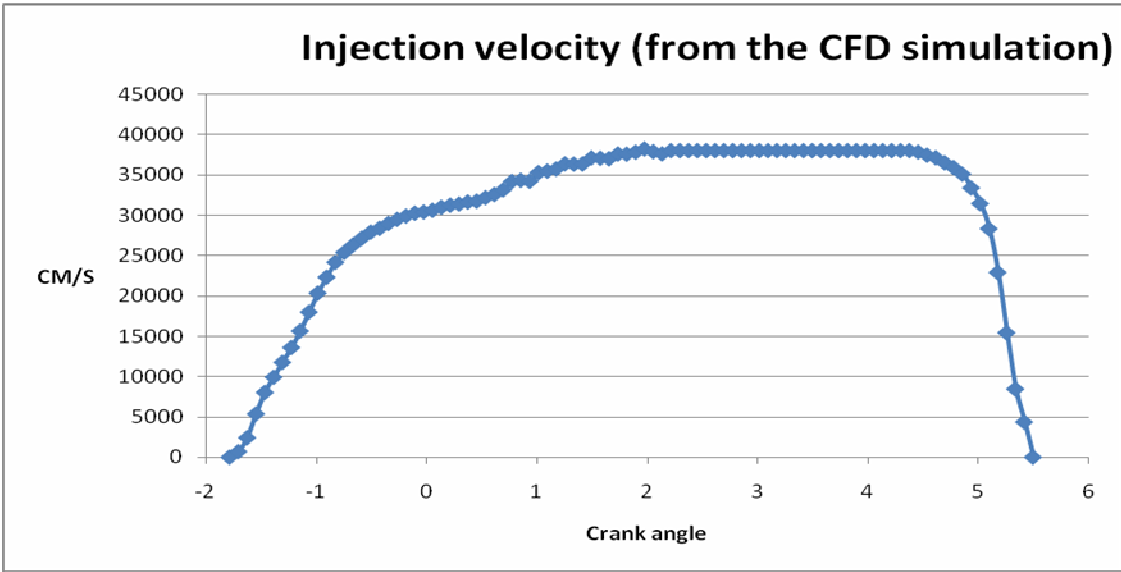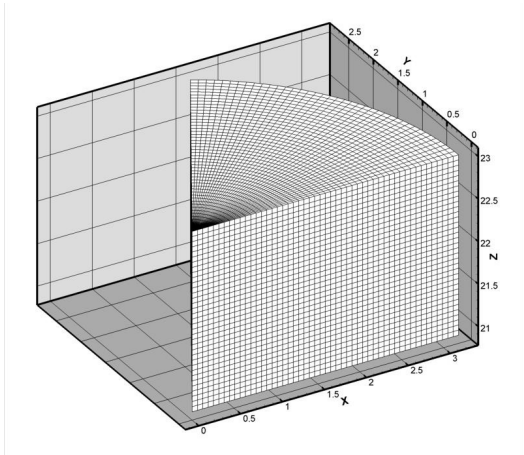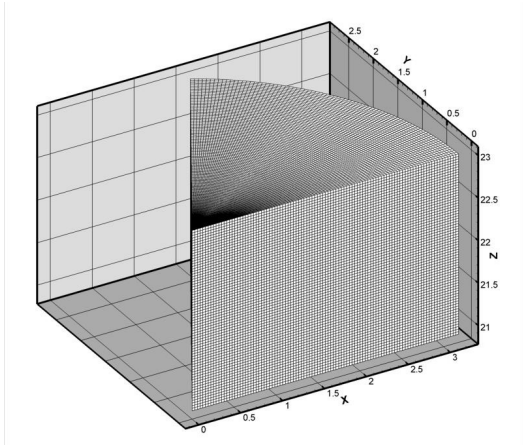
Figure 4-12. Injection velocity with respect to crank angle (duration 7.28)

a)

b)

**Figure 4-13. E16 mesh: a) coarse distribution, b) dense distribution.**

To gain more insight, Figure 4.15 shows a plot of mass penetration with respect to the crank angle. The criterion used is the same as in Section 4.3.2 with 95% accumulated mass distance from the injector. The curves support the graphical presentation of the results with LES_C case under predicting penetration throughout the cycle, bar the initial stage (which should be discarded from analysis due to the reasons mentioned in 4.3.2) and the final stage, above 8° ATDC. The reason why the E16_F curve tapers off at this value is the accumulation of the liquid on the cylinder wall. The penetration criterion does not currently account for spray impingement. Therefore reliable comparison is only possible before spray deposition on the wall occurs. An examination of the Figure 4.14, snapshots c and d, it is noted that the curvature of the spray is larger in the E16_C case. Both the droplets and the vapour do appear at the left side of the domain (due to the periodic boundary condition) suggesting a significantly wider spray cloud in the radial direction. Relatively wide cloud can also be seen in the optical images, although, as mentioned along with substantially higher penetration not captured accurately by the E16_C case.

4.4   Concluding remarks

This Chapter assessed the quality of the mixing of the injected diesel fuel in a non-reacting engine configuration. Both instantaneous and averaged data have been gathered and analyzed. Three computations were performed, RANS and two LES. The logic behind this was to have RANS simulation as a reference point of the code performance in its original formulation. The coarse mesh LES was a bridge between RANS and a full, high resolution LES. The aim was to investigate, whether LES performed on a mesh suited to RANS will still yield benefit that is expected with large eddy simulation. This was confirmed to large extent. Both LES cases

showed much improvement in predicting the penetration of the liquid jet and what follows, presence of the fuel in the cylinder. In some cases the predicted penetration was double that of what RANS simulation was able to capture, brining the results much closer to the real spray behaviour. The differences in droplet breakup intensity were very significant, with LES_F case predicting much more breakup and atomization. Interestingly, analysis of the SMR of droplets showed that LES_C has some limitations as the average droplet size was larger than the one predicted by RANS. This is probably an indication that when attempting LES on a too coarse mesh, one has to adjust the constants of the breakup models, especially the Rayleigh-Taylor model to somehow account for the lack of spatial resolution. Such issues do not seem to exist in LES_F case where the model performed very well, predicting finest droplets as small as 6 microns. RANS was able to capture liquid in sizes of 10 microns, while LES_C was in between with a diameter of 13 microns. Smaller droplets predicted by LES_F case augmented significantly the process of evaporation, leading to much more vapour present in the system at the end of the cycle. This would definitely improve the quality of combustion modelling and will be investigated in Chapter 5. Overall, the LES results were able to capture the affect of the swirl in the cylinder on the injected liquid phase. The presence of fuel in the squish region, near the Top Dead Centre of the piston further proved that fuel mixing is much better reproduced than it is possible by time averaged methods. That was supported by the analysis of fuel contours on a side two-dimensional plane, where fuel was present in the bowl area in the LES_F and to some extent LES_C case.

The additional analysis of the pre-chamber engine showed very good agreement of liquid penetration with the experimental data. Again, LES benefited from increased resolution as dense mesh results were in accordance with the optical dataCareful analysis of the code ability to correctly predict fuel mixing and liquid penetration served as a base for further modification to the LES and combustion models which will be presented in the next Chapter.
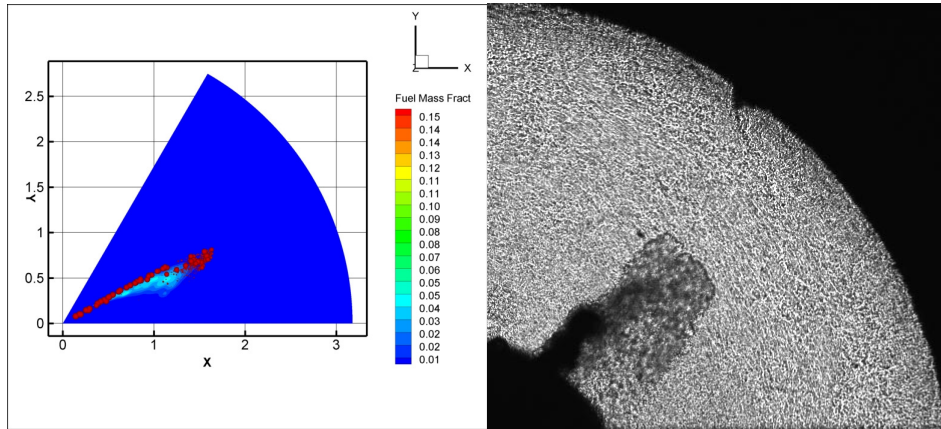
a) -0.4 CA
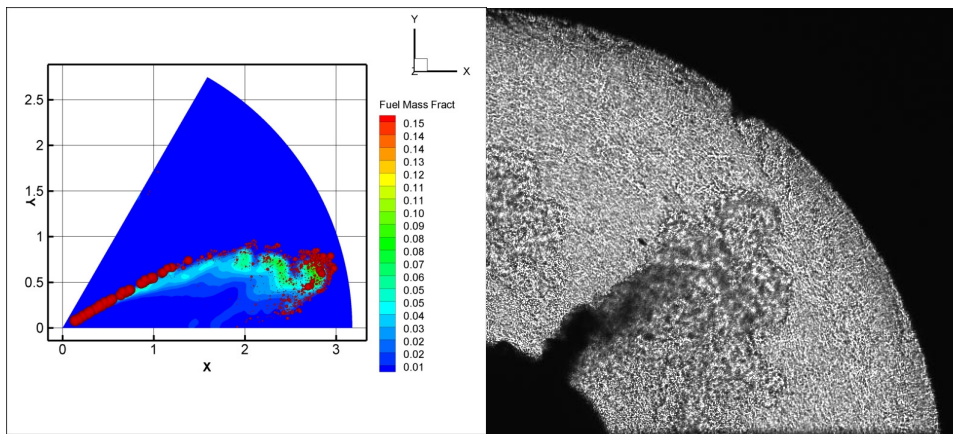
b) 0.8 CA
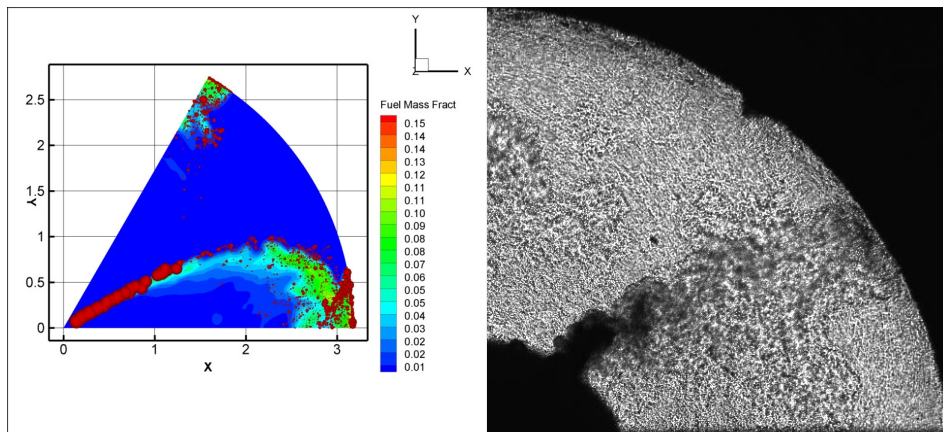
c) 1.6 CA

Figure 4-14. E16 spray development for different crank angles, particles sized by diameter, contours on the plane showing vapour mass fraction.
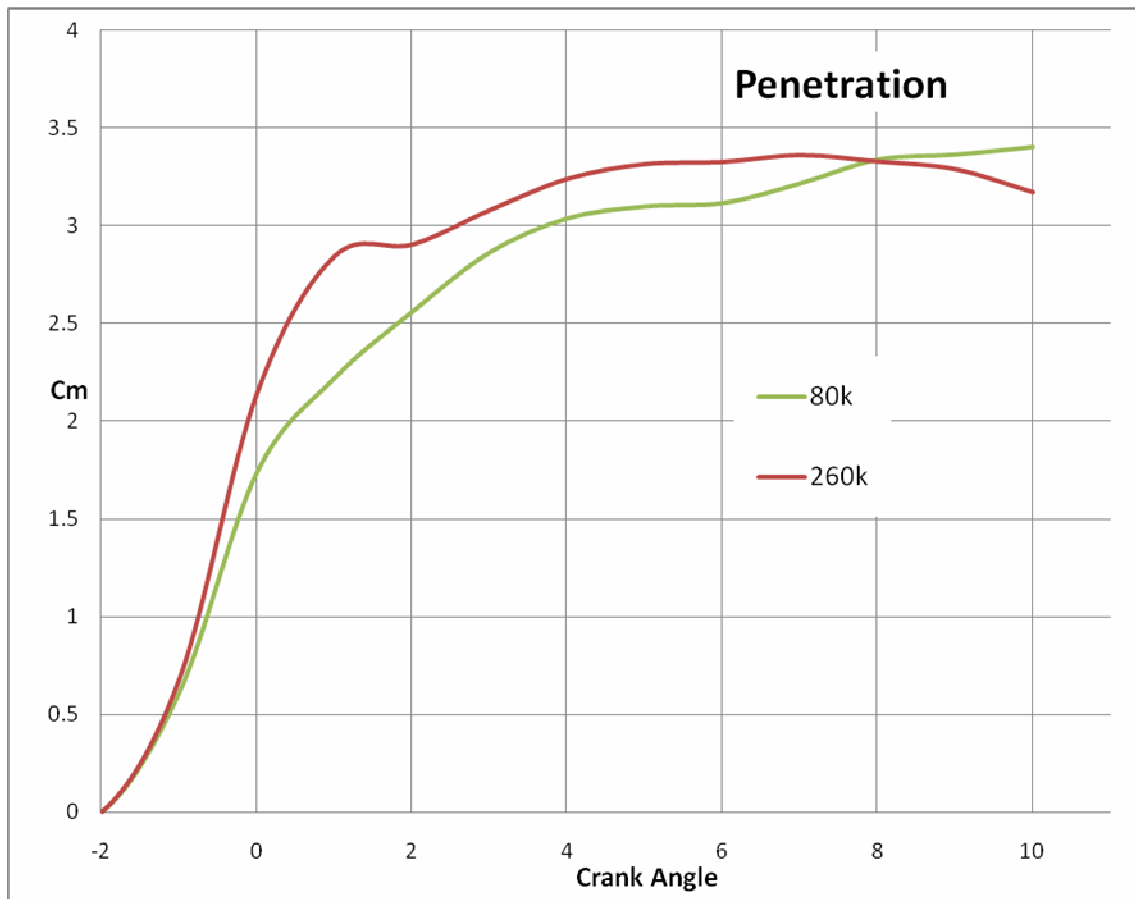
Figure 4-15. E16 liquid penetration for two mesh sets.

5   LES Modelling of Spray Combustion in an Engine Environment

5.1   Introduction

This Chapter describes in detail the simulation of the motored Hydra engine used in Chapter 4 for the investigation of spray penetration predictions. Here however, reaction modelling has been employed resulting in a full LES of reacting multiphase flow of real engine configuration. In order to achieve this, further modifications have been introduced to the code, concentrating on improving the LES scheme and modifying the time-scale based combustion model in order to be compliant with LES framework. The next Section describes the modifications performed, followed by analysis of the result in subsequent Sections.

5.1.1   Improvements to the reacting LES code

The modification to the LES scheme aimed to remove the limitation of ad hoc specification of the filter width. Since cells in computational domain inherently vary in size (this is unavoidable in engine geometries), the production of turbulent kinetic energy is compromised by the fixed size of the LES filter, leading to either over or under prediction depending on the size of the computational cell. When we look at the Equation 2.22, the filter width Δ is responsible for the estimation of dissipation term (second term on the right hand side of the equation, D^{SGS}). In addition to that, the formula for subgrid eddy viscosity also contains the value of filter width

$$\nu_t = C_k \sqrt{k_{SGS}} \Delta \tag{5.1}$$

The eddy viscosity in turn influences the subgrid stress tensor τ_{ij}.

Those correlations prove that in order to get as accurate results as possible, we need to ensure that the underlying assumptions and empirical formulas are absolutely correct and in no way compromised or averaged throughout the domain. Previous ad-hoc specification of the single filter width for whole domain (hundreds of thousands of cells) was just that, an averaging introduced very early on in the algorithm that had an influence on quantities like subgrid stresses, turbulent kinetic energy dissipation and even on the rate of combustion process in the new combustion model.

In the new algorithm, the filter is no more specified as a single value via the input file. Instead the values are calculated for each cell separately, taking into account X, Y and Z dimensions. This ensures that the code utilises information about the cell size and adjusts the filter size accordingly. The formula for the filter width is (Sone et al., 2001):

$$\sqrt[3]{CellVolume} \qquad\qquad\qquad \textbf{(5.2)}$$

The only drawback of this method is a slight increase in the memory requirement of the simulation. This is because the code now needs to store additional variable ready to be accessed by subroutines. This variable is the filter width and the array size equals that of a number of cells. However, as we shall see, the procedure is very beneficial to the results. A simple comparison will be presented here of an annular jet from the Chapter 3, utilizing two versions of the code and variable mesh sizes. The old version with fixed filter width LES_1 and new version LES_2 were run parallel on different mesh size. Table 5.1 briefly summarizes the procedure for the comparison of the two LES codes. It can be seen that the LES_2 calculation uses a mesh that is half the size of LES_1. It would therefore appear that much more detailed flow characteristics would be captured by the LES_1 simulation, because

finer mesh is able to directly resolve smaller structures. Bearing this in mind, we shall now take a look at Figure 5.1 that shows two vector fields at identical time instant for LES_1 and LES_2.

Table 5.1. Computational cases for updated LES scheme performance assessment

|	LES_1	LES_2
Mesh size	730 000	360 000
Filter Width	Ad-hoc specified (6.6e-02[cm])	Variable, cell volume based

The jets are not expected to be identical or even largely resembling due to the different numerical treatment and big difference in mesh resolution. The aim of the Figure 5.1 is to show how much detail can be extracted from the simulation on a two times smaller mesh when the numerical procedure is improved and introduction of averaging avoided. LES_2 shows roughly the same amount of vortices in the inner and outer shear layer that are also comparable in size to those predicted by LES_1. One could even state that the structures in Figure 5.1b appear to be less smeared, especially in the core of the jet. Bearing in mind the mesh resolutions used for respective cases, it is safe to acknowledge that the memory trade-off of LES_2 case does not represent the problem. Contrary, much coarser mesh can be used in certain applications than in LES_1 and accurate results still obtained.

Some caution must be taken when analyzing those promising results when we would deal with reacting cases, as the mesh resolution might be of bigger importance there. For the non-reacting cases however, we can reasonably confidently lower the mesh resolution by a certain amount without compromising on quality of the results. As mentioned before, the additional memory requirement is therefore more than offset by the accuracy improvements. The

computational time increase due to the calculation of the filter width is negligible. Having assessed the positive impact of the variable filter width Δ on the simulation quality, the remainder of the computations were conducted with the LES_2 version of the KIVA3V code, referred to from now on as new LES.
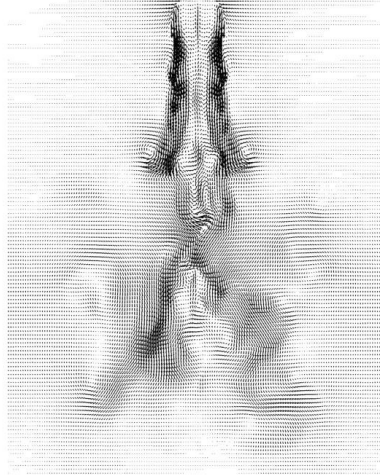
a)
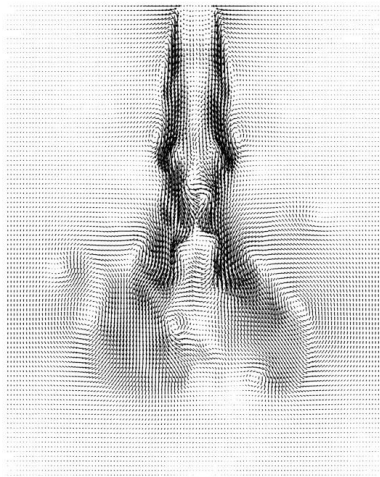
b)

Figure 5-1. Velocity vector fields: a) LES_1, b) LES_2.

5.1.2   Modifications of the Characteristic Timescale Combustion Model

The baseline model used in the code is the Characteristic Timescale Combustion model that originated as a spark ignition engine model (Abraham et al., 1985).   The underlying assumption of species conversion is the change rate of the density of the m-th species governed by the following formula (Xin et al., 1997)

$$\frac{d\rho_m}{dt} = -\frac{\rho_m - \rho_m^*}{\tau_{c,m}}$$

(5.3)

Where ρ_m^* is the local instantaneous thermodynamic equilibrium value of the partial density and $\tau_{c,m}$ characteristic timescale needed to achieve it (Xin et al., 1997). The multiscale model implies that those timescales are different for each of the species, as opposed to original model formulation (Reitz & Bracco, 1983) where only single timescale was calculated for all the species present in the system. The determination of the characteristic timescale is based on two main quantities, namely laminar τ_l and turbulent τ_t:

$$\tau_{c,m} = \tau_l + f\tau_t$$

(5.4)

Where f is a coefficient of the degree of turbulent combustion (Xin et al., 1997).

The laminar timescale is defined as (Xin et al., 1997)

$$\tau_l = A[C_nH_{2n+2}]^{0.75}[O_2]^{-1.5}e^{E_a/RT}$$

(5.5)

A is a model constant equal to 1.625e-11

The turbulent timescale in original formulation is specified as

$$\tau_t = \frac{C_2 k}{\varepsilon} \qquad\qquad (5.6)$$

In Equation (5.6), k is the turbulent kinetic energy and ε its dissipation rate. C_2 is a constant equal to 0.1 (Kong et al., 1995). The most important issue here is that those values are correct for RANS based methods with $k - \varepsilon$ turbulence model employed. The values and indeed physical interpretation of those quantities in LES with k-equation model is very different. The k is subgrid turbulent kinetic energy that accounts only for the subgrid scales (Section 2.1) while ε is not calculated explicitly at all. This poses obvious problem as the magnitude of those values is very different in RANS and LES (See Figure 3.1 for example). Subsequently, incorrect estimation of the turbulent timescale leads to wrong prediction of the change in density of species (Equation 5.3) and what follows errors in pressure and temperature. For accurate predictions of species density within LES, another definition of turbulent timescale is needed, known also as the eddy turnover time. After careful investigation a new estimate for eddy turnover time was used. The formula based on Smagorinsky's assumption that the turbulent energy generation and dissipation should balance each other locally (Smagorinsky, 1963). With regard to subgrid scales that are much more uniform this assumption was found to be reasonable. Following this logic, the formula for the subgrid dissipation is

$$\varepsilon = 2\nu_t \overline{S}_{ij} \overline{S}_{ij} \qquad\qquad (5.7)$$

Where $\overline{S}_{ij}$ is the resolved rate of strain tensor, and the characteristic turbulent timescale is equal to (Yaga et al., 2002)

$$\tau_t = \left(\frac{\nu}{\varepsilon}\right)^{0.5} \qquad\qquad (5.8)$$

Where ν stands for gas phase viscosity. Implementation of this formula ensured that the eddy turnover time would be predicted accurately within LES framework.

5.2   Engine test conditions and numerical cases

Three numerical cases have been thoroughly analyzed. RANS simulation and two LES cases. The differences between two LES cases were different LES treatment (Section 5.1.1) and formulation of the combustion model (Section 5.1.2). Case B contained old version of the model with turbulent timescale calculation from RANS (LES_eps) and ad-hoc specified, constant filter width. Case C uses calculated filter width for each cell and a new numerical procedure for determination of the eddy turnover time (LES_eddy). The data of the engine and simulated cycle are identical to the one described in Chapter 4 and summarized in Table 4.1. Injection rate is presented in Figure 4.7 As can be noted in Table 5.2, mesh has been changed from the one used in Chapter 4. The increase in resolution is mainly limited to the bowl which could influence the LES results especially at the Top Dead Centre. The modification was possible, after a more detailed profile of the bowl was obtained from Delphi Diesel Systems which then allowed construction of more nodes and significantly increased resolution. Increased resolution in the bowl area would also allow more accurate predictions of liquid spray behaviour and effects of turbulent flow field since more energy containing eddies would be directly resolved. This would in turn influence combustion process by means of improved mixing predictions.

Figure 5.2 shows the new mesh. With respect to the RANS mesh, bowl area has also been refined although the mesh is coarser than LES one but was deemed satisfactory for time averaged calculations. RANS based calculations were performed on a more dense mesh with

approximately 340000 elements, but no improvement was found with respect to mesh used in case A. Therefore, remainder of the calculations were performed on a mesh that is suitable for RANS without unnecessarily increasing the computational time

Table 5.2. Numerical cases for the reacting Hydra engine simulation

	Case A (RANS)	Case B (LES_eps)	Case C (LES_eddy)
Formulation	RANS	LES	LES
Mesh resolution	66000	595000	595000
LES Filter width	N/A	0.6 [mm]	Cell specific
Turbulence model	$k-\varepsilon$	$k-$equation	$k-$equation
SOI	-3.5° CA	-3.5° CA	-3.5° CA
Injection duration	30° CA	30° CA	30° CA
Total mass of injected fuel	0.038725 [g]	0.038725 [g]	0.038725 [g]
	2.05	2.05	2.05
Chemistry	Shell ignition model; Multiscale combustion model	Shell ignition model; Multiscale combustion model	Shell ignition model; Modified multiscale combustion
Initial pressure in the cylinder	2.8 [bar]	2.8 [bar]	2.8 [bar]
Initial temperature in the cylinder	371 [K]	371 [K]	371 [K]
Temperature of the cylinder wall	400 [K]	400 [K]	400 [K]
Engine speed	4200 rpm	4200 rpm	4200 rpm
Load	100%	100%	100%
Injection Rate	See Figure 4.7	See Figure 4.7	See Figure 4.7
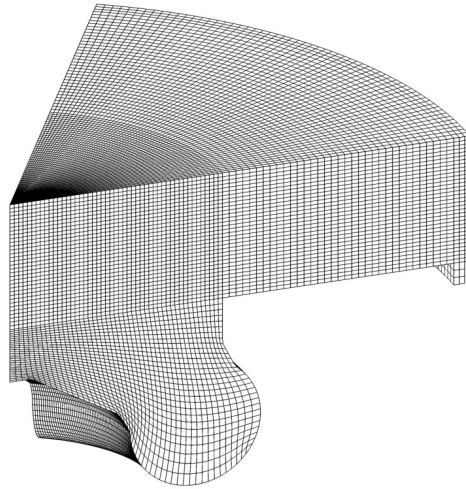
**Figure 5-2. Refined computational mesh for LES cases.**

5.3   Results and discussions

Three sets of instantaneous results have been carefully chosen to investigate the temperature field and presence of fuel throughout the combustion cycle. Snapshots at 5°, 40° and 80° CA were taken to investigate three different stages of the combustion process. The ignition occurs at around -4°CA and lasts until about 75° so the chosen values should give insight on the initial, middle and final combustion stages.

5.3.1   Instantaneous results at the initial combustion stage

Figure 5.3 shows contour plots of fuel vapour mass fraction, along with 3d particle positions at 5° CA and the corresponding temperature field. The contour plane is inclined to cut through the middle of the spray cone. Overall, the presentation in Figure 5.3 follows exactly the one used in Figure 4.3.
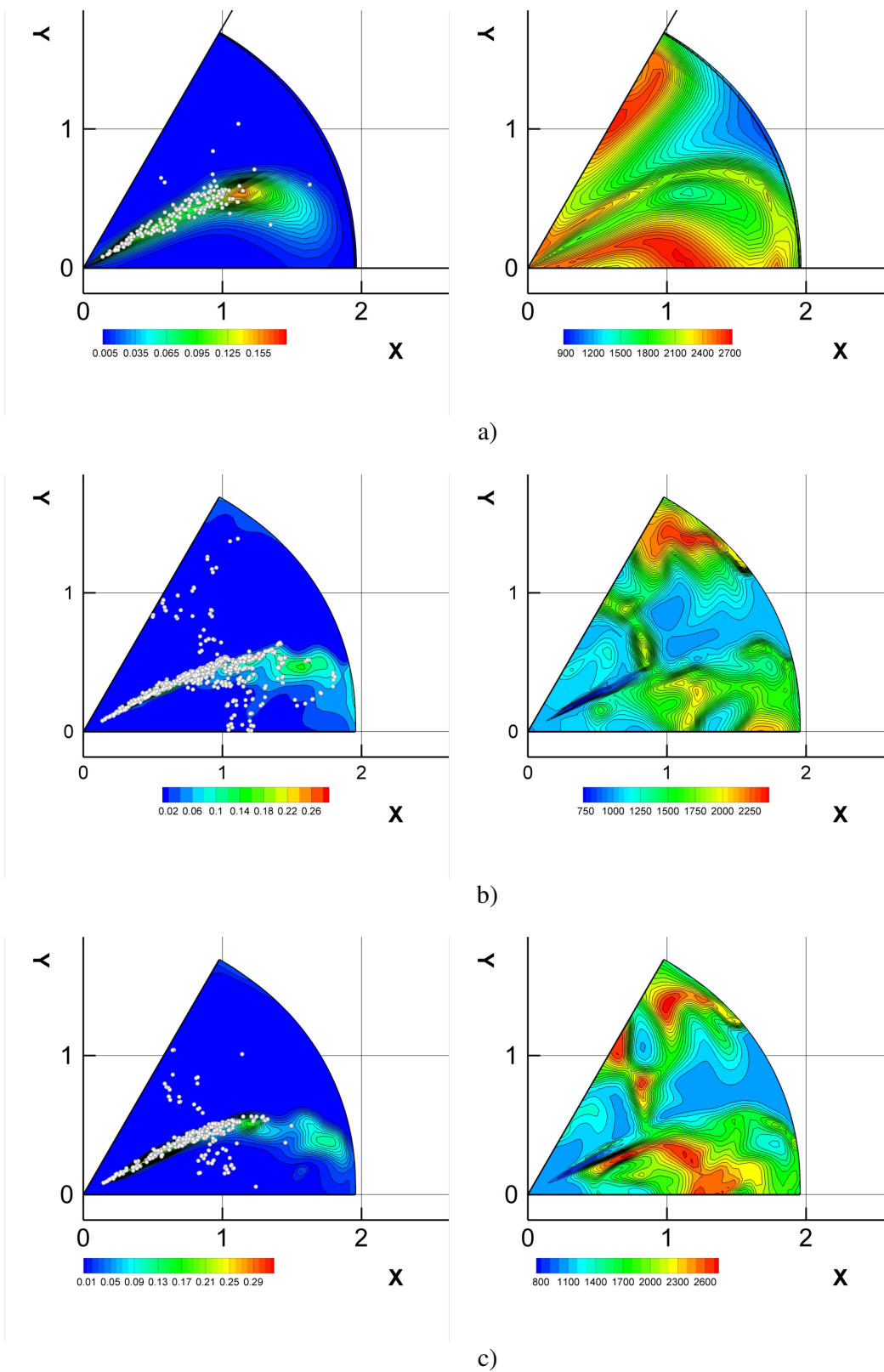
Figure 5-3. Vapour mass fractions, 3D particle positions and temperature field [K] at 5°CA: a) RANS, b) LES_eps, c) LES_eddy.

While fuel distribution can to some extent be compared to the non-reacting cases (curved jet, liquid penetration, excessive radial spreading for the RANS case), the temperature field does give proper insight into the initiated combustion process. The RANS temperature field is very dissipated. While the low temperature region where the spray is present is predicted reasonably, the outer regions where the burning seems to be initiating appear to be smeared and do not show any wrinkled temperature field which is believed not to be realistic as combustion in HSDI engine does not have such a uniform character. The LES_eps case presents temperature field that is much more influenced by the turbulence generated during the expansion stroke. The region where the spray is being injected has much more lower temperature than in RANS. This is correct since burning does not occur within the liquid jet in the upstream region where there is not enough vapour and spray momentum is high.

It is only in the regions where vapour is present that we see increased temperature values (around 1500K). Overall, the temperature in the domain is slightly under predicted by the LES_eps formulation. There appears to be one region of high temperature in the top corner. LES_eddy case seems to predict high temperature, fuel burning regions better. Lower region of the domain contains burning zones that are most likely created by the presence of vapour and influenced by the swirl in the cylinder (improved mixing process). The temperature field seems to follow the spray and vapour pattern more closely, although both models predict low temperature region in the middle of the domain, where liquid phase is present. The correlation between fuel presence and temperature is largely absent in the RANS simulation. Overall, the LES predicted temperature fields are much more wrinkled due to the unsteadiness and action of turbulence, something RANS cannot capture.

In the LES_eddy case the regions of the highest temperature (red colour) seem to exist just in the vicinity of the vapour phase presence (near the jet). This means that fuel is gradually consumed as the liquid evaporates from the jet core and the equivalence ratio is optimal for efficient burning. Interesting feature of the LES_eddy case is the lack of vapour in the upper corner of the periodic domain (please note that this region is in fact continuation of the lower portion – periodicity). LES_eps does predict presence of liquid there. This is because the old combustion model under predicts the temperature and the vapour can travel further downstream before being consumed by the flame (again, Figure 5.3 must be viewed with periodicity in mind, so that the upper portion of the domain is in fact continuation of the lower bound). In the LES_eddy case fuel is burnt in the lower region and this affects the liquid and vapour distribution further downstream. This is evident when looking at the temperature field as there are three regions of high temperature that are most likely responsible for fuel consumption in that area in the new LES case.

In Figure 5.3 and LES cases, it can be deducted from both the temperature and fuel distribution contours that the flame follows the action of the swirl and therefore is subjected and influenced by the turbulent flow field, something RANS fails to capture in the simulation. Especially important are the three hot region patches in LES_eddy (Figure 5.3c) with the cold one in the middle (X=1, Y=1). They support the claim that LES is able to capture instantaneous data very well, and that those vortical structures play a significant role in the development and shape of the flame during the combustion process. The coupling between turbulent flow field, distribution of fuel and chemistry effects is well captured.

115

5.3.2   Instantaneous results at the advanced combustion stage

At the later stage of the simulation, the combustion process is in an advanced state and practically all the fuel will have evaporated. Figure 5.4 specifies the location of the plane that was use to display the temperature contours in Figure 5.5, the plane was located at Z = 10.1.
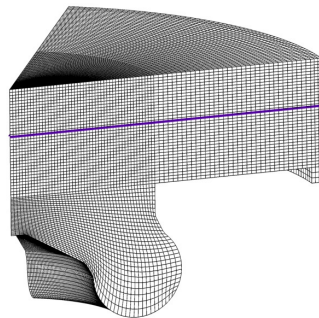
**Figure 5-4. The contour plane location at Z=10.1**

Figure 5.5 shows contours of the temperature. At 40°CA the combustion process is very well developed. Again, there is a strong contrast between RANS and LES calculations. LES shows much more wrinkled structure and influence of transient turbulence structures that penetrate into high temperature regions and affect the behaviour of the flame. With regard to differences between LES cases, the important is the unrealistic, almost vertical region of moderate temperature levels at about X=2 that is captured by LES_eps (Figure 5.5b). It looks like a discontinuity and cannot be observed in the Figure 5.5c. The large patch of high temperature region in Figure 5.5b between X=1 and X=2 can also be questionable to some extent. LES_eddy does not predict such a large and uniform region. Instead, much more irregular field is observed in that area.
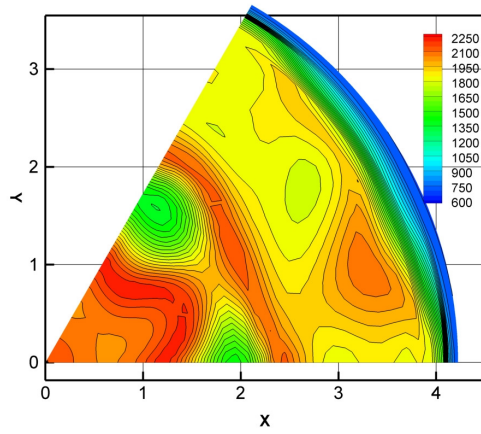
a)
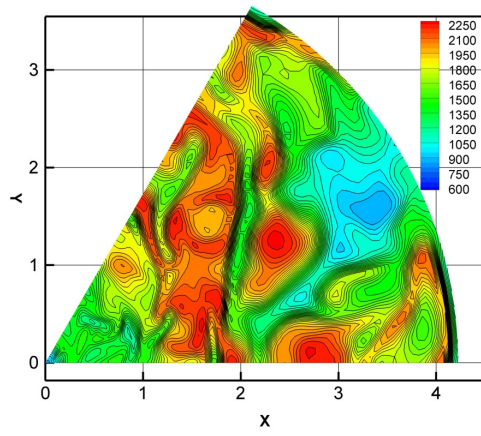
b)
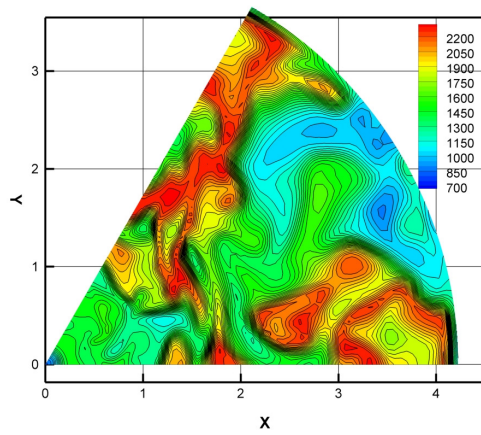
c)

Figure 5-5. Temperature contours at 40° CA [K]: a) RANS, b) LES_eps, c) LES_eddy.

This may be explained of course by the difference in chemistry modelling, but also by the more accurate prediction of the LES_eddy code with dynamically calculated filter width. There are also most likely effects of large temperature and pressure gradients modifying the flow field, although those are difficult to assess. Looking at the cylinder wall, there are further marked differences between all three cases investigated. Since the walls are cooler than the combusting gas, it would be expected that temperature distribution would to some extent reflect that. Here, the RANS case seems to capture the correct trend while at the same time over predicting the influence of cool cylinder walls. LES_eddy captures a large portion of lower temperatures in the vicinity of the wall on most of the radius, except for the regions in the corners where most likely very intense combustion process occurs.

For an insight into the temperature distribution and influence of turbulent flow field on the quality of combustion, side plots have been constructed on a plane that cuts through the middle of the 60 degree grid. Those plots are presented in the Figure 5.6. In addition to the temperature field, visualization of the flow field by means of vectors has been superimposed in the contours. Velocity levels predicted by LES are very high, especially in the region up to X=2. Reasons for this being most likely tumble flow generated by the downstream piston motion and the influence of the bowl area which augments the turbulence generation. The temperature distribution closely follows the velocity field. When we look at the Figure 5.6c at X=1.8 where two high temperature regions exist and observe the velocity field it becomes clear how the turbulent vortices are able to influence the temperature distribution and most likely flame behaviour. In this region, flame might be subjected to quenching by the strong flow and that could be the reason for separation of those two hot regions.
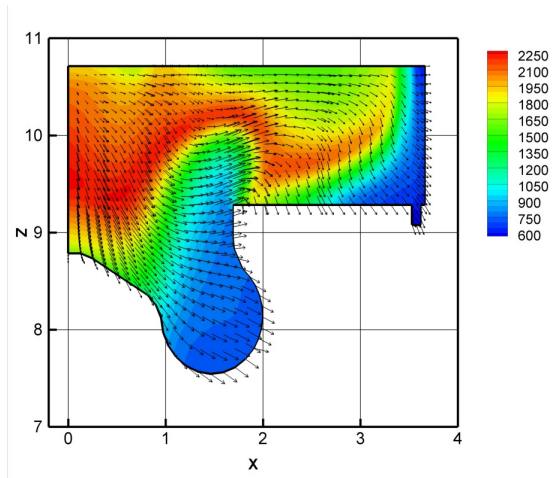
a)
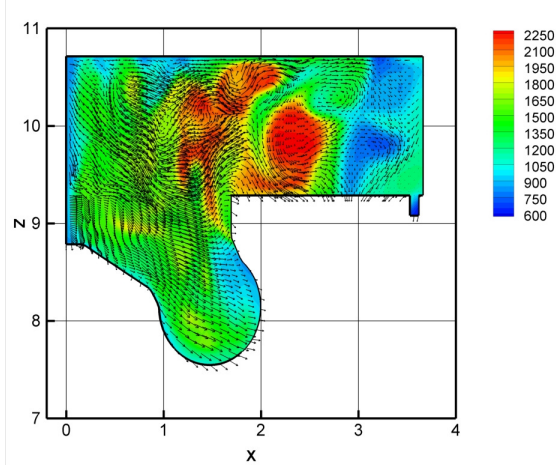
b)
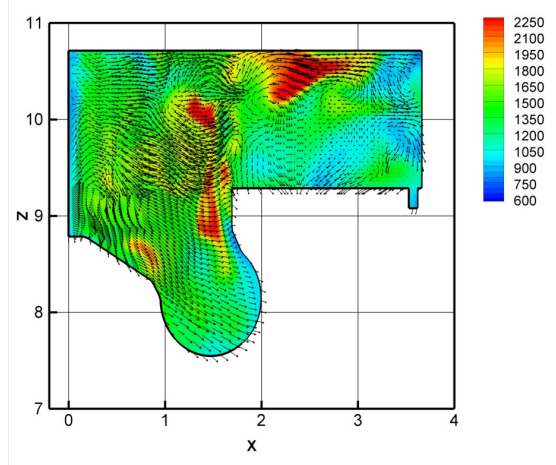
c)

Figure 5-6. Side temperature contours [K] and velocity field on a vertical plane: a)

RANS, b) LES_eps, c) LES_eddy.

In the near wall region there is a strong clockwise rotating vortex and relatively low temperatures in that region (around 1000K) could be explained by the high activity of the flow and the presence of walls. On the other hand, large temperature gradients in that area (high temperature on one side and cool walls on the other) may lead to buoyancy effects and generate additional flow motion.

Indeed, a look at the Figure 5.6b shows a very pronounced vortex at X=2.9 that is visible both when examining the velocity vectors but also when analyzing temperature field in that region. This is strong evidence that the coupling of turbulence and combustion is of twofold nature in LES. Case C (LES_eddy) captures vortices at X=2.8, Z=10.2 and X=1.9, Z=10.2 that clearly modify the shape of the high temperature front. Examining the bowl area, much higher values are predicted by LES than RANS which essentially fails to account for presence of hot gases in that region completely. From the plots in Figure 5.6 it can be established that generally high velocity of the fluid and presence of swirling transient turbulent structures profoundly influences the combustion process. Efficient mixing prediction by LES allows for constant fuel burning and oxygen supply in high temperature regions. Unfortunately, RANS simulation fails to capture those effects. The combustion process is largely decoupled from the motion of the gas phase. The latter is also much more uniform throughout the cylinder, failing to capture the unsteady vortices.

Figure 5.7 gives insight into the pressure distribution on the same plane that was used in Figure 5.6. The units are in CGS, which means that pressure is provided in dynes/cm^2. The unit range is presented in an individual manner, meaning that each of the cases has its own respective range. There are marked differences not only between RANS and LES but between performances of the two LES formulations.
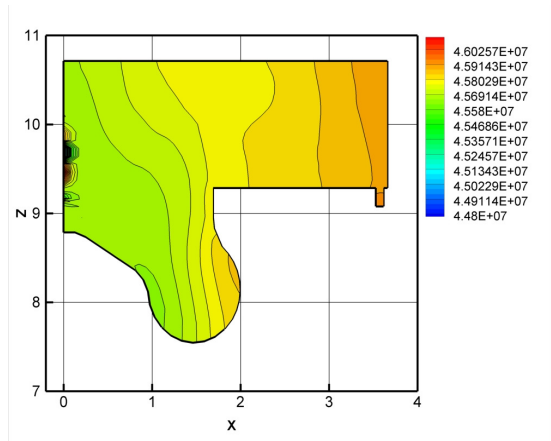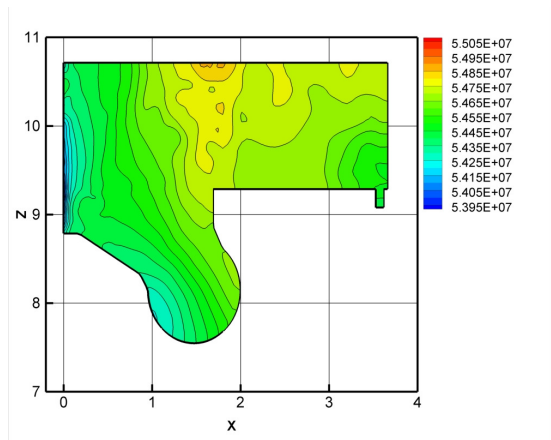
a)
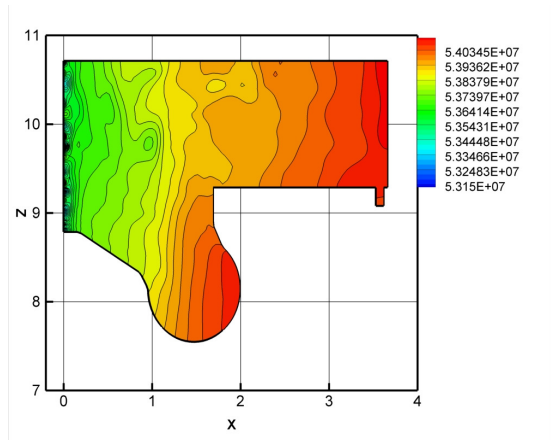
b)

c)

Figure 5-7. Pressure distribution [dynes/cm^2] on a vertical plane: a) RANS, b) LES_eps,

c) LES_eddy.

Pressure prediction is very important for comparison with experimental data and gives a very good insight into the actual performance of the model. Section 5.3.4 will elaborate on this in detail. The pressure prediction is markedly different for all three cases and this is where the LES_eddy case again proves to be superior. The distribution of pressure values in Figure 5.7c is most realistic and follows the temperature distribution. When we look at the Figure 5.6c it can be observed that high temperature regions correspond exactly to the pressure values in the domain (Figure 5.7c). Area with the centre in X=1.9 and Z=10.5 can be distinguished in both Figures. Overall, the distribution is more realistic than cases other two cases. The poor performance of RANS is augmented by the fact that the pressure values are significantly under-predicted. LES_eps gives better quantitative results but the distribution is not very realistic and quite decomposed from the temperature field. The RANS and LES_eps show strange vertical "segmentation" of the pressure contours which does not look realistic. Especially LES_eps with its large gradients throughout vertical direction of the domain does not appear to be accurate. It is clear that the prediction of pressure is best with the LES_eddy model with smaller gradients and in general more uniform distribution that reflects both the temperature and flow fields.

5.3.3   Instantaneous results at the final combustion stage

In this sub-section, snapshots of the temperature with corresponding velocity vectors taken at the 80° after TDC will be presented. This is the final stage of combustion, fuel in liquid state is not present in the system anymore, and the amount of diesel vapour is close to zero. There is no additional heat release. The vertical plane for contours shown in Figure 5.8 is placed at

30° (middle of the domain). Extensive differences between LES and RANS are again apparent.

RANS still predicts regions with unrealistically low temperature of around 600K (the bowl area and lower portion of the cylinder wall). Those are not present in either of the LES cases. The whole flow and temperature RANS-calculated field is diffused and lacks the presence of unsteady structures. The velocity values are significantly smaller in the RANS case (vector length is scaled by the velocity magnitude) and flow is again largely decoupled from the combustion process. Regions of high temperature do not correspond to the velocity at all. LES cases seem to perform much better, as it was the case at the earlier crank angles. Figure 5.8b does show an interesting region of high temperature at the top of the piston (Z=6.3). It is unlikely that in real engine configuration we would encounter intensive fuel burning in such area right next to the wall. LES_eddy (Figure 5.8c) does not detect any increased temperature region there. Instead, burning still occurs roughly in the middle of the domain which is believed to be more realistic. At Z=8, X=0.5 there is a very interesting structure in the temperature field resembling a typical vortex. Its presence is reflected by the velocity vectors again confirming that the coupling of turbulent effects and flame propagation is of two way nature. If we compare Figure 5.8b with Figure 5.8c we may notice that the temperature contours are slightly less wrinkled in the new LES case. This is due to the fact that the combustion process is at the more advanced stage which is more in accordance with experimental data.
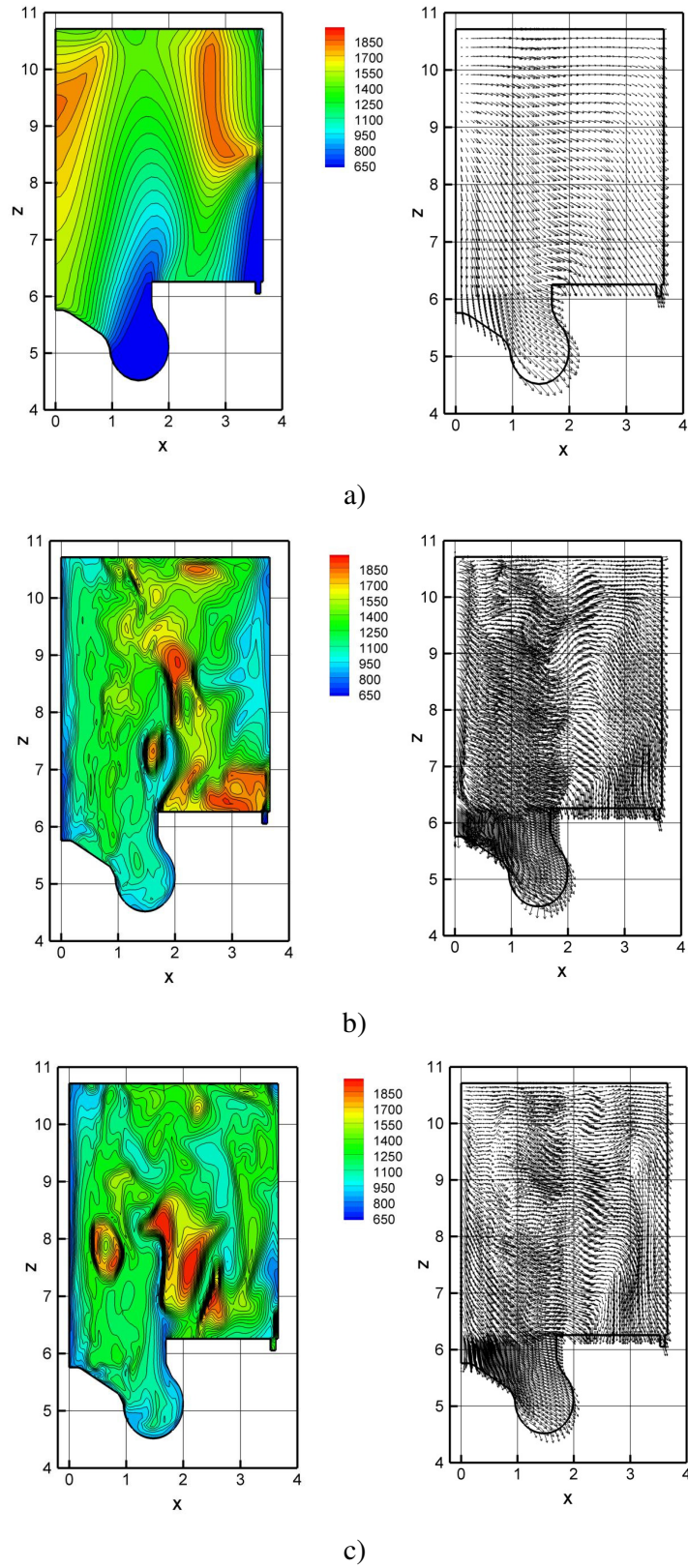
Figure 5-8. Temperature contours [K] and velocity vectors at 80°: a) RANS, b) LES_eps,
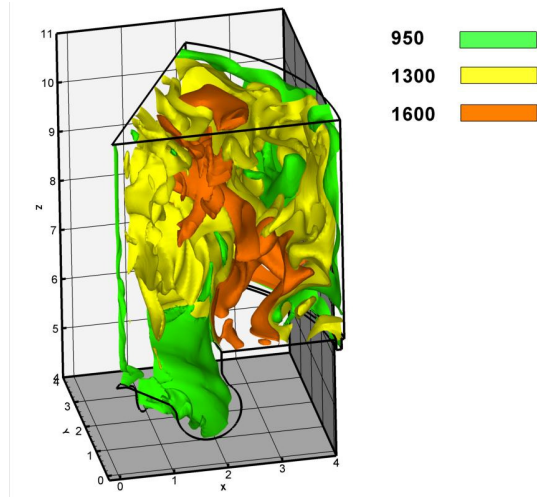
c) LES_eddy.

This will be confirmed in Section 5.3.4 where heat release rate will be analyzed. Moreover, high temperature regions are concentrated in the middle of the domain, without scattering throughout the whole cylinder as in LES_eps. At this final stage of combustion it is believed that having burning region concentrated in the middle of the domain is a more realistic representation of the actual process.

For a more detailed examination of the concentration of high, medium and low temperature regions, three dimensional plots have been constructed and plotted in Figure 5.9. They show ISO-surfaces of 950K, 1300K and 1600K. The already mentioned highly unsteady character of the flow and interaction of flame and turbulence of LES are in stark contrast to the diffused field shown by RANS. LES predicted field is both a consequence of the presence of turbulent structures, some of them created by the expansion stroke and to some extent by the strong density changes due to the ongoing reaction process.

Instantaneous data, while very important in terms of giving an overview of the combustion process, should always be backed up by the averaged data across the engine volume and cycle. This is crucial in terms of predicting pressure throughout the cycle which can then be compared with experimental data taken from a real engine configuration. Next Section will present analysis of the model performance in terms of predicting space averaged values.
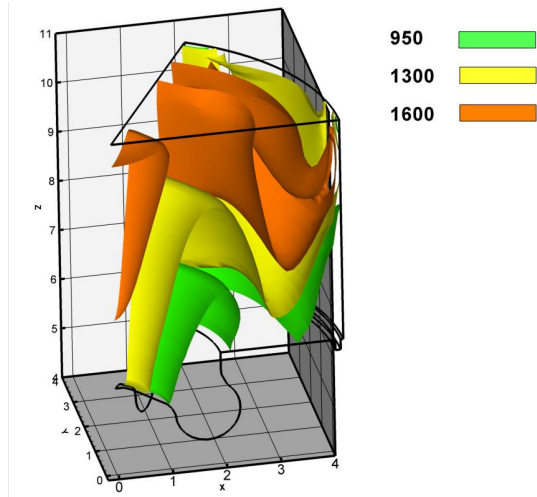
a)

b)
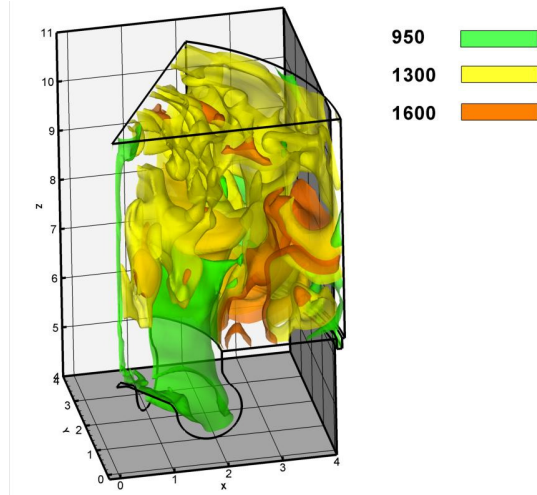
c)

Figure 5-9. Iso-surfaces of temperature [K]: a) RANS, b) LES_eps, c) LES_eddy.

5.3.4 Comparison of averaged data with experimental results

This section will focus on assessing the performance of the RANS and two LES models when compared with experimental data. In addition to that, a mesh sensitivity study has been performed for two LES cases to investigate sensitivity of the results to the mesh size. Some very interesting results have been obtained. While some LES studies have been performed with regard to non-reacting flow-field and mesh resolution dependence (Vreman et al., 1996), (Meyers et al., 2003), (Prière et al., 2005), the performance of the combustion models with respect to mesh size within LES framework is scarce in the literature. Recently Boudier et al. (2008) conducted a study of reacting LES on mesh size dependence and found out that RMS of temperature is quite sensitive to the grid resolution while at the same time velocity values are comparable for different grids.

Figure 5.10 shows pressure distribution throughout most of the engine cycle for different cases along with experimental data obtained from Delphi Diesel Systems. It must be noted that strictly speaking the mesh sensitivity study concerns LES only, as RANS should produce grid independent results when the resolution is sufficient. This was confirmed earlier on and appropriate RANS mesh was used. In addition to that, the aim of the Thesis is focused on detailed investigation of LES and its improved modelling procedures. Therefore all the subsequent Figures show a single resolution RANS simulation at a reached grid-independent state. This would indicate the possible improvements by LES with respect to the best possible results obtained by RANS method.
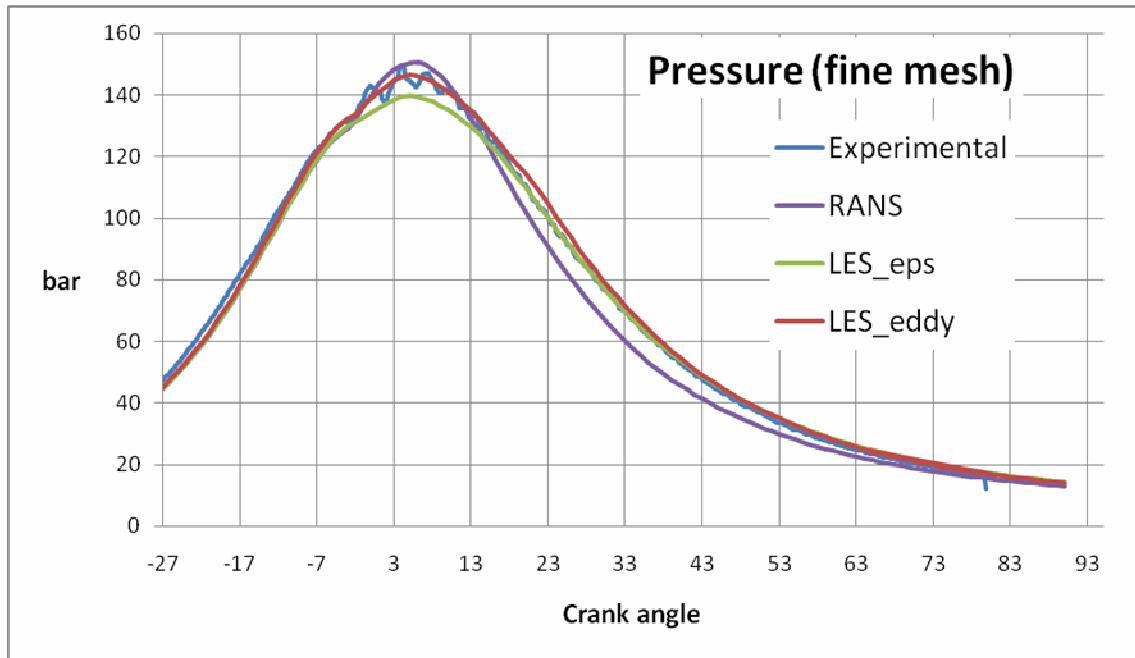
a)
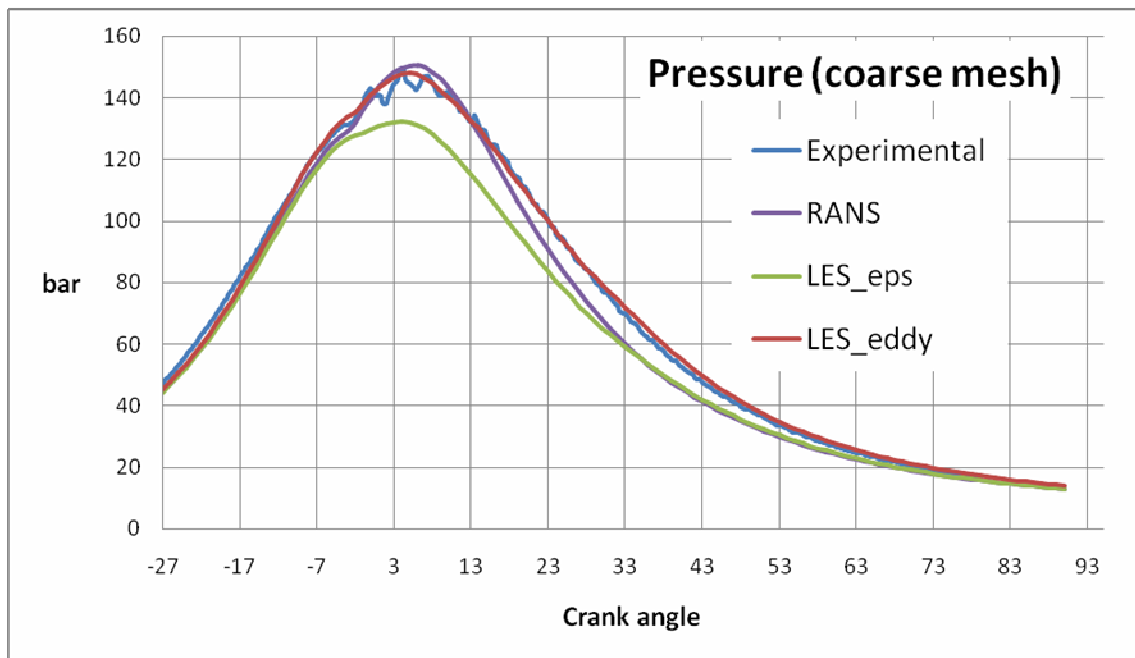
b)

Figure 5-10. Pressure in the cylinder for LES, RANS and experimental data: a) fine mesh, b) coarse mesh.

From Figure 5.10a it is evident, that the updated LES model has a very good agreement with experimental pressure traces throughout the engine cycle. The prediction just after the top dead centre where combustion process is developing quickly is spot on. The only visible discrepancy is between 20°and 30° where the model slightly over-predicts the pressure

Interestingly, this is also the area where LES_eps performs best giving good agreement with the experimental curve. In general, LES_eps performs worst when the piston is near Top Dead Centre. Reason for this is of twofold nature. First of all, the ad-hoc specified filter width is most likely not suitable for the mesh at the top dead centre and as a result performance of the subgrid stress tensor model may be compromised. This would directly influence production of subgrid kinetic energy and consequently estimation of its rate of dissipation. Old combustion model in LES_eps formulation relies on dissipation to estimate turbulent timescale. Hence the performance in areas where mesh/filter width correlation is poor is severely compromised. The prediction by RANS is still worse with peak pressure over-predicted and under-prediction at later crank angles. The shape of the curve least resembles the experimental data.

An examination of Figure 5.10b where results performed on coarse mesh are plotted reveals even more pronounced differences. The agreement of LES_eddy is very good and virtually not influenced by the mesh resolution. This is very important in terms of real life industrial applications, where mesh for LES always tends to be too coarse and the size is limited by either hardware or calculation time. In such circumstances it is crucial that the combustion model still gives good agreement with experiment. As can be se in Figure 5.10b, the LES_eps curve gives very poor prediction on the coarse mesh. Near the peak, the pressure is under-estimated by over 20 bars, rendering the results useless for any trustworthy analysis.
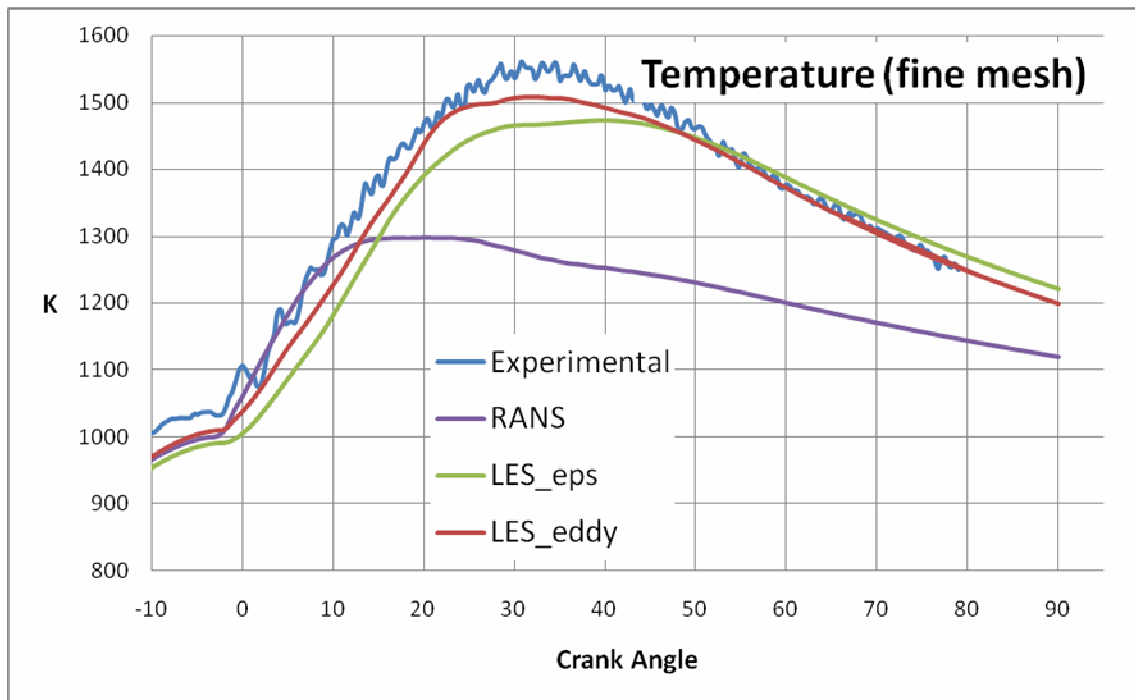
a)
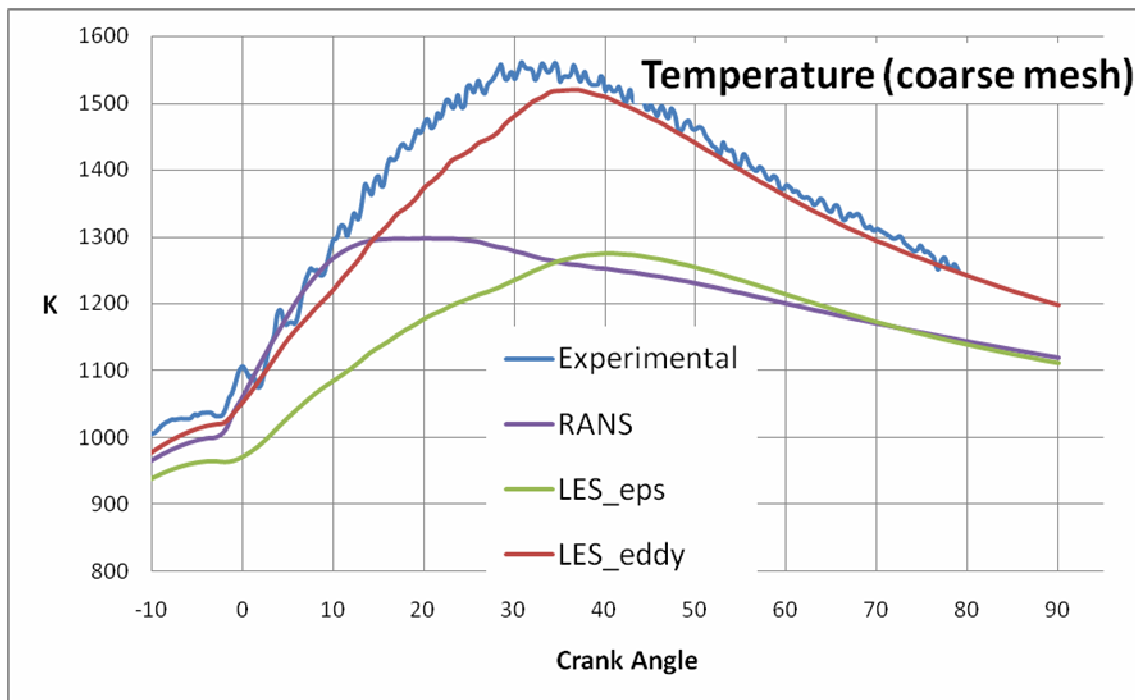
b)

Figure 5-11. Temperature in the cylinder for LES, RANS and experimental data: a) fine mesh, b) coarse mesh.

The agreement before injection start at -3.5° ATDC is good for all cases, however as soon as ignition occurs, the LES_eps curve tapers off failing to reach the values of experimental and LES_eddy values. A look at the values of temperature in cylinder should provide us with additional feedback regarding the performance of the models.

Figure 5.11 presents temperature in the cylinder with respect to crank angle, again for fine and coarse mesh sets. As expected, the differences between results confirm those established on the basis of pressure plots. The best overall agreement is again presented by the LES_eddy model. Although even on the fine mesh (Figure 5.11a) LES_eddy slightly under-predicts temperature up to 50K the overall qualitative agreement is very good. This small difference is probably easily remedied by some constants adjustments within the combustion model. When new code was used in conjunction with low resolution mesh (Figure 5.11b) the shape of the curve still reflected very well the experimental results. Interestingly, for the LES_eddy case, the agreement is very good from about 50° onwards. The only visible discrepancies exist in the region of most intensive combustion process (up to approximately 40°). It is especially evident on the coarse mesh where the difference with respect to experiment can reach up to 100K. Analysis of the LES_eps shows clearly that the model has a much poorer performance regardless of the mesh size. Results from coarse mesh show massive under-prediction of more than 200K suggesting clearly that RANS-developed CTC model cannot be used in LES without the necessary modifications. Again, the great sensitivity of the LES_eps to mesh resolution is a deciding factor. Bearing in mind the mentioned constraint of LES in industrial applications, where basically every mesh is under-resolved, the limitations of the LES_eps formulation are obvious. The LES_eddy although suffering slightly between 0° and 40° in terms of accuracy due to the changed mesh, is nevertheless much more able to cope with grid resolution limitations.

There is a difference between crank angle where the peak of pressure and temperature occur in Figure 5.10 and 5.11. One has to bear in mind that only volume averaged data is shown. In addition to that, the heat release at later crank angles is still very intense as was confirmed by Figure 5.5, where many patches of very high temperature of over 1800K are still present. The combination of heat release, heat transfer and volume change determine the peak pressure and after that the ongoing reaction process and volume change can still increase temperature (Heywood, 1988). In addition to that, the injection duration is very long (30° CA) and that accounts for the specific temperature distribution and heat release. Figure 5.12 shows heat release rates in Joules per crank angle. We can see that the experimental data as well as simulation results show peak at around 20° and heat release continues up until around 80° CA.
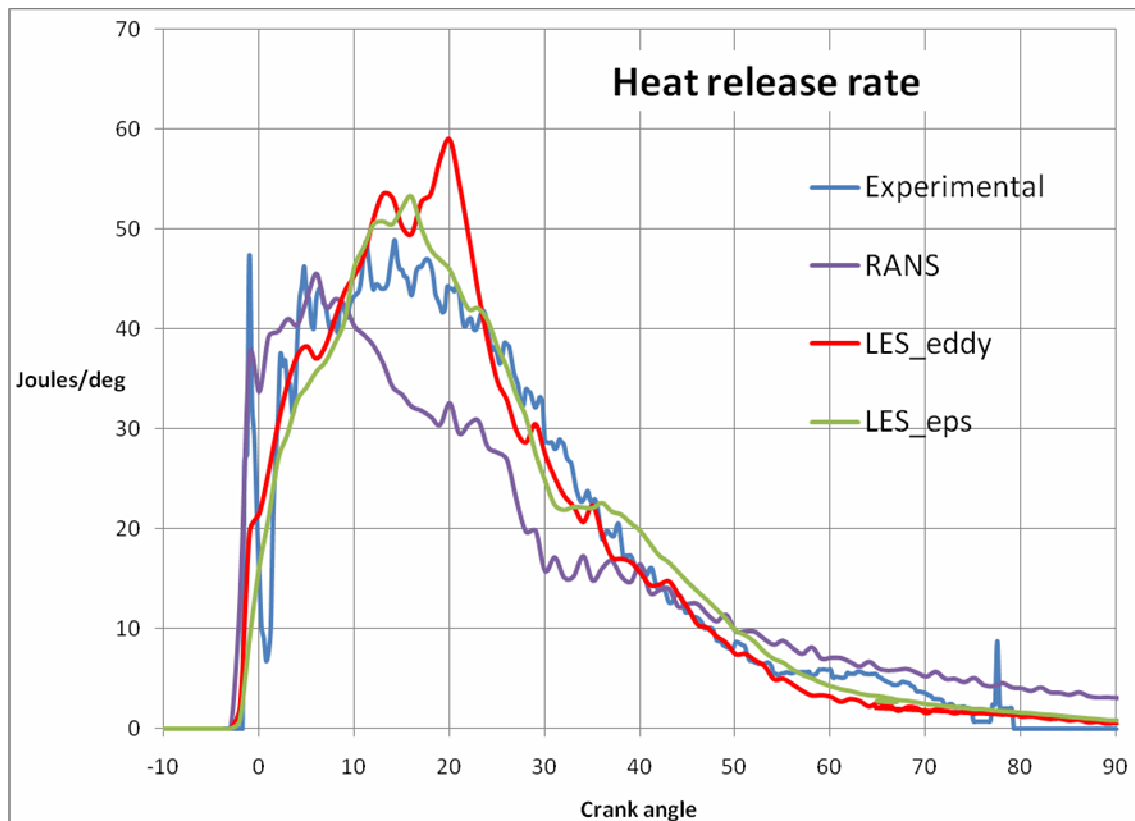

**Figure 5-12 Heat release rates for LES, RANS and experimental data.**

It is necessary to give more information on why the models give poorer prediction in the region of intensive chemical heat release region. Since the heat release occurs at the molecular scales, all the reaction modelling effectively takes place at the subgrid scales. Therefore the mesh resolution has most influence on those results. Dense grids are able to directly resolve more turbulent structures and heat release and are less dependent on modelling. Increase in resolution is therefore likely to reveal more flame wrinkling and lead to accurate predictions of the combustion process. This is proved by the progress of LES_eddy curves between 0° and 40° where agreement is much better when dense mesh is used.

Finally, an analysis of accumulated heat release will be conducted. This is an important quantity as RANS has difficulties with estimating the correct trend, let alone correct values. Accumulated heat release depends largely on the correct prediction of spray structure, rate of evaporation and distribution of fuel vapour mass fractions. Those quantities then directly affect the combustion rates. Based on the findings described in Chapter 4, where it was found that LES is much more capable of accurate liquid spray and vapour penetration predictions it is expected that this will be reflected in the accumulated heat release rate analysis. Figure 5.13 shows results for LES_eps code, LES_eddy code, experimental data and reference RANS.

One of the important aspects is that the heat release must stabilize after the combustion process is completed. This is reflected in the experimental curve where at 80° there is no more rise and the values remain constant. RANS results fail to capture the trend, under-predicting throughout the engine cycle bar the initial stage of combustion between 0° and 18°. What is also important is that the curve does not reach steady state. The LES gives much better agreement.
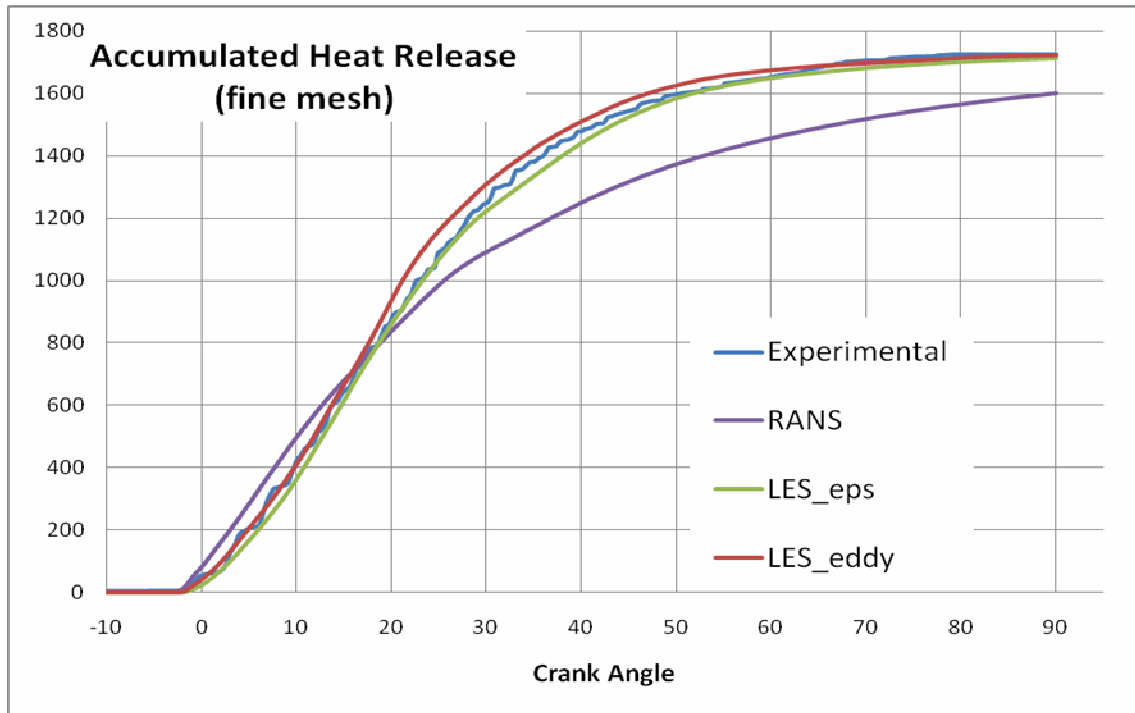
a)
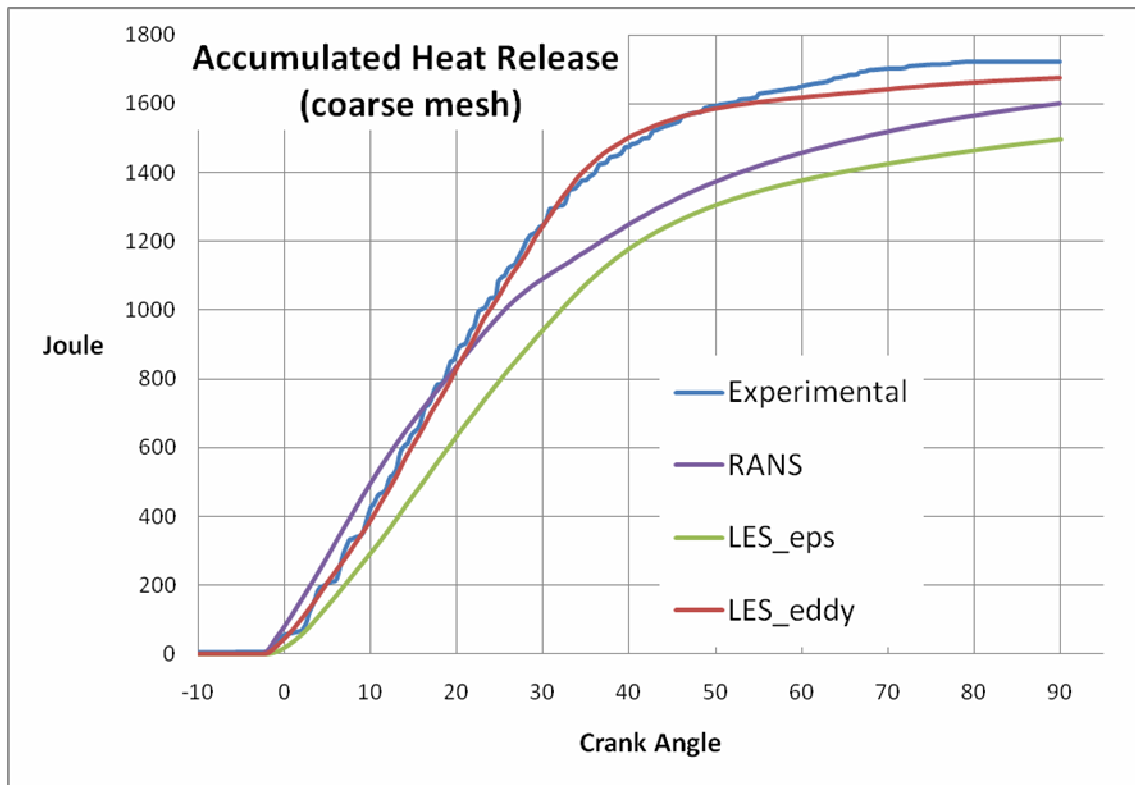
b)

Figure 5-13. Accumulated heat release rate: a) fine mesh, b) coarse mesh.

The relatively good performance of the LES_eps model in Figure 5.13a is more than offset when we look at the Figure 5.13b. Computations on coarse mesh again reveal the impact of mesh resolution on the LES_eps model abilities. At the end of combustion the discrepancy reaches 200 Joules and no steady state is achieved. Even RANS calculations give better quantitative agreement, although the shape of the curve is better matched by both LES results.

With respect to coarse mesh computation, the LES_eddy model predicts the accumulated heat release very well up to a value of approximately 50°. After that the values are lower than experimental. Also, the steady state is reached later than it was the case when dense mesh was used. However, bearing in mind large difference in resolution, the agreement of the LES_eddy is very encouraging. This means that when care is taken, LES could be attempted for real engine configurations even on a mesh that is equal to the resolution of RANS (under the condition that RANS solution had reached mesh-independent state). Obviously, the postulate of using as fine mesh as possible is still valid. Same cannot be said of previous LES formulation that is very sensitive to mesh resolution and even for large node numbers, the agreement is not on par with the LES_eddy.

5.4   Concluding remarks

This Chapter investigated in detail the performance of a new LES modelling procedure, with modified treatment for scale range separation and improvements to the characteristic timescale combustion model that allowed successful simulations of two phase reacting flow. Real engine configuration was used and both averaged and instantaneous data were carefully analyzed. Reference RANS simulation was also performed to study the improvements and capabilities of LES that are beyond reach of time averaged methods. Finally, careful

validation using available experimental data was performed to support the claims of LES superiority when predicting unsteady, two-phase reacting flows. The analysis confirmed that LES is capable of showing time dependent turbulent structures that directly influence the distribution of temperature in the cylinder. By avoiding time averaging, existence of vortical structures was found that corresponded directly to the flame propagation. The LES_eddy was also able to capture the pressure differences due to the vorticity in the flow field, something old formulation was limited at. Comparison with experiment confirmed good ability of the new LES models to predict volume averaged pressure, temperature and accumulated heat release values throughout the engine cycle. Much better qualitative and quantitative agreement was achieved than that obtained using RANS method. Additionally, mesh dependence study was conducted, further highlighting the strengths of the LES_eddy model. While old formulation gave very poor results when the resolution was decreased, the updated model has shown remarkably small mesh dependence. It was found that temperature curve is mostly affected by the resolution decrease. This was attributed to the fact that combustion occurs almost exclusively at the smallest scales. Therefore dense mesh can capture more small structures directly which would otherwise be modelled in the subgrid scales.

This had a direct impact on temperature values, both in terms of flame wrinkling and more realistic chemistry modelling.

Overall, the new LES formulation has shown a marked improvement over RANS in terms of ability to capture instantaneous data, and equally importantly, prediction of volume averaged quantities.

6   Conclusions and Future Work

6.1   Concluding remarks

The work presented here concentrated on applying large eddy simulation technique to a complex, two phase reacting flows that are present in industrial configurations. This task was accomplished in clearly outlined steps which would allow gradual development and what is more important, detailed investigation of issues and limitations that needed addressing.

The performance of the original LES version of the KIVA3V code was assessed by studying the behaviour of a liquid annular jet issuing into a high pressure domain with varying amount of initial gas-phase swirl. Strong dependence of the jet structure on swirl number was found. The high swirl number case had limited downstream penetration, while the radial penetration and air entrainment were increased comparing to low or non-swirling cases. Turbulent structures that are exclusive to an annular jet were captured by the code and included the stagnation point, reversed flow and head vortices. Generation of those was attributed to the existence of two liquid shear layers (inner and outer) that are in vicinity of each other. Overall, the code was able to capture highly instantaneous data and turbulent structures whose existence was earlier confirmed by Researchers.

A detailed study on fuel mixing and atomization was then conducted in a non-reacting environment and compared to RANS simulation of exactly the same configuration. It was found that LES predicts much higher spray (both vapour and liquid) penetration into the domain that subsequently influences the quality of mixing. The effect of initial swirl in the cylinder was very well captured by the LES, acting both on the liquid and gas phases of the fuel. The turbulent structures present in the domain had a profound impact on the jet. In

contrast, RANS predicted liquid jet structure and vapour concentration appeared decoupled from the flow field and driven almost exclusively by the initial injection parameters. The images from experimental rig confirmed that LES is able to accurately reproduce the shape and penetration of the spray. Mesh sensitivity study performed for LES showed that refining the mesh reveals more detail in the flow field and vapour phase distribution. Analysis of the droplet radius in the cylinder during the injection process showed a big improvement with increased mesh size, the code predicting much finer droplets. LES performed on coarse mesh predicted presence of significantly higher radiuses, suggesting that when LES on coarse mesh is attempted, some adjustments of the breakup constants might be necessary.

Finally, after careful code validation reacting simulations of an engine configuration were attempted. Modifications to the existing LES scheme and combustion model were performed. The former ensured that the subgrid kinetic energy levels are as accurate as possible, without introducing averaging; the latter ensured that the reaction modelling is compatible with updated LES scheme. Changes to the LES code guaranteed that the filter width is explicitly calculated for each computational cell, not specified in an *ad-hoc* manner. Combustion model was presented with different formula of turbulent timescale that was suitable for LES.

Encouraging results were obtained, with the new LES code giving a very good agreement with experimental data. It was found that the new formulation is much less sensitive to the mesh resolution than the old LES code which gave poor results on a coarse mesh. This is crucial to industrial applications, as generally LES mesh tends to be under resolved and governed by the available computational resourced and/or calculation time. It was shown that under certain circumstances, RANS mesh (provided it reached mesh-independent state) might be used for basic LES calculations and still give a good insight into averaged data like temperature, pressure or heat release. Caution must however be taken, as some constants may

need additional adjustments (especially for the breakup models) and it is always advisable to use finest mesh possible, as the LES accuracy is increased. Especially temperature prediction in the reacting simulations benefits from smaller cell element size as the combustion occurs at smallest scales. Ability to capture instantaneous turbulent structures also increases greatly with smaller element size.

Overall, it was proved that LES is a viable and promising tool for simulation of complex two-phase reacting flows and can in certain circumstances compete with the well established RANS formulations giving superior results.

6.2   Further recommendations

Additional development in specific areas is without a doubt necessary. Wall treatment in LES is an area where much research is needed, especially with regard to internal combustion engine applications where effects like spray impingement, heat transfer to the walls and influence of the strong swirl are very important. Near wall region cannot be directly resolved by LES due to the mesh constraints and this makes development of LES specific wall functions even more necessary. Current estimation of the wall heat transfer using turbulent kinetic energy results in under-prediction of the wall cooling effect.

Subgrid models for droplet evaporation are also scarce and need much more development. Especially treatment of the dense sprays and fine droplets is crucial as injection pressures are very high and correct prediction of droplet breakup and atomization necessary for accurate heat release rates and emissions predictions.

Finally, state of the art subgrid combustion models like subgrid PDF, Linear Eddy Model or CMC (Conditional Moment Closure) need to be carefully looked at and possibly employed in the code. This would further increase the ability to predict heat release rates. Especially the Linear Eddy Model appears to be promising and is well suited to the subgrid formulation and subgrid species transport as well as chemistry.

Pollutant formation is another challenging problem in numerical simulations (not limited to LES) and work is needed before we can obtain trustworthy results of soot prediction and NOx emissions.

Those goals however cannot be achieved without parallelization of the code, as memory and CPU limitations of single processor put a severe constraint on modelling possibilities and especially mesh size.

References

Abraham, J., Bracco, F.V., Reitz, R.D., 1985. Comparisons of Computed and Measured Premixed Charge Engine Combustion. *Combustion and Flame*, 60, pp. 309-322.

Almeida, T.G., Jaberi, F.A., 2008. Large-eddy simulation of a dispersed particle-laden turbulent round jet. *International Journal of Heat and Mass Transfer*, 51, pp. 683-695.

Amsden, A. A., 1993. KIVA-3: A KIVA Program with Block-Structured Mesh for Complex Geometries, LA-12503-MS (March 1993), Los Alamos National Laboratory.

Amsden, A.A., 1997. *A Block-Structured KIVA Program for Engines with Vertical or Canted Valves*. Los Alamos National Laboratories

Apte, S.V., Gorokhovski, M., Moin, P., 2003. LES of atomizing spray with stochastic modeling of secondary breakup. *International Journal of Multiphase Flow*, 29(9), pp. 1503-1522.

Apte, S.V., Mahesh, K., Gorokhovski, M. and Moin, P., 2009. Stochastic modeling of atomizing spray in a complex swirl injector using large eddy simulation. *Proceedings of the Combustion Institute.*

Auriemma, M., Corcione, F. E., Valentino, G., 1998. Interpretation of air motion in reentrant bowl in-piston engine by estimating Reynolds stresses. *SAE Technical Paper*, SAE 980482.

Befrui, B., Corbinelli, G., Robart, D., Reckers, W. 2008. LES Simulation of the Internal Flow and Near-Field Spray Structure of an Outward-Opening GDI Injector and Comparison with Imaging Data. *SAE Technical Paper*, 2008-01-0137.

Birouk, M., Gokalp, I., 2006. Current status of droplet evaporation in turbulent flows. *Progress in Energy and Combustion Science*, 32, p. 408-423.

Boris, J.P., Grinstein, F. F., Oran, E. S., Kolbe, R. L. 1992. New insights into large eddy simulation. *Fluid Dyn Res.*, 10, pp. 199-228.

Boudier, G., Gicquel, L. Y. M., Poinsot, T. J. 2008. Effects of mesh resolution on large eddy simulation of reacting flows in comlex geometry combustors. *Combustion and Flame,* Vol. 155, pp. 196-214.

Bray, K.N.C., 1996. The challenge of turbulent combustion. *Proceedings of the Combustion Institute*,. pp.1-26.

Calhoon, W.H., 1996. *On subgrid combustion modeling for large-eddy simulations*. PhD Thesis. Georgia Institute of Technology

Camarri, S., Salvetti, M. V., Koobus, B., Drevieux, A., 2004. A low-diffusion MUSCL scheme for LES on unstructured grids. *Computers & Fluids*, 33(9), pp. 1101-1129.

Candel, S., 2002. Combustion dynamics and control: progress and challenges. *Proceedings of the Combustion Insitute*,. pp.1-28.

Caraeni, D., Bergstroem, C. & Fuchs, L., 2002. Modeling of liquid fuel injection, evaporating and mixing in a gas turbine burner using large eddy simulation. *Flow, Turbulence and Combustion*, 65, p. 223-244.

Chan, W. T., Ko, N. W. M., 1979. The inner regions of annular jets. *Journal of Fluid Mechanics,* Vol. 93, Issue 03, pp. 549-584.

Chen F., Tsaur, J., Durst, F., Das, S. K., 2003. On the axisymmetry of annular jet instabilities. *Journal of Fluid Mechanics,* Vol. 488, pp. 355-367.

Chigier, N, Reitz, R.D., 1996. Regimes of jet break-up and break-up mechanisms (physical aspects). *Recent Advances in Spray combustion: Spray Aromization and Drp Burning Phenomena*,.

Del Taglia, C., Blum, J., Gass, J., Ventikos, Y., Poulikakos, D. 2004. Numerical and experimental investigation of an annular jet flow with large blockage. *Journal of Fluids Engineering,* Vol. 126, pp. 375-384.

Devesa, A., Moreau, J., Poinsot, T., 2004. Large Eddy Simulations of Jet/Tumble Interaction in a GDI Model Engine Flow. *SAE paper*, 2004-01-1997.

De Villiers, E., Gosman, A.D. & Weller, H.G., 2004. Large Eddy Simulation of Primary Diesel Atomization. *SAE Technical paper*, SAE 2004-01-0100.

Deardfoff, J.W., 1970. A numerical study ofthree-dimensional turbulent channel flow at large Reynolds numbers. *Journal of Fluid Mechanics*, 41, p. 453-480.

Dinkelacker, F. et al., 1998. Structure of locally quenched highly turbulent lean premixed flames. *Proceedings of the Combustion Institute*,. pp.857-865.

Domaradzki, J.A., Saiki.E. M., 1997. Backscatter Models for Large-Eddy Simulations. *Theoretical and Computational Fluid Dynamics*, 9, p. 75-83.

Erlebacher, G., Hussaini, M.Y., 1992. Towards the large-eddy simulation of compressible turbulent flows. *Journal of Fluid Mechanics*, 238, pp. 155-185.

Faeth, G.M., Lazar, R.S., 1971. Fuel droplet burning rates in a combustion gas environment. *AIAA Journal*, 9, p. 1593-1612.

Faeth, G.M., 1987. Mixing, Transport and Combustion in Sprays. *Progress in Energy and Combustion Science*, 13(4), p. 293-345.

Ferziger, J., 1983. *Higher-level simulations of turbulent flows.*: Hemisphere Publishing Corporation, Washington.

Froehlich, J., Rodi, W., 2002. *Closure strategies for turbulent and transitional flows*. Cambridge: Cambridge University Press.

Fureby, C., 1996. On subgrid scale modelling in large eddy simulations of compressible fluid flow. *Physics of Fluids*, 8, p. 1301-1311.

Garcia-Villalba, M., Froehlich, J. & Rodi, W., 2006. Identification and analysis of coherent structures in the near field of a turbulent unconfined annular swirling jet using large eddy simulation. *Physics of Fluids*, 18(055103).

Gelfand, B.E., 1996. Droplet break-up phenomena in flows with velocity lag. *Progress in Energy and Combustion Science*, 22, p. 201-265.

Gorokhovski, M.A., 2001. The stochastic Lagrangian model of drops breakup in the computation of liquid sprays. *Atomization Sprays*, 11, p. 505-520.

Haenlien, A., 1932. Disintegration of a liquid fuel. *NACA TM 659*.

Haworth, D.C., 1999. Large-eddy simulation of in-cylinder flows. *Oil and Gas Sci. Technology Rev.*, 54(2), pp. 175-185.

Haworth, D.C., Jansen. K., 2000. Large-eddy simulation on unstructured deforming meshes: towards reciprocating IC engines. *Computers & Fluids*, 29, p. 493-524.

Heywood, J., B. 1988. Internal Combustion Engine Fundamentals. Mc-Graw Hill.

Hori, T., Kuge, T., Senda, J., Fujimoto, H., 2008. Effect of Convective Schemes on LES Fuel Spray by Use of KIVALES. In *Diesel Fuel Injection and Sprays2008*. SAE 2008-01-0930

Itoh, Y., Tanigucchi, N. & Kobayashi, T., 2003. Numerical Prediction of Vaporizing Spray by using Large Eddy Simulation in Swirling Flows. In *The 5th Asian Comp. Fluid Dynamics Conf.* Busan.

Jagus, K., Jiang, X., Zhao, H., Dober, G., Greeves, G., Milovanovic, N., 2008. Annular fuel jet in a swirling/non-swirling diesel environment. 5th European Thermal-Sciences Conference. Netherlands.

Jagus, K., Jiang, X., Dober, G., Greeves, G., Milanovic, N., Zhao, H., 2009. Assessment of large eddy simulation feasibility in modelling the unsteady diesel fuel injection and mixing in a high speed direct injection engine. Proceedings of the Institution of Mechanical Engineers, Part D. Volume 223, Number 8, pp. 1033-1048.

Jhavar, R., Rutland, C. J., 2006. Using large eddy simulations to study mixing effects in early injection diesel engine combustion. *SAE paper, 2006-01-0871*

Kerstein, A.R., 1988. A linear-eddy model of turbulent scalar transport and mixing. *Combustion Science and Technology*, 60, p. 391-421.

Kerstein, A.R., 1992. Linear-eddy model of turbulent transport 4. Structure of diffusion-flames. *Combustion Science and Technology*, 81, p. 75-96.

Kimura, S., Kosaka, H., Matsui, Y., Himeno, R., 2004. A numerical simulation of turbulent mixing in transient spray by LES (comparison between numerical and experimental results of transient particle laden jets). *SAE Transactions*, 113(4), p. 1492-1500.

Kolmogorov, A.N., 1991. The local structure of turbulence in incompressible viscous fluid for very large Reynolds numbers. *Proceedings: Mathematical and Physical Sciences*, 434, pp. 9-13.

Kong, S. C., Han, Z., Reitz, R. D., 1995. The Development and Application of a Diesel Ignition and Combustion Model for Multidimensional Engine Simulation. *SAE Technical Paper,* No. 950278.

Lee, D., Pomraning, E., Rutland, C.J., 2002. LES modeling of Diesel Engines. *SAE Paper 2002-01-2779*.

Leonard, A., 1974. Energy cascade in large eddy simulations of turbulent fluid flows. *Advanced Geophysics*, 18A, p. 237.

Lesieur, M., Metais, O., Compte, P., 2005. *Large-eddy simulations of turbulence.* Cambridge: Cambridge University Press.

Lin, S.P., Reitz, R.D., 1998. Drop and spray formation from a liquid jet. *Annual Rev. Fluid Mechanics,*. pp.85-105.

Liu, A.B., Mather, D., Reitz, R.D., 1993. Modelling the Effects of Drop Drag and Breakup on Fuel Sprays. *SAE Paper*, SAE 930072.

Lumley, J.L., 1999. *Engines: an introduction*. Cambridge: Cambridge University Press.

Magnussen, B.F., Hjertager, B.H., 1976. *On mathematical modelling of turbulent combustion with special emphasis on soot formation and combustion*. Proceedings of the Combustion Insitute.

Meneveau, C., Lund, T. S., Cabot, W. H., 1996. A Lagrangian dynamic subgrid-scale model of turbulence. *Journal of Fluid Mechanics*, 319, pp. 353-385.

Menon, S., Calhoon, W., 1996. Subgrid mixing and molecular transport modelling for large-eddy simulations of turbulent reacting flows. *Proceedings of the Combustion Institute*,. pp.59-66.

Menon, S., McMurtry, P.A. & Kerstein, A.R., 1993. In *LES of complex engineering and geophysical flows*.: Cambridge University Press. p. 287-314.

Menon, S., Patel, N., 2006. Subgrid modeling for simulation of spray combustion in large-scale combustors. *AIAA Journal*, 44, pp. 709-723.

Menon, S., Yeung, P., Kim, W., 1996. Effect of subgrid models on the computed interscale energy transfer in isotropic turbulence. *Computers and Fluids*, 25, p. 165-180.

Meyers, J., Geurts, B. J., Baelmans, M. 2003. Database analysis of errors in large-eddy simulation. *Physics of Fluids,* Volume 15, No. 9 pp. 2740-2755.

Miller, R.S., Bellan, J., 1999. Direct numerical simulation of a confined three-dimensional gas mixing layer with one evaporating hydrocarbon-droplet-laden stream. *Journal of Fluid Mechanics*, 384, p. 293-338.

O'Rourke, P.J., Amsden, A.A., 1987. The TAB method for numerical calculation of spray droplet breakup. *SAE Paper*, SAE Paper 872089.

Pannala, S., 1999. On LEM/LES methodology for two-phase flows. In *AIAA/ASME/SAE/ASEE Joint Propulsion Conference and Exhibit, 35th*. Los Angeles.

Patte-Rouland, B., Lalizel, G., Moreau, J. & Rouland, E., 2001. Flow analysis of an annular jet by particle image velocimetry and proper orthogonal decomposition. *Measurement Science and Technology*, 12, p. 1404-1412.

Patterson, M.A., Reitz, R.D., 1998. Modeling of the effects of fuel spray characteristics on diesel engine combustion and emission. *SAE paper*, SAE Paper 980131.

Pinho, F. T., Whitelaw, J. H., 1991. Flow of non-Newtonian fluids over a confined baffle. *Journal of Fluid Mechanics,* Vol. 226, pp. 475-496.

Pitsch, H., 2006. Large-eddy simulation of turbulent combustion. *Annual Review of Fluid Mechanics,* Vol. 48, pp.453-482.

Pope, S.B., 1985. PDF methods for turbulent reacting flows. *Progress in Energy and Combustion Science*, 11, p. 119-162.

Pope, S.B., 2008. *Turbulent Flows*. Cambridge University Press.

Prière, C., Gicquel, L. Y. M., Gajan, P., Strzelecki, A., Poinsot, T., Bérat, C. 2005. Experimental and Numerical Studies of Dilution Systems for Low-Emission Combustors. *AIAA Journal,* Vol. 43, No.8 p. 1753-1766.

Reitz, R., Diwakar, R., 1986. Effect of drop breakup on fuel sprays. *SAE paper*, (SAE Paper 860469).

Reitz, R.D., 1987. Modeling atomisation processes in high-pressure vaporizing sprays. *Atomisation and Spray Technology*, 3, p. 309-337.

Reitz, R. D., Bracco, F. V., 1983. Global Kinetics Models and Lack of Thermodynamic Equilibrium. *Combustion and Flame,* Vol. 53, pp. 141-143.

Reitz, R. D., 1999. In Challen, B., Baranescu, R., editors. Diesel engine reference handbook, Boston Elsevier Butterworth-Heinemann, pp.153-172.

Riber, E., Moureau, V., Garcia, M., Poinsot, T., Simonin, O. 2009. Evaluation of numerical strategies for large eddy simulation of particulate two-phase recirculating flows. *Journal of Computational Physics*, Vol. 228, Issue 2, pp. 539-564.

Richardson, L. F., 1922. *Weather prediction by numerical process*. Cambridge University Press.

Salewski, M., Fuchs, L., 2007. Consistency issues of Lagrangian particle tracking applied to a spray jet in crossflow. *International Journal of Multiphase Flow*, 33, p. 394-410.

Sankaran, V., 2003. Subgrid combustion modeling for compressible two-phase reacting flows. *PhD Thesis*, Georgia Institute of Technology

Schumann, U., 1995. Stochastic backscatter of turbulence energy and scalar variance from random subgrid-scale fluxes. *Proc. Roy. Soc. London Ser. A.*, 451, p. 193.

Siamas, G.A., Jiang, X., Wrobel, L.C., 2009. Parallel Direct Numerical Simulation of an Annular Gas-Liquid Two-Phase Jet with Swirl. In *Parallel Scientific Computing and Optimization*.: Springer New York. p. 223-236.

Smagorinsky, J., 1963. General Circulation experiments with the primitive equations, Part I: The basic experiment. *Monthly Weather Review*, 91, p. 99-164.

Sone, K., Menon, S., 2003. The effect of subgrid modeling on the in-cylinder unsteady mixing process in a direct injection engine. *ASME Journal of Engineering for Gas Turbines and Power*, 125, pp. 435-443.

Sone, K., Patel, N., Menon, S., 2001. *KIVALES: large-eddy simulations of internal combustion engines*. Technical Report. Georgia Institute of Technology

Sone, K., Patel, N., Menon, S., 2001. Large-eddy simulation of fuel-air mixing in an internal combustion engine. *AIAA Paper 2001-0635*.

Speziale, C.G., 1985. Galilean invariance of subgrid-scale stress models in the large-eddy simulation of turbulence. *Journal of Fluid Mechanics*, 156, pp. 55-62.

Su, T.F., Patterson, M.A., Reitz, R.D., 1996. *Experimental and numerical studies of high pressure multiple injection sprays*. Technical Report 960861. SAE International

Tennison, P.J., Reitz, R.D., 2001. An Experimental Investigation of the Effects of Common-Rail Injection System Parameters on Emissions and Performance in a High-Speed Direct-Injection Diesel Engine. *Journal of Engineering for Gas Turbines and Power*, 123(1), p. 167-175.

Valentino, M., 2006. *Numerical Simulations of Transient Gas and Spray Jets under Diesel Conditions*. PhD Thesis. Brunel University

Valentino, M., Jiang, X., Zhao, H., 2007. A comparative RANS/LES study of transient gas jets and sprays under diesel conditions. *Atomization and Sprays,* 2007, 17, pp. 451-472.

van Wachem, B. G. M., Almstedt, A. E., 2003. Methods for multiphase computational fluid dynamics. *Chemical Engineering Journal*, 96, p. 81-98.

Vinkovic, I., Aguirre, C., Simoens, S., Gorokhovski, M., 2006. Large eddy simulation of droplet dispersion for inhomogeneous turbulent wall flow. *International Journal of Multiphase Flow*, 32, pp. 344-364.

Vreman, B., Geurts, B., Kuerten, H. 1996. Comparison of Numerical Schemes in Large-Eddy Simulation of the Temporal Mixing Layer. *International Journal for Numerical Methods in Fluids,* Vol. 22, pp. 297-311.

Xin, J., Montgomery, D., Han, Z., Reitz, R. D., 1997. Multidimensional Modeling of Combustion for a Six-Mode Emissions Test Cycle on a DI Diesel Engine. *Journal of Engineering for Gas Turbines and Power,* Vol. 119, pp. 683-691.

Yaga, M., Endo, H., Yamamoto, T., Aoki, H., Miura, T., 2002. Modeling of eddy characteristic time in LES for calculating turbulent diffusion flame. *International Journal of Heat and Mass Transfer,* Vol. 45 pp. 2343-2349.

Yavuz, I., Celik, I., Smith, J., Gel, A., Amine, E., 1998. Bowl induced flow instability in a typical engine cylinder. *ASME ICE-Division Fall Conference*. Clymer, New York.